ARO 21139.11-EL

(2)

Final Report

Millimeter Wave Antennas

Department of Electrical Engineering
University of Houston
Houston, Texas 77204

September 1, 1984 to August 31, 1988

ARO Project No. 21139-EL
Contract No. DAAG29-84-K-0166

Dr. Stuart A. Long
Dr. David R. Jackson

DISCLAIMER NOTICE

THIS DOCUMENT IS BEST QUALITY PRACTICABLE. THE COPY FURNISHED TO DTIC CONTAINED A SIGNIFICANT NUMBER OF PAGES WHICH DO NOT REPRODUCE LEGIBLY.

UNCLASSIFIED
SECURITY CLASSIFICATION OF THIS PAGE (When Data Entered)

MASTER COPY - FOR REPRODUCTION PURPOSES

REPORT DOCUMENTATION PAGE

READ INSTRUCTIONS BEFORE COMPLETING FORM

1. REPORT NUMBER: ARO 21139.11-EL	2. GOVT ACCESSION NO.: N/A
	3. RECIPIENT'S CATALOG NUMBER: N/A
4. TITLE (and Subtitle): Millimeter Wave Antennas	5. TYPE OF REPORT & PERIOD COVERED: Final Report Sept. 1, 1984-Aug. 31, 1988
	6. PERFORMING ORG. REPORT NUMBER:
7. AUTHOR(s):	8. CONTRACT OR GRANT NUMBER(s): Contract No. DAAG29-84-K0166 ARO Project No. 21139-EL
9. PERFORMING ORGANIZATION NAME AND ADDRESS: Department of Electrical Engineering University of Houston Houston, Texas 77204-4793	10. PROGRAM ELEMENT, PROJECT, TASK AREA & WORK UNIT NUMBERS:
11. CONTROLLING OFFICE NAME AND ADDRESS: U. S. Army Research Office Post Office Box 12211 Research Triangle Park, NC 27709	12. REPORT DATE: October 28, 1988
	13. NUMBER OF PAGES: 01
14. MONITORING AGENCY NAME & ADDRESS (if different from Controlling Office):	15. SECURITY CLASS. (of this report): Unclassified
	15a. DECLASSIFICATION/DOWNGRADING SCHEDULE:

16. DISTRIBUTION STATEMENT (of this Report)

Approved for public release; distribution unlimited.

17. DISTRIBUTION STATEMENT (of the abstract entered in Block 20, if different from Report)

NA

18. SUPPLEMENTARY NOTES

The view, opinions, and/or findings contained in this report are those of the author(s) and should not be construed as an official Department of the Army position, policy, or decision, unless so designated by other documentation.

19. KEY WORDS (Continue on reverse side if necessary and identify by block number)

Antennas, millimeter wave, microstrip, dielectric resonator

20. ABSTRACT (Continue on reverse side if necessary and identify by block number)

The properties of two types of antennas suitable for operation at millimeter wave frequencies (100 to 300 GHz) have been investigated both theoretically and experimentally. The type of radiators considered were printed-circuit or microstrip antennas and dielectric resonator antennas. Special emphasis was placed on the problem of integrating the antenna with the waveguiding structure. The ultimate objective of the research was to provide aid in the selection and design of millimeter wave antennas for given systems applications within this frequency range.

DD FORM 1 JAN 73 1473 EDITION OF 1 NOV 65 IS OBSOLETE

UNCLASSIFIED
SECURITY CLASSIFICATION OF THIS PAGE (When Data Entered)

TABLE OF CONTENTS

STATEMENT OF PROBLEM STUDIED

Antennas are being used presently, or have been proposed for use on systems now under development, on military hardware such as missiles, projectiles, aircraft, satellites, and tanks. They may be used for the purpose of remote guidance, communications, terrain sensing, fusing, navigation, or position location. In recent years the frequency range of interest for military systems has gradually progressed upward. For several applications today frequencies beyond those of the usual microwave band are required. Of special importance is the millimeter wave regions from 100 to 300 GHz (with a resulting wavelength in air of 3.0 to 1.0 mm).

Many of the same properties that are important for more usual microwave antennas are also required for uses at millimeter wave frequencies. Some of the physicai properties that can be important include, ruggedness, ease of fabrication, and the ability to be mounted conformally to the object on which it is attached. Electrical properties which may be important include efficiency, bandwidth, input impedance, and radiation pattern. In addition to these usual considerations, a new set of criteria also arises. Since the millimeter wave energy is not always guided by standard coaxial lines, or even rectangular waveguides, additional problems arise in the integration of suitable antennas with the desired waveguiding system. Thus the transition region between the waveguide and the antenna and the particular feeding structure is an important part of the antenna design problem.

The properties of two types of antennas suitable for operation at millimeter wave frequencies (100 to 300 GHz) have been investigated both theoretically and experimentally. The type of radiators considered were printed-circuit or microstrip antennas and dielectric resonator antennas. Special emphasis was placed on the problem of integrating the antenna with the waveguiding structure. The ultimate objective of the research was to provide aid in the selection and design of millimeter wave antennas for given systems applications within this frequency range.

SUMMARY OF MOST IMPORTANT RESEARCH

1) Dielectric cylinders of very high permittivity have been used in the past as resonant cavities, but since the structure is not enclosed by metallic walls, electromagnetic fields do exist beyond the geometrical boundaries of the structure and part of the power is radiated. Through the proper choice of geometry and permittivity this radiation can become the dominant feature of the structure and become an efficient antenna for use at millimeter wave frequencies. Both experimental and theoretical investigations of a variety of these dielectric resonator antennas have been undertaken. In particular, the input impedance of a probe-fed cylindrical structure was examined in detail and a comparison of theoretical and experimental results was made. [4]

2) An approximate theory was derived for the modes in a cylindrical dielectric resonator antenna. The air-dielectric interface was approximated as a perfect magnetic conductor and expressions for the resonant frequency and radiation from the equivalent surface magnetic currents were derived. A broad beam with a maximum normal to the ground plane was obtained for the lowest mode. A more directive beam or a beam with a single sharp null was obtained for the next mode depending on the cylinder geometry. Good agreement was obtained between theory and experiment.

An experimental investigation was also undertaken to demonstrate that the coplanar waveguide was an effective excitation mechanism for the cylindrical dielectric resonator antenna. Data showing the coupling behavior and the radiation patterns for various cylinder aspect ratios, dielectric constants, and feed positions were presented. The results show that efficient and practical antenna systems can be designed using such a feed structure which is much more practical at millimeter wave frequencies.

3) A systematic investigation of the excitation of a cylindrical dielectric resonator antenna

by a microstrip transmission line was undertaken to illustrate the possibility of such a feed structure and to characterize the coupling behavior and radiation patterns of the system.[18]

4) The electromagnetic properties of electrically thick rectangular microstrip antennas were investigated experimentally. Antennas were fabricated with different patch sizes and with electrical thicknesses ranging from 0.03 to 0.23 wavelengths in the dielectric substrate. The resonant frequencies were measured and compared to existing formulas. The bandwidth was calculated as a function of electrical thickness and the antenna radiation patterns were measured.

5) An algebraic formulation for the resonant frequency of a rectangular microstrip antenna has been derived which is valid for electrically thick substrates. Predicted values of resonance are compared with previous theories, as well as actual experimental measurements, for radiators approaching one-quarter wavelength in thickness, which may correspond to physically thin printed circuit boards at millimeter wave frequencies.

6) The design and experimental measurement of a dual-band, monolithic microstrip antenna is presented. The structure utilizes a short-circuited length of microstrip transmission line to provide reactive loading and, thereby, retains the low-profile characteristic of a normal microstrip patch radiator and allows accurate fabrication for high frequency applications.

7) An experimental study of reactively loaded rectangular microstrip antennas has been undertaken. The reactive loads used were either a single pin, or a symmetrically located pair of pins, short circuiting points on the patch to corresponding points on the ground plane. A set of points forming a single curve for the case of one shorting pin or two symmetrically located curves for the case of two shorting pins was found. A single, or a pair, of short circuits placed at any point on these curves results in an element having a fixed resonant frequency and a fixed radiation pattern independent of the point selected. The input impedance, however, varies over a very large range when the short circuit or pair of short circuits is moved along these curves. The major application of this work is the study of the feasibility of maintaining an impedance match for the elements of a microstrip antenna array with changing scan angle by moving the position of one or more short-circuiting pins. An experimental and theoretical study of the mutual impedance for microstrip array elements was conducted and used in a computer program simulating a finite array. Though the model used for mutual impedance was somewhat crude, the simulation program predicted a variation of active element impedance with scan angle. For a number of different scan angles, the position of shorting pins was adjusted to obtain a match for all of the array elements thus indicating that this dynamic matching technique may be feasible for scanned arrays.

8) A dual mode microstrip antenna element was investigated which had two independently excitable modes resonant at the same frequency. This element has been shown to be capable of producing a broadside maximum, a broadside null, or an end-fire type pattern by suitable choices of its reactive loads and suitable excitation of its degenerate modes. Appropriately located loads can be used to resonate modes normally resonant at quite different frequencies, at a single, common frequency. The results indicate that the nodal lines of the loaded element are accurately predicted by the generalized theory of loaded microstrip antennas, and that two modes can be excited independently of each other by feeding each mode along the nodal line of the other. To verify the theoretical predictions an actual dual mode microstrip element was fabricated and tested. The results of this experiment correlate well with the theoretical model for the overall characteristics of the radiator.

9) One of the initial studies during this contract concerned the properties of microstrip radiators in a two-layered substrate-superstrate geometry. It was observed previously that certain phenomena occur when a printed antenna element is embedded within such a structure. For example, a superstrate layer may be used to eliminate surface waves excited by a horizontal current element, resulting in 100% efficiency for such an element. A phenomenon termed

"radiation into the horizon" may also be produced, in which the far-field radiation pattern of an element in a layered microstrip geometry may extend down to the horizon with a nonzero value. Using this effect, a substrate-superstrate geometry may be chosen so that the radiation pattern from an embedded element will be nearly omnidirectional. Alternatively, a substrate-superstrate geometry may be used to produce the opposite effect, to produce patterns which have narrow beams. Some of these effects may have practical uses in modifying the properties of microstrip elements, as well as the radiation patterns. For example, in [6] it is noted that using a superstrate to eliminate the excitation of surface waves may significantly reduce the mutual coupling between microstrip elements. The effect of a superstrate layer on other types of microstrip elements such as the electromagnetically coupled (EMC) dipole and the microstrip line are also discussed in [6].

During the course of this investigation, a technique for efficiently evaluating the Sommerfeld integrals which occur in microstrip analysis was used, which is explained in [5]. This technique overcomes most of the difficulty in computing the Sommerfeld integrals for source and observation points which are widely separated, which would otherwise be a serious limitation in the computation of mutual impedance in many cases.

10) One of the main projects which was initiated during this contract was a leaky-wave investigation of the narrow-beam effect which may be created in a multiple-layer dielectric geometry. This project, started with an investigation of the two-layered substrate-superstrate structure, which had already been found previously to produce narrow beams as the permittivity of the superstrate increases, for a particular choice of layer thicknesses. This effect was found to be attributable to the existence of weakly attenuated leaky waves which are excited on the structure in this high-gain condition. The layer thicknesses essentially determine the propagation constant of the waves, and hence the beam scan angle, while the permittivity determines the attenuation of the waves, which in turn determines the beamwidths. An asymptotic solution of the characteristic equations for the TE and TM leaky waves allowed for closed-form expressions for the propagation constants. By using scalar radiation theory, radiation patterns for the case of a two-dimensional source within the structure were obtained. A comparison with exact patterns showed excellent agreement near the beam maximum, where the leaky waves contribute significantly to the total pattern. Details of the analysis, as well as the results, are given in [9].

The next phase in the leaky-wave research project was the investigation of the multiple-layer dielectric structure, which consists of an arbitrary even number of layers having alternating low and high permittivities. It was observed in previous work by others (H. Y. Yang and N. G. Alexopoulos, "Gain Enhancement Methods for Printed Circuit Antennas Through Multiple Superstrates", *IEEE Trans. Antennas Propagat.*, vol. AP-35, pp. 860-863, July 1987) that very narrow beams could be obtained when using more than two layers in the structure. Such a structure may find applications at millimeter-wave frequencies, where the thickness would not be a serious limitation. A leaky-wave antenna constructed from only dielectric layers, with a simple source mechanism, would have the advantages of durability and simplicity. A leaky-wave analysis of this structure revealed the same leaky wave behavior as for the two-layered case. A more general analysis technique was developed to calculate the propagation constants of the leaky waves, however. This technique utilized the similarity in field structure between the leaky wave fields and the fields existing inside the layered structure when illuminated with a plane wave excitation. A power calculation inside the structure was then used to derive asymptotic formulas for the leaky-wave propagation constants. A comparison with exact values of propagation constants showed very good agreement, which improves as the beamwidth decreases. The derivation of these formulas is given in [15].

During the leaky-wave investigation, another topic which was explored was the extension of leaky-wave radiation formulas to the case of cylindrically propagating leaky waves. Previously, leaky-wave radiation formulas existed only for the case of a one-dimensional wave, where the radiation pattern could be determined from a Kirchoff-Huygens scalar radiation equation (T. Tamir and A. A. Oliner, "Guided Complex Waves: Part 2, Relation

to Radiation Patterns", *Proc. IEE*, vol. 110, pp. 325-334, Feb. 1963). For leaky-wave antennas consisting of a cylindrical leaky wave propagating on a planar interface, scalar radiation theory no longer suffices, due to the vector nature of the aperture fields. A microstrip source within a layered structure is one example where the leaky wave is cylindrical, so it is clearly important from a practical standpoint to have radiation formulas available for cylindrical waves. By using the equivalence principle and integrating over the equivalent sources, closed-form expressions for the far-field radiation patterns of TE and TM cylindrical leaky waves were obtained. One practically important aspect of these formulas was that the results allowed for arbitrary aperture size, so that the radiation from a truncated aperture could be studied. This is practically important, since all planar structures must be truncated at some finite radius. The formulas which were developed were used together with the asymptotic analysis of the multiple-layered structure in order to accurately predict the radiation patterns from sources within this structure. The radiation formulas are derived in [14].

11) Another project which was investigated under the contract was the accurate computation of mutual coupling in large phased arrays of patch antenna elements. This investigation led to a formulation of mutual impedance from which series expansions for the impedance matrix could be easily obtained. For large sparce arrays, the first few terms of this matrix series usually gives accurate results for the patch impedances, while requiring much less computation time than the matrix inversion required in a moment-method formulation of the phased array impedance matrix. A derivation of these series expansions may be found in [11].

12) Also initiated during the contract was a design study of an array of EMC dipoles. The EMC dipole is a very promising microstrip element due to its small size and simplicity. At higher frequencies where the substrate thickness may be .05 wavelengths or more, the EMC dipole also exhibits a large bandwidth. It also has the advantage of easy matching with the feeding transmission line, by simply adjusting the dipole length and offset. An array of these elements would make an attractive design for many applications. Previously, a design procedure for an array of such elements was developed by Elliott and Stern (R. S. Elliott and G. J. Stern, "The Design of Microstrip Dipole Arrays Including mutual Coupling, Part I: Theory", *IEEE Trans. Antennas Propagat.*, vol. AP-29, pp. 757-760, Sept. 1981). This design procedure was more directly compatible with experimental measurements than with numerical calculation, however. During the present investigation a design procedure was developed which was well-suited to a direct moment-method analysis. One of the key features of this design procedure is the introduction of coupling coefficients which may be determined numerically by considering only two EMC dipole pairs at a time, resulting in a relatively small moment method problem. The use of traveling-wave basis functions on the transmission lines further improved the efficiency of the calculation. Once the coupling coefficients are determined, a matrix description of the line and dipole currents is used to formulate a matrix set of design equations, which accounts for all of the necessary interactions between all of the lines and dipoles in the array. This matrix set of equations allows for the design of a feed network which will excite the required dipole currents in order to produce a specified radiation pattern. In order to test the theory, an experimental four element linear array was constructed and tested, with good agreement between the theoretical and measured patterns. Details of the design procedure, along with the results, may be found in [13].

13) An investigation of the scattering properties of conductive bodies embedded within lossy media was undertaken during the contract period. One particular example of such a configuration would be a microstrip patch antenna on top of or below a lossy dielectric layer. A general scattering formula was derived which shows the fundamental dependence of the radar cross section of the body on the parameters of the lossy media. One important result of this formula is that the body radar cross section (RCS) is directly related to the radiation efficiency of the body, so that the RCS may be directly controlled by introducing loss into a surrounding layer.

A numerical study was performed for a rectangular patch antenna embedded within a lossy substrate-superstrate geometry, as a specific case. Results were obtained for three particular configurations: a lossy substrate, a lossless substrate with a lossless superstrate on top, and a lossless substrate with a lossy superstrate on top. In each case, the results confirmed the general trend predicted by the scattering formula. Details and results may be found in [12].

14) During the contract period a feasibility study of an array of electromagnetically coupled patch antennas was performed. In this array, the patch antennas are electromagnetically coupled between adjacent neighbors by short sections of transmission line which are embedded within the substrate. This eliminates the need for a corporate feed network, and greatly simplifies the array construction. The feasibility study determined that it is possible to design such an array to produce a beam scanned to any specified direction, with reasonable coupling values between adjacent patches required. A moment method calculation was used to determine the coupling coefficients between adjacent patches, and a matrix equation using these values was then formulated to predict the patch current amplitudes assuming a given feed source on the first patch and a specified load termination on the last patch. A synthesis procedure was then developed, whereby the coupling coefficients between adjacent patches may be determined from the desired set of patch current amplitudes, which determines the radiation pattern. Hence, the dimensions of the embedded line sections between the patches are determined from the specified pattern. To test the theory, a four element linear array of patches was built, designed for a 45^{0} beam. The measured pattern showed good agreement with the predicted result, and demonstrated the feasibility of this type of array. The details of the design technique, along with the results, are given in (11).

15) An investigation of the properties of a traveling-wave array of monopoles embedded within a substrate, fed by a meandering stripline, was conducted during the contract period. Such an array may make a useful scanned-beam antenna for some applications. Because individual monopoles which are electrically short do not radiate significantly, it is possible to construct arrays of this type many wavelengths long, with control of the monopole currents achieved by variation of the monopole heights and length of the meandering stripline between monopoles. A quasi-periodic structure analysis of the array was used to obtain design equations for the monopole heights and line lengths required to produce a specified constant phase shift between elements, and a specified amplitude taper in the monopole currents along the length of the array. As an experimental verification of the theory, a ten-element linear array with a 60^{0} beam was designed and constructed. The measured pattern showed good agreement with the theoretical one. A detailed discussion of the theory and results may be found in [2].

LIST OF PUBLICATIONS

PAPERS PUBLISHED

[1] S. E. Davidson, S. A. Long and W. F. Richards, "Dual-Band Microstrip Antennas with Monolithic Reactive Loading", *Electronics Letters*, vol. 21, no. 20, pp. 936-937, September 26, 1985.

The design and experimental measurement of a dual-band, monolithic microstrip antenna is presented. The structure utilizes a short-circuited length of microstrip transmission line to provide reactive loading and, thereby, retains the low-profile characteristic of a normal microstrip patch radiator.

[2] E. Chang, S. A. Long, and W. F. Richards, "An Experimental Investigation of Electrically Thick Rectangular Microstrip Antennas", *IEEE Trans. Antennas and Propagation*, vol. AP-34, June 1986.

The electromagnetic properties of electrically thick rectangular microstrip antennas were investigated experimentally. Antennas were fabricated with different patch sizes and with electrical thicknesses ranging from 0.03 to 0.23 wavelengths in the dielectric substrate. The resonant frequencies were measured and compared to existing formulas. The bandwidth was calculated as a function of electrical thickness and the antenna radiation patterns were measured.

[3] W. F. Richards and S. A. Long, "Reactively Loaded Microstrip Antennas," *IEEE Antennas and Propagation Society Newsletter*, vol. 28, No. 5, pp. 11-17, October 1986.

Microstrip elements have proven to be very versatile and have found uses in a variety of applications from satellite arrays to automobile anti-collision warning systems. This versatility stems mainly from their structural simplicity, ease of construction, ruggedness, conformability, low profile, and low cost. In addition to these features, microstrip elements are capable of producing a variety of different patterns and polarization. Most research efforts, however, have been limited to basic applications using only a single, unperturbed mode of a rectangular or circular element. Additional applications are possible through the used of reactive loading. These include multiband, frequency-agile and polarization-diverse, adaptable-impedance, and multimode-pattern antennas. Some experimental work has been done in these areas but very little theoretical work has been done. In this paper, a very simple theory is presented which will guide a designer who wished to take advantage of the added flexibility that reactive loading provides. In addition, several application are discussed with corresponding theoretical and experimental results.

[4] S. A. Long and M. W. McAllister, "The Input Impedance of the Dielectric Resonator Antenna", *International Journal of Infrared and Millimeter Waves*, vol. 7, no.4, pp. 555-570, 1986

Dielectric cylinders of very high permittivity have been used in the past as resonant cavities, but since the structure is not enclosed by metallic walls, electromagnetic fields do exist beyond the geometrical boundaries of the structure and part of the power is radiated. Through the proper choice of geometry and permittivity this radiation can become the dominant feature of the structure and become an efficient antenna for use at millimeter wave frequencies. Both experimental and theoretical investigations of a variety of these dielectric resonator antennas have been undertaken. In particular, the input impedance of a probe-fed cylindrical structure was examined in detail and a comparison of theoretical and experimental results was made.

[5] D. R. Jackson and N. G. Alexopoulos, "An Asymptotic Extraction Technique for Evaluating Sommerfeld-Type Integrals", *IEEE Transactions on Antennas and Propagation*, vol. AP-34, pp. 1467-1470, Dec. 1986.

An asymptotic extraction technique is developed, which leads to an efficient evaluation of the electric field from a Hertzian dipole in a layered geometry. This technique allows for a rapidly converging expression for the electric field, which remains well behaved as the source and observation heights above the ground plane coincide. A useful application of this method is in the calculation of mutual impedance between printed dipoles.

[6] D. R. Jackson and N. G. Alexopoulos, "Analysis of Planar Strip Geometries in a Substrate-Superstrate Configuration", *IEEE Transactions on Antennas and Propagation*, vol. AP-34, pp. 1430-1438, Dec. 1986.

A moment method procedure is used to analyze the behavior of several different configurations consisting of planar strips in a substrate-superstrate geometry. These include the microstrip transmission line,
center-fed dipole, the mutual impedance between two dipoles, and the transmission-line coupled dipole. In each case some of the basic superstrate effects are discussed.

[7] R. Garg and S. A. Long, "Resonant Frequency of Electrically Thick Rectangular Microstrip Antennas" *Electronics Letters*, vol. 23, no. 21, pp. 1149-1151, October 8, 1987.

An algebraic formulation for the resonant frequency of a rectangular microstrip antennas has been derived which is valid for electrically thick substrates. Predicted values of resonance are compared with previous theories, as well as actual experimental measurements, for radiators approaching one-quarter wavelength in thickness.

[8] R. Garg and S. A. Long, "An Improved Formula for the Resonant Frequencies of the Triangular Microstrip Patch Antenna", *IEEE Trans. on Antennas and Propagation*, vol.AP- 36, no. 4, pp. 570-575, April 1988.

An improved formula is derived to predict the resonant frequency of the triangular microstrip patch antenna. The techni ue previously used for the case of a circular disk is modified to produce greater accuracy than previous investigations.

[9] D. R. Jackson and A. A. Oliner, "A Leaky-Wave Analysis of the High-Gain Printed Antenna Configuration", *IEEE Transactions on Antennas and Propagation*, vol. AP-36, July 1988.

A leaky-wave analysis is used to explain the narrow-beam "resonance gain" phenomenon, in which narrow beams may be produced from a printed antenna element in a substrate-superstrate geometry. The leaky-wave approach furnishes insight into the physical nature of this phenomenon, as well as providing new practical information. The leaky-wave approach also permits the derivation of simple asymptotic formulas for the leaky-wave propagation constants, which determine the radiation patterns.

[10] R. A. Kranenburg and S. A. Long "Microstrip Transmission Line Excitation of Dielectric Resonator Antennas", *Electronics Letters*, vol. 24, no. 18, pp. 1156-1157, September 1, 1988.

A systematic investigation of the excitation of a cylindrical dielectric resonator antenna was undertaken to illustrate the possibility of such a feed structure and to characterize the coupling behavior and radiation patterns of the system.

PAPERS SUBMITTED

[11] D. R. Jackson, W. F. Richards, and A. Ali-Khan, "Series Expansions for the Mutual Coupling in Microstrip Patch Arrays", *IEEE Transactions on Antennas and Propagation* (accepted for publication).

A dominant-mode mutual coupling theory is developed for an array of microstrip patches. A formulation is used which is compatible with either a cavity model or a spectral-domain

calculation, or with measurements. This formulation allows for the simple derivation of series expansions for the impedance, admittance, and scattering matrices, which do not require inversion of a moment-method matrix. These expansions are computationally efficient for large, sparce arrays.

[12] D. R. Jackson, "The RCS of a Rectangular Microstrip Patch in a Substrate-Superstrate Geometry", *IEEE Transactions on Antennas and Propagation* (accepted for publication).

A general scattering formula is developed for the radar cross section of a general resonant conductive body embedded within lossy media. This formula shows that the RCS of the body is directly related to the radiation efficiency of the body. The specific case of a rectangular microstrip patch within a lossy substrate-superstrate geometry is analyzed, with results presented for three different cases: a lossy substrate only, a lossless substrate with a lossless superstrate, and a lossless substrate with a lossy superstrate. It is concluded that the lossy superstrate case gives the most RCS reduction with the least detrimental effect on the input impedance of the patch.

[13] D. R. Jackson, A. E. Dinbergs, and S. A. Long, "A Moment Method Design Procedure for an Array of EMC Dipoles", submitted to *IEEE Transactions on Antennas and Propagation*.

A design procedure based on a moment-method analysis is given for an array of microstrip dipoles electromagnetically coupled (EMC) to microstrip transmission lines. One of the key features of the design procedure is that only one pair of EMC dipoles needs to be analyzed at a time numerically, in order to develop the necessary coupling coefficients which account for the interactions between all of the EMC line-dipole pairs. A convenient set of matrix design equations are obtained, which allows for the design of a feed network to excite the desired dipole currents.

[14] A. Ip and D. R. Jackson, "Radiation from Cylindrical Leaky Waves", submitted to *IEEE Transactions on Antennas and Propagation*.

Formulas for the far-field pattern of cylindrical leaky waves propagating on a planar surface are derived. These formulas may be used to predict the radiation pattern of a general class of leaky-wave antennas, consisting of a finite-size source which excites a radially propagating leaky wave on some planar surface. Leaky-wave antennas comprised of microstrip antenna elements fall into this category. Formulas are derived for both TE and TM leaky waves of arbitrary aperture size, which allows the practical effects of a truncated aperture to be determined.

[15] D. R. Jackson, A. A. Oliner, and A. Ip, "Leaky-Wave Propagation and Radiation for a Multiple-Layer Dielectric Structure", submitted to *IEEE Transactions on Antennas and Propagation*.

A leaky-wave analysis is used to predict the beamwidth of a narrow-beam multiple layer dielectric structure, consisting of an alternating arrangement of low and high permittivity dielectric layers. A power-flow analysis is used to derive asymptotic formulas for the phase and attenuation constants of the leaky waves which propagate on this structure, which directly determines the beamwidths and scan angle. The asymptotic formulas show that the beam width decreases very rapidly as the number of layers increases, so that very narrow beams may be obtained with only a modest number of layers.

[16] H. Y. Yang, N. G. Alexopoulos, and D. R. Jackson, "Microstrip Open-End and Gap

Discontinuities in a Substrate-Superstrate Structure", submitted to *IEEE Transactions on Microwave Theory and Techniques.*

An analysis of both open-end and gap discontinuities in microstrip lines within a substrate-superstrate geometry is given. The analysis uses both subdomain and semi-infinite traveling-wave basis functions for an efficient moment-method calculation of the scattering parameters. Results show that the superstrate may significantly affect the discontinuity parameters, by increasing the space wave and surface-wave radiation at the discontinuity.

[17] P. B. Katehi, D. R. Jackson, and N. G. Alexopoulos, "Microstrip Dipoles", submitted as Chapter 5 of *The Handbook of Microstrip Antennas*, J. R. James and P. S. Hall, Eds.

A general overview of the analytic and numerical aspects of modeling microstrip dipole configurations is presented, along with results showing some of the basic properties of the microstrip dipole. Particular attention is devoted to the EMC dipole, both as a single element and as an element in a finite array. Practical considerations include bandwidth and impedance behavior, and the trade-off between dipole bandwidth and line radiation for the EMC dipole.

[18] R. A. Kranenburg, S. A. Long and J. T. Williams, " Coplanar Waveguide Excitation of Dielectric Resonator Antennas", *IEEE Transactions on Antennas and Propagation.*

An approximate theory is derived for the modes in a cylindrical dielectric resonator antenna. The air-dielectric interface is approximated as a perfect magnetic conductor and expressions for the resonant frequency and radiation from the equivalent surface magnetic currents are presented. A broad beam with a maximum normal to the ground plane is obtained for the lowest mode. A more directive beam or a beam with a single sharp null is obtained for the next mode depending on the cylinder geometry. Good agreement is obtained between theory and experiment. An experimental investigation was also undertaken to demonstrate the coplanar waveguide as an effective excitation mechanism for the cylindrical dielectric resonator antenna. Data showing the coupling behavior and the radiation patterns for various cylinder aspect ratios, dielectric constants, and feed positions are presented. The results show that efficient and practical antenna systems can be designed.

PAPERS PRESENTED

[1] S. A. Long, 'Dielectric Resonator Antennas" presented at U. S. Army Research Office Workshop on Millimeter Wave Technology, New York Institute of Technology, Old Westbury, NY, December 1984.

[2] S. E. Davidson S. A. Long, W. F. Richards, "Monolithic Design of Dual-Band Microstrip Antennas Using Reactive Loading" presented at IEEE International AP-S Symposium, Vancouver, British Columbia, June 1985.

[3] W. F. Richards and S. A. Long, "Pattern Adaptation Using Loaded Dual-Mode Microstrip Antennas presented at IEEE International AP-S Symposium, Vancouver, British Columbia, June 1985.

[4] M. W. McAllister and S. A. Long, "The Dielectric Resonator Antenna", presented at Tenth International Conference on Infrared and Millimeter Waves, Lake Buena Vista, Florida, December 1985.

[5] W. F. Richards and S. A. Long, "Impedance Matching of Microstrip Antennas with Reactive Loads" presented at National Radio Science Meeting, Boulder, Colorado, January 1986.

[6] E. Chang, S. A. Long and W. F. Richards, "The Resonant Frequency of Electrically Thick Rectangular Microstrip Antennas" presented at IEEE International AP-S Symposium, Philadelphia, PA, June 1986.

[7] W. F. Richards and S. A. Long, "Matching Microstrip Antennas Using Reactive Loads" presented at IEEE International AP-S Symposium, Philadelphia, PA, June 1986.

[8] D. R. Jackson and S. A. Long, "A Moment-Method Approach for the Array of Transmission Line Coupled Dipoles", presented at the IEEE AP-S Intl. Symp., Philadelphia, PA, June 1986.

[9] D. R. Jackson and N. G. Alexopoulos, "An Asymptotic Extraction Technique for the Real-Space Evaluation of Sommerfeld-Type Integrals", presented at the URSI National Radio Science Meeting, Philadelphia, PA, June 1986.

[10] S. A. Long, "The Cylindrical Dielectric Resonator Antenna" presented at the U. S. Army Research Office Workshop on Fundamental Issues in Millimeter and Submillimeter Waves, Los Angeles, CA, September 1986.

[11] W. F. Richards and S. A. Long, "Impedance Control of Microstrip Antennas Utilizing Reactive Loading" presented at International Telemetering Conference, Las Vegas, NV, October 1986.

[12] W. F. Richards and S. A. Long, "Adaptive Pattern Control of a Reactively Loaded Dual-Mode Microstrip Antenna" presented at International Telemetering Conference, Las Vegas, NV, October 1986.

[13] D. R. Jackson, W. F. Richards, and A. Ali-Khan, "An Exact Mutual Coupling Theory for Microstrip Patches", presented at the IEEE AP-S Intl. Symp., Blacksburg, VA, June 1987.

[14] D. R. Jackson and A. A. Oliner, "A Leaky Wave Analysis of the High-Gain Printed Antenna Configuration", presented at the URSI Radio Science Meeting, Blacksburg, VA, June 1987.

[15] S. A. Long, "An Investigation of the Use of Reactive Loading to Control the Impedance of Microstrip Antennas" presented at Missile/Projectile/Airborne Test Instrumentation Antennas Workshop, Atlanta, GA, October 1987.

[16] S. A. Long and A. Ali Khan, "An Investigation of the Impedance of Reactively Loaded Microstrip Antennas" presented at National Radio Science Meeting, Boulder, Colorado, January 1988.

[17] N. G. Alexopoulos, H. Y. Yang, and D. R. Jackson, "Analysis of Microstrip Open-End and Gap Discontinuities in a Substrate-Superstrate Configuration", presented at the IEEE MTT-S Intl. Symp., New York City, NY, May 1988.

[18] D. R. Jackson and N. G. Alexopoulos, "Scattering from a Microstrip Patch in a Lossy Substrate-Superstrate Geometry", presented at the IEEE AP-S Intl. Symp., Syracuse, NY, June 1988.

[19] D. R. Jackson, A. A. Oliner, and A. Ip, "Radiation from Leaky Waves on Multiple-Layer Dielectric Structures", presented at the URSI Radio Science Meeting, Syracuse, NY, June 1988.

PARTICIPATING PERSONNEL

Stuart A. Long, Professor
William F. Richards, Associate Professor
David R. Jackson, Assistant Professor
Jeffery T. Williams, Assistant Professor
Ramesh Garg, Visiting Associate Professor

Esin Chang, Graduate Research Assistant
Arturs Dinbergs, Graduate Research Assistant
Antonio Ip, Graduate Research Assistant
Jia-Xiang Jiang, Graduate Research Assistant
Ajaz Ali Khan, Graduate Research Assistant
Roger Kranenburg, Graduate Research Assistant
Sai Kwok, Graduate Research Assistant
Prakash Manghnani, Graduate Research Assistant
Steve Slawson, Graduate Research Assistant
S. Toomsawasdi, Graduate Research Assistant

DEGREES EARNED

(1) E. Chang, "An Experimental Study of Electrically Thick Rectangular Microstrip Antennas," M.S.E.E., University of Houston, December 1985.

The electromagnetic properties of electrically thick rectangular microstrip antennas are investigated. Antennas are fabricated with different patch sizes and with electrical thicknesses ranging from 0.03 to 0.23 wavelengths in the dielectric substrate. The resonant frequency and bandwidth are measured and compared to existing theories. The radiation patterns are also measured and the 3 dB beamwidths for the antennas are determined.

(2) S. Toomsawasdi, "Moment Method Analysis of a Microstrip Antenna Using a Patch-Edge *Integral Equation*", Ph.D. University of Houston, May 1987.

A method of computing the input impedance of a microstrip antenna in free space and in a modified environment is presented. A pair of integral equations in terms of the patch-edge electric and magnetic currents are solved using the method of moments. One of these integral equations is based on an approximate exterior-region Green's function. An appropriately chosen magnetic current distributed on the side of a conducting mesa in the presence of the dielectric is capable of reproducing the exact field of a patch element. This mesa is formed by connecting the edge of the patch to the ground plane with conductor. The approximate Green's function used in this theory ignores the presence of both the dielectric substrate and the conducting mesa. It is, therefore, just the free-space Green's function and its use instead of an exact Green's function considerably reduces the computational complexity of the analysis. Results for the input impedance computed using other approximate theories and measurements are presented for comparison with this theory. Comparison with measured results shows the this theory, though approximate, very accurately predicts the locus of the input impedance of microstrip antennas of practical thicknesses. Surprisingly, the antenna quality factor was also predicted very accurately by this technique although the approximate Green's function cannot account for the presence of a surface wave. The

resonant frequencies predicted by this theory are somewhat higher than those measured, an effect attributable to ignoring the presence of the dielectric. The approximate Green's function was also modified to account for the presence of an elevated dielectric slab for applications to microstrip image arrays. Measurements were made for an element in this modified environment; theoretically predicted impedances agreed well with the measured results.

(3) A. Ali Khan, "Study of Loaded Microstrip Antennas and Their Application To Arrays," M.S.E.E., University of Houston, December 1987.

An experimental study of reactively loaded rectangular microstrip antennas is presented in this thesis. The reactive loads used here were either a single pin, or a symmetrically located pair of pins, short circuiting points on the patch to corresponding points on the ground plane. A set of points forming a single curve for the case of one shorting pin or two symmetrically located curves for the case of two shorting pins was found. A single or a pair, of short circuits placed at any point on these curves results in an element having a fixed resonant frequency and a fixed radiation pattern independent of the point selected. The input impedance, however, varies over a very large range when a short circuit or pair of short circuits is moved along these curves. The major application of this work is the study of the feasibility of maintaining an impedance match for the elements of a microstrip antenna array with changing scan angle by moving the position of one or two short-circuiting pins. An experimental and theoretical study of the mutual impedance for microstrip array elements was conducted and used in a computer program simulating a finite array. Though the model used for mutual impedance was somewhat crude, the simulation program predicted a variation of active element impedance with scan angle. For a number of different scan angles, the position of shorting pins was adjusted to obtain a match for all of the array elements thus indicating that this dynamic matching technique may be feasible for scanned arrays.

(4) Antonio Ip, "Radiation and Propagation of Cylindrical Leaky Waves on a Planar Dielectric Multi-Layer Structure", M.S.E.E., University of Houston, May 1988.

Radiation formulas for cylindrical leaky waves on a planar surface are derived. These formulas predict the far-field patterns of either TE or TM waves, with an arbitrary finite-sized aperture assumed, so that the effects of aperture truncation may be determined. A narrow-beam antenna obtained by embedding a printed antenna element within a multiple-layer dielectric structure is then explained from the existence of weakly attenuated leaky waves which exist on this structure. Analytical methods for asymptotically calculating the leaky-wave propagation constants for small beamwidths are presented. Radiation patterns based on the leaky waves are compared with the exact patterns for horizontal and vertical electric and magnetic dipoles in the structure, with excellent agreement obtained near the beam maximum, where the leaky wave contribution is most significant.

(5) Sai C. Kwok, "Analysis and Design of a Traveling-Wave Array of Vertical Monopoles in a Substrate", M.S.E.E., University of Houston, Aug. 1988.

This thesis presents an analysis and design technique for a traveling-wave array of monopoles embedded within a substrate, fed by a meandering stripline. A Block analysis is used to analyze the structure, which is approximated as a periodically loaded transmission line, with the loads being the active impedances of the monopoles. An iterative design procedure is established which determines the necessary monopole heights and meandering line section lengths in order to produce a desired inter-element phase shift and current amplitude taper for the set of monopole currents, and hence a desired radiation pattern. Special attention is devoted to the efficient evaluation of the Sommerfeld integrals which are needed in the self and mutual impedance calculations. As an experimental verification of the theory, a ten element linear array is built

and tested, with good agreement obtained between theory and experiment.

(6) Arturs E. Dinbergs, "Analysis and Design of an Array of Electromagnetically Coupled Microstrip Dipoles", M.S.E.E., University of Houston, Aug. 1988.

This thesis presents an analysis and design technique for an array of microstrip dipoles electromagnetically coupled to microstrip lines (EMC dipoles). A general analysis technique using a combination of piecewise
sinusoidal and traveling-wave basis functions is used to analyze the coupling between elements in the array. A design approach is formulated in which coupling coefficients between only two isolated EMC dipole elements are needed. These coefficients are used together with a matrix description of the line and dipole currents in the array in order to account for the necessary mutual interactions between all of the elements in the array. A four element linear array is built and tested, with good agreement obtained between the predicted and measured patterns.

(7) Prakash Manghnani, "Design and Analysis of an Array of Electromagnetically Coupled Microstrip Patches", M.S.E.E., University of Houston, Aug. 1988.

In this thesis, an analysis and design of an array of microstrip patches that are electromagnetically coupled by transmission lines embedded within the substrate is presented. A method of moments formulation is used to calculate the coupling coefficients between elements, using piecewise sinusoidal basis functions on the transmission lines and dominant-mode cavity basis functions on the patches. An analysis procedure is then developed in which the coupling coefficients between adjacent elements are used in a matrix equation which then determines the patch current amplitudes on all of the elements in the array. A synthesis procedure is then developed, in which the coupling coefficients are determined in order to produce a desired set of patch currents, which determines the radiation pattern. A four element linear array having a 45^{0} beam is built and tested, with the measured far-field pattern showing good agreement with the predicted pattern.

(8) Roger Kranenburg "Planar Transmission Line Excitation of Dielectric Resonator Antennas", M.S.E.E., University of Houston, November 1988.

An approximate theory is derived for all the modes in a cylindrical dielectric resonator antenna. The air-dielectric interface is approximated as a perfect magnetic conductor and expressions for the resonant frequency and radiation from the equivalent surface magnetic currents are presented. A broad beam with a maximum normal to the ground plane is obtained for the lowest mode. A more directive beam or a beam with a single sharp null is obtained for the next mode depending on the cylinder geometry. Good agreement is obtained between theory and experiment.

An experimental investigation was also undertaken demonstrating the microstrip transmission line and the coplanar waveguide as effective excitation mechanisms for the cylindrical dielectric resonator antenna. Results showing the coupling behavior and the radiation patterns for various cylinder aspect ratios, dielectric constants, and feed positions are presented. The results show these feed structures may result in efficient and practical antenna systems.

APPENDIX A

Electronic Letters, Vol. 21. no. 20, pp. 936-937, Sept. 26, 1985

DUAL-BAND MICROSTRIP ANTENNAS WITH MONOLITHIC REACTIVE LOADING

Indexing terms: Antennas, Microstrip

The design and experimental measurement of a dual-band, monolithic microstrip antenna is presented. The structure utilises a short-circuited length of microstrip transmission line to provide reactive loading and, thereby, retains the low-

Introduction: For a variety of applications in telecommunications it is often necessary to utilise two separate operating frequencies. Previous work[1,2] has shown that a single microstrip radiating element could be used in this fashion by employing reactive loading. A general theory has been formulated and preliminary experimental measurements have been made for radiators using a variable-length, short-circuited coaxial stub as the mechanism for the loading.[1] These investigations have demonstrated the general techniques involved and have verified the accuracy of the analysis in predicting the resonant frequencies of the structure.

The presence of the coaxial load which protrudes into the region behind the low-profile, printed-circuit antenna is usually not desirable in practical systems. For this reason alternative forms of loading which are monolithic in nature and thus retain the low-profile characteristics of the more usual single frequency microstrip antenna have been investigated. A set of antennas have been designed and tested which use microstrip transmission lines etched on the same printed-circuit board as the patch radiator for the reactive loading. Such a structure has been shown to display dual-band behaviour while retaining the usual, quite attractive physical characteristics of a microstrip radiator.

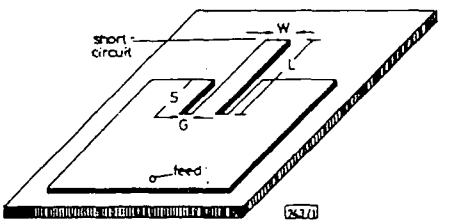

Fig. 1 *Geometry of monolithic design*

Design: To model most simply the previously investigated coaxially loaded antennas one can straightforwardly substitute a short-circuited microstrip line attached to the edge of a rectangular patch element. Use of a coaxial load was considerably more flexible, however, since the separation between resonances as well as the resonant frequencies themselves could also be adjusted by moving the load position away from the edge. To emulate this variation the microstrip line has also been designed with a specified 'inset' dimension S as shown in Fig. 1. Unfortunately, positioning the load in the interior of the patch results in yet another parameter G, the gap spacing between the line and the radiator. This parameter seems to have little effect on the upper resonance but tends to reduce the lower resonant frequency as the gap spacing is increased. The effect of the inset distance, however, is precisely the same as for the coaxial loads. As the inset is increased, the two resonant frequencies come closer together, thereby reducing the overall separation between resonances.

Results: Several antennas were fabricated with varying insets and gap spacings with stub lengths predicted by theoretical calculations to give dual-band behaviour. Two illustrative

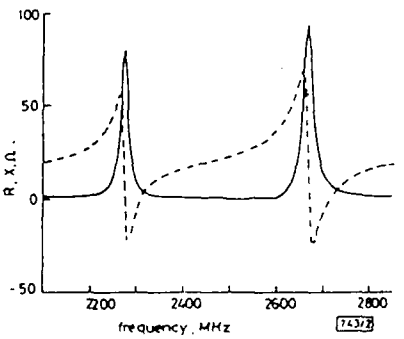

Fig. 2 *Impedance of edge-loaded, 4 × 6 cm patch antenna*

cases are presented. First an edge-loaded antenna consisting of a 6 cm by 4 cm patch with a short-circuited microstrip transmission line of length $L = 4{\cdot}0$ cm and width $W = 0{\cdot}33$ cm (inset: $S = 0$, $G = 0$), was measured. All antennas were etched on a dielectric substrate with a relative permittivity of 2·17 and a thickness of 0·079 cm and coaxially fed near the edge and at the centre of the 6 cm side. Good pattern performance was observed at each of the resonant frequencies (2·275 GHz and 2·666 GHz, respectively) with the overall impedance behaviour shown in Fig. 2.

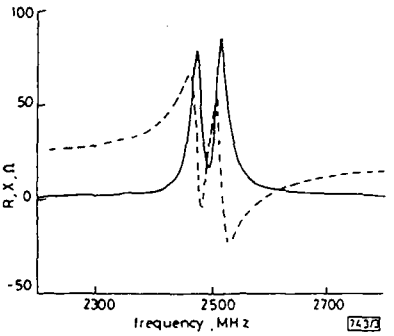

Fig. 3 *Impedance of inset-loaded, 4 × 6 cm patch antenna*
$L = 4{\cdot}0$ cm, $W = 0{\cdot}33$ cm, $G = 0{\cdot}3$ cm, $S = 1{\cdot}5$ cm

Secondly, a similar radiator with $L = 4{\cdot}0$ cm, $W = 0{\cdot}33$ cm and an inset of $S = 1{\cdot}5$ cm in from the edge with a gap spacing $G = 0{\cdot}3$ cm was investigated. Similar patterns were measured and the resulting impedance is shown in Fig. 3. The dual-band behaviour is still apparent, but the separation between resonances (2·471 GHz and 2·514 GHz) is seen to be greatly reduced.

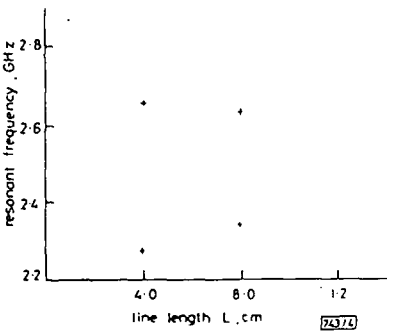

Fig. 4 *Resonant frequency against line length for edge-loading 4·0 × 6·0 cm patch*
$W = 0{\cdot}33$ cm, $S = 0$, $G = 0$

A complete listing of the measured upper and lower resonant frequencies for various dual-band radiators is shown in tabular form in Table 1 and graphically in Figs. 4 and 5. Fig. 4 shows the decrease in spacing between the two resonances as the length of the loading stub is increased for two otherwise identical edge-loaded patches (4·0 × 6·0 cm patch and $W = 0{\cdot}33$ cm). Fig. 5 illustrates the effect of changing the gap size for radiators with inset, $S = 1{\cdot}5$ cm, $L = 4{\cdot}0$ cm and $W = 0{\cdot}33$ cm. The upper resonance is seen to remain relatively stable but the lower one tends to decrease somewhat as the gap size is increased.

Table 1 RESONANT FREQUENCIES OF MONOLITHIC MICROSTRIP ELEMENTS

W	L	G	S	F	Γ
cm	cm	cm	cm	GHz	GHz
0·33	4·0	1·0	1·5	2·356	2·494
0·33	4·0	0	0	2·275	2·666
0·33	8·4	0	0	2·339	2·628
0·33	4·0	0·7	1·5	2·437	2·494

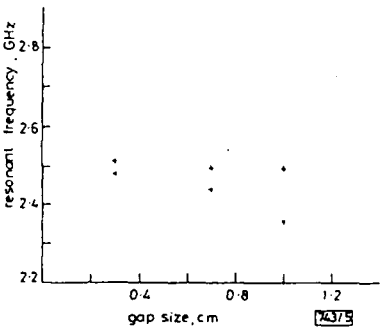

Fig. 5 *Resonant frequency against gap size*
4·0 × 6·0 cm patch, $W = 0{\cdot}33$ cm, $S = 1{\cdot}5$ cm, $L = 4{\cdot}0$ cm

Conclusions: The utilisation of reactive loading to produce dual-band behaviour in microstrip antennas has been implemented in a more practical manner by the use of monolithic microstrip transmission lines. This technique eliminates the more cumbersome coaxial stubs used in previous investigations.

Acknowledgment: This work was supported in part by the US Army Research Office through contract DAAG29-84-K-0166.

S. E. DAVIDSON
NASA/Johnson Space Center
Houston, Texas, USA

S. A. LONG
W. F. RICHARDS
Department of Electrical Engineering
University of Houston-University Park
Houston, TX 77004, USA

19th August 1985

References

1 RICHARDS, W. F., DAVIDSON, S. E., and LONG, S. A.: 'Dual band, reactively loaded microstrip antenna', *IEEE Trans.*, 1985, AP-33, pp. 556–561
2 KERR, J. L.: 'Microstrip antenna development'. Proceedings of Workshop on printed-circuit antenna technology, Las Cruces, NM, USA, 1979, pp. 3:1–3:20

APPENDIX B

An Experimental Investigation of Electrically Thick Rectangular Microstrip Antennas

ESIN CHANG, MEMBER, IEEE, STUART A. LONG, SENIOR MEMBER, IEEE, AND WILLIAM F. RICHARDS, MEMBER, IEEE

Abstract—**The electromagnetic properties of electrically thick rectangular microstrip antennas were investigated experimentally. Antennas were fabricated with different patch sizes and with electrical thicknesses ranging from 0.03 to 0.23 wavelengths in the dielectric substrate. The resonant frequencies were measured and compared to existing formulas. The bandwidth was calculated as a function of electrical thickness and the antenna radiation patterns were measured.**

I. Introduction

DURING THE PAST TEN YEARS, microstrip antennas experienced a great gain in popularity and have become a major research topic in both theoretical and applied electromagnetics. They are well known for their highly desirable physical characteristics such as low profile, light weight, low cost, ruggedness, and conformability. Numerous researchers have investigated their basic characteristics and recently extensive efforts have also been devoted to the design of "frequency agile," "polarization agile," or dual-band microstrip antennas [1], [2], [3]. Most of the previous theoretical and experimental work has been carried out only with electrically thin microstrip antennas. Recent interest has developed in radiators etched on electrically thick substrates. This interest is primarily due to two major reasons. First, as these antennas are used for applications with increasingly higher operating frequencies, and consequently shorter wavelengths, even antennas with physically thin substrates become thick when compared to a wavelength. Second, microstrip antennas have inherently narrow bandwidths and are normally not suitable for broad bandwidth applications. Increasing the bandwidth is possible, but the methods used [4], [5], [6] invariably increase the volume of the antenna by either extending the radiating surface or by increasing the overall antenna thickness. To aid in the design of broader band microstrip antennas, a careful experimental study of the resonant frequency, bandwidth, and radiation patterns of rectangular microstrip antennas as a function of electrical thickness of the substrate was undertaken. The measured resonant frequencies were compared to formulas previously developed for predicting the resonant frequency of electrically thin rectangular microstrip antennas.

Manuscript received October 4, 1985; revised December 23, 1985. This work was supported in part by the U.S. Army Research Office under Contract DAAG-29-84-K-0166.

E. Chang was with the Department of Electrical Engineering, University of Houston-University Park, Houston, TX. He is now with the Information Center, Shell Oil Company, P. O. Box 20329, Houston, TX 77025.

S. A. Long and W. F. Richards are with the Department of Electrical Engineering, University of Houston-University Park, Houston, TX 77004.

IEEE Log Number 8608073.

II. Experimental Procedures

The microstrip antennas investigated are rectangular patches with geometry as illustrated in Fig. 1. They are fabricated on 3M CuClad 233 and on Rogers RT/duroid 5870 microwave substrates. The CuClad material is made of a polytetrafluoroethylene (PTFE) woven glass laminate material while the RT/duroid material is made of a glass microfiber reinforced PTFE composite. Both substrates have a nominal dielectric constant (ϵ_r) of 2.33, and all the antennas are fed using an SMA coaxial feed. In this investigation the feed is located at the midpoint of the longer side ($x' = a/2$) and at a distance from the edge ($y' = 0.15$ cm). In each case the dimension "a" has been chosen to be approximately one and one-half times the dimension "b" with a 10 cm × 10 cm ground plane. Two sets of regular microstrip antennas have been fabricated. The ones in the first set have the same substrate thickness "h" but have nine different patch sizes; the ones in the second set have the same patch size but have three different substrate thicknesses. In addition a so-called "air-dielectric" model radiator has been fabricated to allow an even more detailed study of the resonant frequency. Its geometry models that of the regular rectangular microstrip antenna shown in Fig. 1 but with a substrate whose height can be changed by placing sheets of styrofoam ($\epsilon_r \approx 1.05$) with varying thicknesses between the ground plane and the radiating patch. The 1.78 cm × 2.67 cm aluminum radiating patch has a thickness of $t = 0.16$ cm and is coaxial fed over a 14 cm × 14 cm aluminum ground plane. This fixture allows the resonant frequency to be measured for a wide range of electrical thicknesses using exactly the same rectangular radiating patch.

The resonant frequency, impedance and radiation pattern measurements were all performed at the University of Houston-University Park, Applied Electromagnetics Laboratories, using an automated network analyzer system and dedicated computer programs. Accuracy enhancement techniques [7] have been used to partially correct for effective directivity, effective source match, and frequency tracking errors when taking impedance measurements. The radiation pattern measurements were taken with the antenna under test placed inside an anechoic chamber and mounted on a one meter diameter circular aluminum ground plane.

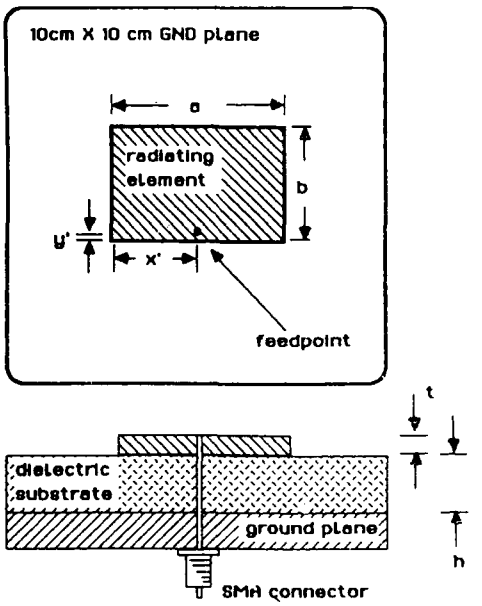

Fig. 1. Rectangular microstrip antenna geometry.

III. Experimental Results

A. Impedance

During the course of this research, the input impedances ($Z = R + jX$) and the radiation patterns of each of the antennas have been measured. Before the impedance data were used to determine the resonant frequencies (f_r) and the bandwidths (BW), they were smoothed in order to take out any residual ripples or oscillations that are due to reflections internal to the measurement equipment and have not been corrected by the accuracy enhancement routines. The values of admittance, $Y = G + jB$, as a function of frequency (f) were computed from the measured impedance versus frequency data through the relation $Y = Z^{-1}$. Depending on the values of admittance, either a cubic or quadratic least squares regression polynomial is fitted through the values of the admittance versus frequency curve. From this fitted polynomial, the smoothed admittance at each measured value of frequency is computed and then the reciprocal is taken to obtain the smoothed impedance. The actual smoothing operation is carried out with the admittance data since both the real and imaginary parts of the admittance are monotonic functions in the neighborhood of resonance and thus result in a better polynomial fit. The smoothed curves follow the general form of the measured traces very closely and allow the true peak of the resistance curve to be determined more accurately for resonant frequency measurements. Fig. 2 shows a comparison of typical smoothed and measured impedance versus frequency curves with data points taken every 10 MHz for an antenna with $h/\lambda_d = 0.110$.

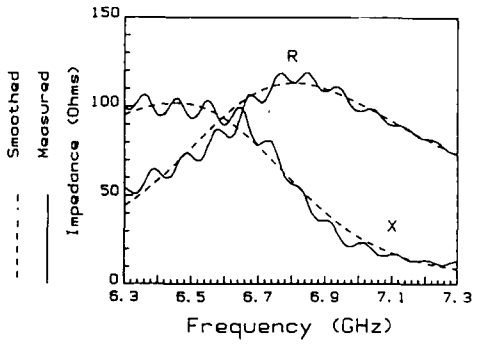

Fig. 2. Comparison of measured and smoothed impedance (1.1 cm x 1.7 cm radiating patch, 0.3175 cm substrate, $\epsilon_r = 2.33$).

B. Resonant Frequency

Generally, the resonant frequency of a microstrip antenna is defined as the frequency at which the reactance is equal to zero. For electrically thin antennas, this point is also very close to the frequency where the resistance reaches a maximum. However, in this investigation many of the reactance curves exhibit an inductive shift due to the coaxial feed passing through the electrically thick substrate [8], [9]. In fact, for the thicker antennas, the reactance curve never passes through zero at all (see Fig. 2). For this reason, the resonant frequency has been redefined as the point at which the resistance reaches a maximum, independent of the value of reactance. Furthermore, since the bandwidth of an electrically thin microstrip antenna is commonly defined in terms of the impedance (and thus is dependent on the reactance), an alternate definition of bandwidth that is not affected by the inductive shift of the reactance is used to obtain the antenna bandwidths of this paper. This last point will be discussed in detail in a later section.

Since the main concern in the measurement of the resonant frequency is the effect of the changing electrical thickness of the substrate, a normalized resonant frequency is defined where $f_{norm} = f_r/f_{r0}$, and f_{r0} is the zeroth-order prediction of the resonant frequency. This approximation for f_{r0} assumes that the antenna thickness is infinitesimally thin and that b is equal to $\lambda_d/2$. Then knowing that $\lambda_d = c/(f_{r0}\sqrt{\epsilon_r}) = 2b$, f_{r0} can be computed. For the units of c in m/s and those of b in cm,

$$f_{r0} = 15/(b\sqrt{\epsilon_r}) \text{ GHz}. \quad (1)$$

Table I shows the measured resonant frequency, zeroth order prediction, physical dimensions, and electrical thickness of each antenna. Fig. 3 shows a plot of the normalized resonant frequency plotted as a function of electrical thickness for the nine antennas etched on the same thickness of substrate and for the three identically sized antennas on different substrate thicknesses.

Table II shows the measured resonant frequencies and the

TABLE I
MEASURED AND PREDICTED ANTENNA RESONANT FREQUENCIES

a (cm)	b (cm)	h (cm)	Meas'd (GHz)	James (GHz)	Hammerstad (GHz)	h/λ_d
5.7	3.8	0.3175	2.31	2.30	2.38	0.037
4.55	3.05	0.3175	2.89	2.79	2.90	0.047
2.95	1.95	0.3175	4.24	4.11	4.34	0.068
1.95	1.3	0.3175	5.84	5.70	6.12	0.094
1.7	1.1	0.3175	6.80	6.47	7.01	0.110*
1.4	0.9	0.3175	7.70	7.46	8.19	0.125
1.2	0.8	0.3175	8.27	8.13	9.01	0.141
1.05	0.7	0.3175	9.14	8.89	9.97	0.148
0.9	0.6	0.3175	10.25	9.02	11.18	0.166
1.7	1.1	0.1524	7.87	7.46	7.84	0.061
1.7	1.1	0.3175	6.80	6.47	7.01	0.110*
1.7	1.1	0.9525	4.73	4.32	5.27	0.229

*These two are the same antennas.

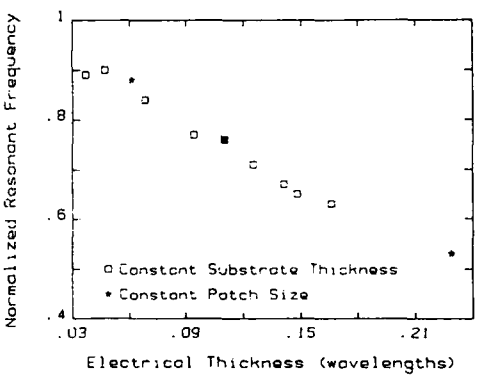

Fig. 3. Normalized antenna resonant frequency versus electrical thickness.

TABLE II
RESONANT FREQUENCY VERSUS h FOR AIR-DIELECTRIC FIXTURE (1.78 cm × 2.67 cm RADIATING PATCH)

h (cm)	Meas'd (GHz)	James (GHz)	Hammerstad (GHz)	h/λ_d
0.64	5.14	4.54	5.75	0.112
0.79	5.12	4.18	5.42	0.138
0.99	4.33	3.78	5.07	0.146
1.19	4.27	3.46	4.77	0.174
1.44	3.32	3.13	4.46	0.163
1.64	3.06	2.91	4.25	0.171
2.04	2.56	2.55	3.91	0.178
2.34	2.29	2.34	3.70	0.193

corresponding electrical thicknesses of the air dielectric fixture, while the circles in Fig. 4 represent the same data in graphical form. It is evident from Figs. 3 and 4 that the resonant frequency indeed decreases as the antennas become electrically thicker as has been shown in previously published results [10], [11]. It is perhaps unexpected, however, that this trend continues even to thicknesses approaching one quarter wavelength.

C. Bandwidth

The percent bandwidth of the antennas was determined from the impedance data. For ease of notation the term bandwidth refers to percent bandwidth unless otherwise specified. Bandwidth is normally defined as

$$\text{percent BW} = [(f_{r2} - f_{r1})/f_r]\ 100 \text{ percent} \qquad (2)$$

where f_r is the resonant frequency, while f_{r2} and f_{r1} are the frequencies between which the magnitude of the reflection coefficient of the antenna is less than or equal to 1/3 (which corresponds to a voltage standing-wave ratio (VSWR) ≤ 2.0). However, this definition is found not to be directly applicable

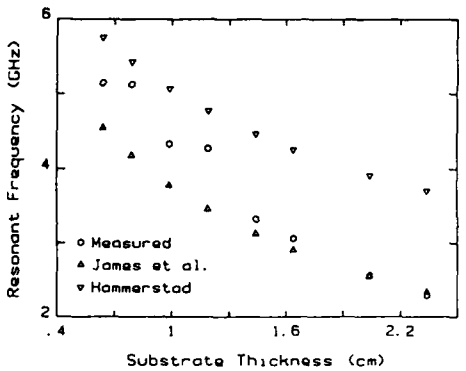

Fig. 4. Air-dielectric fixture resonant frequencies versus substrate thickness (1.78 cm × 2.67 cm radiating patch, $\epsilon_r \approx 1.05$).

to the experimental data because of the inductive shift. Thus, an alternate definition is found in order to determine the bandwidth of the test antennas.

The case where the impedance at resonance is purely resistive ($Z_{res} = R_{max}$) may be represented by a parallel RLC circuit, and an analytical expression for the input impedance in terms of the antenna Q-factor, R_{max} and f_r may be written as

$$Z(f) = \frac{\frac{1}{R_{max}} + j\left[\frac{Qf_r}{R_{max}f_r} - \frac{fQ}{R_{max}f_r}\right]}{\frac{1}{R_{max}^2} + \left[\frac{Qf}{R_{max}f_r} - \frac{Qf_r}{R_{max}f_r}\right]^2}. \quad (3)$$

Using (3), it was found that R and the magnitude of Z had a definite relationship to R_{max} that is independent of the other parameters. Namely,

$$|Z(f_{r1})| = |Z(f_{r2})| = 0.818R_{max}, \quad (4)$$

and

$$R(f_{r1}) = R(f_{r2}) = 0.670R_{max}. \quad (5)$$

For the special case of a prescribed VSWR = 2.0, this method is equivalent to the previously derived analytical expression [12]

$$\mathrm{BW} = (\mathrm{VSWR} - 1)/(Q\sqrt{\mathrm{VSWR}}). \quad (6)$$

For electrically thick radiators with the associated large inductive shift in the impedance, the VSWR may not be below 2.0 for any range of frequencies. Using only the resistance data a projected bandwidth can be calculated, however, following this resonant circuit model by locating the frequencies where the resistance is equal to 0.670 times the value of R_{max}. Table III shows the bandwidths so obtained arranged in order of increasing electrical thickness along with the corresponding f_{r1} and f_{r2}, while Fig. 5 shows the same bandwidth data in graphical form. It is seen that values of bandwidth on the order of 20 percent may be achieved using electrically thick antennas.

It should be noted, however, that no attempt has been made in this investigation to actually match the antennas to a standard 50 Ω transmission line by a technique such as moving the feed point away from the edge. Thus the bandwidths reported in Table III and Fig. 5 are, in effect, projected ones that might be obtainable under the more usual definition of bandwidth. These values are most useful for comparison purposes to characterize the dependence of the bandwidth on the various antenna parameters.

D. Radiation Pattern

The radiation pattern for each element was measured at its resonant frequency in both the E-plane and the H-plane. The experimental results show that the radiation patterns of electrically thick antennas are very similar to those of electrically thin antennas. The H-plane patterns remain virtually unchanged while the E-plane ones begin to show some asymmetries only for the larger substrate thicknesses. Fig. 6 shows the radiation patterns of a representative thicker antenna ($h/\lambda_d = 0.110$, taken at 6.8 GHz in 0.5° steps) and it is typical of the remaining antennas.

IV. Comparison of Measured and Predicted Resonant Frequencies

The measured resonant frequencies can be compared to the predicted resonant frequencies as a mutual check of the experimental data and of the validity of the theories. The equations for the resonant frequency proposed by Hammerstad [13] and by James, Hall, and Wood [11] are used for these comparisons. Both methods share the concept of an effective dielectric constant (ϵ_{eff}) given by [14]

$$\epsilon_{eff}(w) = \frac{(\epsilon_r + 1)}{2} + \frac{(\epsilon_r - 1)(1 + 10h/w)^{-1/2}}{2} \quad (7)$$

where w is a variable and can be either the patch dimension "a" or "b." Hammerstad gives a predicted

$$f_r = \frac{c}{2(b + 2\Delta b)\sqrt{\epsilon_r}}, \quad (8)$$

$$\Delta b = \frac{0.412h(\epsilon_{eff}(a) + 0.3)(a/h + 0.264)}{(\epsilon_{eff}(a) - 0.258)(a/h + 0.8)}. \quad (9)$$

James *et al.* give a predicted

$$f_r = \frac{f_{r0}\epsilon_r}{\sqrt{\epsilon_{eff}(a)\epsilon_{eff}(b)}(1 + \delta)}, \quad (10)$$

where

$$\delta = (h/b)0.882 + \left[\frac{0.164(\epsilon_r - 1)}{\epsilon_r^2}\right] + \left[\frac{(\epsilon_r + 1)[0.758 + \ln(b/h + 1.88)]}{\pi\epsilon_r}\right]. \quad (11)$$

The predicted resonant frequencies obtained using these two methods are shown in Tables I and II for the test antennas and for the air-dielectric fixture.

TABLE III
PROJECTED VALUES OF BANDWIDTH AND CORRESPONDING F_{r1} AND F_{r2}

h/λ_d	f_{r1} (GHz)	f_{r2} (GHz)	BW (%)
0.037	2.280	2.352	3.117
0.047	2.834	2.952	4.083
0.061	7.632	8.152	6.607
0.068	4.120	4.396	6.509
0.094	5.632	6.140	8.699
0.110	6.494	7.272	11.441
0.125	7.314	8.468	14.987
0.141	7.848	9.024	14.220
0.148	8.380	10.560	23.850
0.166	9.442	11.560	20.660
0.229	4.320	5.180	18.180

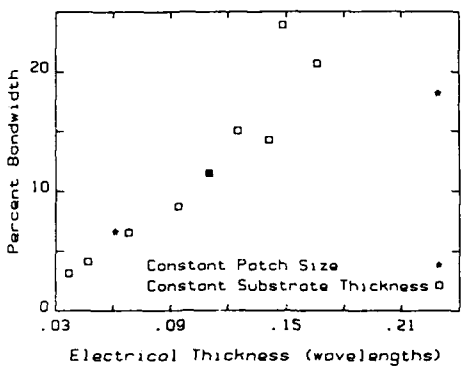

Fig. 5. Projected antenna bandwidth versus electrical thickness.

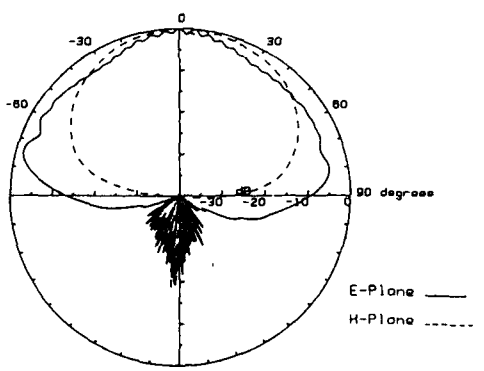

Fig. 6. Antenna radiation pattern (1.1 cm × 1.7 cm radiating patch, 0.3175 cm substrate, ϵ_r = 2.33).

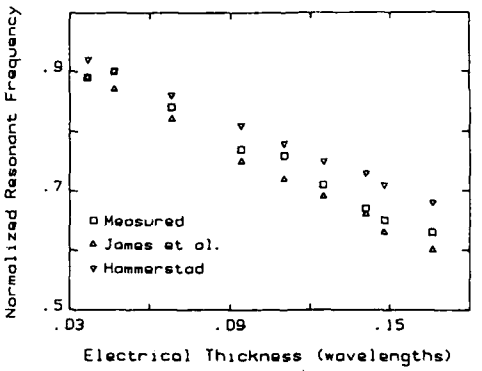

Fig. 7. Comparison of normalized antenna resonant frequencies versus electrical thickness (h = 0.3175 cm, ϵ_r = 2.33).

The predicted resonant frequencies are normalized to the zeroth order predictions and are compared to the measured, normalized resonant frequencies. Fig. 7 shows this comparison for the nine different patches on the substrates with identical physical thickness, while Fig. 4 shows the predicted values of resonant frequency for the air-dielectric fixture compared to the actual measured values. It should be noted that the theoretical data in Fig. 7 are presented as discrete points rather than a continuous curve so that the theory can correspond to the exact cases of the experimental cases, some of which have slightly varying values of a/b ratio and of dielectric constant. This use of individual points causes the data to no longer be aligned along smooth curves. In both cases it is clear that the theories follow the trend of the experimental data quite well even for electrically thick substrates. In fact, based on the information presented here and on additional research data [15], some general observations may be made concerning these two methods. Both predict the resonant frequency very closely for electrically thin rectangular microstrip antennas, but as h becomes greater than $0.1\ \lambda_d$, James *et al.* give consistently better predictions than the method by Hammerstad. Specifically, James *et al.* usually predict values approximately 4 percent lower than the measured resonant frequency while Hammerstad predicts values around 8 percent higher than the measured resonant frequency. It should be noted, however, that these two theories are not intended for use with electrically thick substrates. For $h \leqslant 0.1\ \lambda_d$, the measured resonant frequency is very nearly the mean of the predicted resonant frequencies from the two different formulas. A third algebraic formula for the resonant frequency has been proposed by Sengupta [16], but as the author states, it only applies to electrically thin structures and does not predict the proper behavior for the thicker substrates measured in this investigation.

V. Conclusion

The effect of varying the electrical thickness for rectangular microstrip antennas has been investigated experimentally during the course of this research. In addition, an air-dielectric model radiator has been fabricated with a single patch size and

a variable substrate thickness. The resonant frequency, bandwidth, and radiation pattern have been measured over a range of substrate thickness from 0.03 to 0.23 of a wavelength in the dielectric.

The resonant frequency of a rectangular microstrip antenna was found to decrease as a function of electrical thickness. The validity of this finding is confirmed by previously published results and by the existing theories of Hammerstad and of James *et al.* The predicted resonant frequencies are all very close to the measured resonant frequency for electrically thin substrates. As the electrical thickness is increased, the theories due to Hammerstad and to James *et al.* generally predict values that are approximately 8 percent high and 4 percent low respectively when compared to the actual values. The impedance of the thicker antennas is characterized by an inductive shift in the reactance away from zero at resonance.

The projected bandwidth of the unmatched antennas was calculated to determine the effect of substrate thickness on this characteristic as well. The resulting data show that bandwidths as high as 20 percent could be achieved by simply using electrically thick substrates. Finally, the radiation patterns of electrically thick antennas were seen to be very similar to those of the more usual thin ones. Overall it has been shown that electrically thick rectangular microstrip antennas retain most of the desirable electrical characteristics of thinner ones and may be utilized for broad-band applications assuming a reactive network is used for impedance matching.

References

[1] D. H. Schaubert, F. G. Farrar, A. R. Sindoris and S. T. Hayes, "Microstrip antennas with frequency agility and polarization diversity," *IEEE Trans. Antennas Propagat.*, vol. AP-29, pp. 118–123, 1981.

[2] S. A. Long and M. D. Walton, "A dual-frequency stacked circular-disk antenna," *IEEE Trans. Antennas Propagat.*, vol. AP-27, pp. 270–273, 1979.

[3] W. F. Richards, S. E. Davidson, and S. A. Long, "Dual-band reactively loaded microstrip antenna," *IEEE Trans. Antennas Propagat.*, vol. AP-33, pp. 556–561, 1985.

[4] A. Sabban, "A new broadband stacked two-layer microstrip antenna," in *IEEE Antenna Propagat. Soc. Int. Symp. Digest*, 1983 pp. 63–66.

[5] K. F. Lee, K. Y. Ho, and J. S. Dahele, "Circular-disk microstrip antenna with an air gap," *IEEE Trans. Antennas Propagat.*, vol. AP-32, pp. 80–884, 1984.

[6] G. Kumar and K. C. Gupta, "Broadband microstrip antennas using coupled resonators," in *IEEE Antennas Propagat. Soc. Int. Symp. Dig.*, 1983, pp. 67–70.

[7] Hewlett Packard Appl. Note AP-221A, pp. 5–8, June 1980.

[8] W. F. Richards, J. R. Zinecker, R. D. Clark and S. A. Long, "Experimental and theoretical investigation of the inductance associated with a microstrip antenna feed," *Electromagn.*, vol. 3, pp. 327–346, 1983.

[9] D. M. Pozar, "Considerations for millimeter wave printed antennas," *IEEE Trans. Antennas Propagat.*, vol. AP-31, pp. 740–747, 1983.

[10] K. R. Carver and J. W. Mink, "Microstrip antenna technology," *IEEE Trans. Antennas Propagat.*, vol. AP-29, pp. 2–24, 1981.

[11] J. R. James, P. S. Hall, and C. Wood, *Microstrip Antennas-Theory and Design*. Stevenage, U.K.: Peter Peregrinus Ltd., 1981.

[12] A. G. Derneryd, "The circular microstrip antenna element," in *Proc. Inst. Elec. Eng. Int. Conf. Antennas Propagat.*, Oct. 1978, pp. 307–310.

[13] E. O. Hammerstad, "Equations for microstrip circuit design," in *Proc. 5th European Micro. Conf.*, Hamburg, Sept. 1975, pp. 268–272.

[14] M. V. Schneider, "Microstrip dispersion," *Proc. IEEE*, pp. 144–146, Jan. 1972.

[15] E. Chang, "An experimental study of electrically thick rectangular microstrip antennas," M.S. thesis, Dept. Elec. Eng., Univ. Houston, University Park, 1985.

[16] D. L. Sengupta, "Approximate expressions for the resonant frequency of a rectangular patch antenna," *Electron. Lett.*, pp. 834–835, July 29, 1983.

Esin Chang (S'84–M'85) was born on September 20, 1963. He received the B.S. (magna cum laude) and M.S. degrees in electrical engineering from the University of Houston-University Park, Houston, TX, in 1984 and 1985, respectively.

He was employed by Schlumberger Well Services in Houston, TX and was involved in the engineering support of electromagnetic propagation tools. He also worked as a Graduate Research and Teaching Assistant at the University of Houston in the area of applied electromagnetics while completing the M.S. degree. He is currently employed as an Engineer with Shell Oil Company in communications in Houston, TX. His primary interests are in microstrip antenna technology, high speed telecommunications, and digital telephony.

Mr. Chang is a member of Eta Kappa Nu, the Texas Society of Professional Engineers, and M.A.E.S.

Stuart A. Long (S'65–S'72–M'74–SM'80), for a photograph and biography please see page 561 of the May 1985 issue of this TRANSACTIONS.

William F. Richards (S'69–M'70–M'80), for a photograph and biography please see page 561 of the May 1985 issue of this TRANSACTIONS.

IEEE Antennas and Propagation Society Newsletter, October 1986

Feature Article

Reactively Loaded Microstrip Antennas

William F. Richards
Stuart A. Long

Department of Electrical Engineering
University of Houston - University Park
Houston, Texas 77004

1 Introduction

Microstrip elements have proven to be very versatile and have found uses in a variety of applications from satellite arrays to automobile anti-collision warning systems. This versatility stems mainly from their structural simplicity, ease of construction, ruggedness, conformability, low profile, and low cost. In addition to these features, microstrip elements are capable of producing a variety of different patterns and polarizations [1], [2], [3], [4], [5], [6], [7], [8]. Most research efforts, however, have been limited to basic applications using only a single, unperturbed mode of a rectangular or circular element. Additional applications are possible through the use of reactive loading. These include multiband, frequency-agile and polarization-diverse, adaptable-impedance, and multimode-pattern antennas. Some experimental work has been done in these areas [2], [3], [4], but very little theoretical work with the exception of [3], [5], [7], [8], [9], [10] has been done. In this paper, a very simple theory is presented which will guide a designer who wishes to take advantage of the added flexibility that reactive loading provides. In addition, several applications are discussed with corresponding theoretical and experimental results.

2 Theory

A simple theory that makes use of a graphical interpretation of the characteristic equation for the resonant frequency of a loaded microstrip element is presented in this section. By a "reactively loaded element" we mean a simple microstrip antenna to which one or more, two-terminal lumped, lossless, linear load impedances are attached—one terminal to the patch and the other to the ground plane. Also included in the set of reactive loads are sections of transmission lines attached at one or more points on the patch. The simplest form of the theory results when the original, unloaded antenna has one of the separable shapes which fall into four classes: rectangular, circular, elliptical, and parabolic. In this paper, we will deal only with rectangular elements.

Foundation—the cavity model— The foundation upon which the theory is built is the so-called cavity model [11] as modified in [12]. This model is best suited for understanding loaded elements because it can reconstruct the localized field in the vicinity of the loads, yet it is simple enough that basic physical principles useful in design can be developed and is also surprisingly accurate. It is based on two observations.

1. The real part of the resonant frequency of a microstrip antenna is approximately the same as that of a cavity formed by introducing a magnetic conductor between the patch edge and the ground plane.
2. The quality factor of the microstrip element can be determined with good accuracy using the resonant *cavity field* rather than the exact *antenna field*. Once the quality factor Q is determined, an artificially lossy dielectric with a loss tangent equal to the reciprocal of Q can be imagined to be filling the cavity. The field within such a cavity approximates the field between the patch and ground plane of the original antenna.

Thus, the most fundamental step in determining the properties of a loaded antenna is to determine the resonant frequency and mode distribution within the corresponding loaded *cavity*.

If the reactive load is imagined as being contained within a small cylinder extending between the ground plane and the patch, then Huygen's principle can be used to replace the load by equivalent magnetic and electric surface currents impressed in a now *empty* cavity. Since microstrip elements are thin, the magnetic surface current is primarily a horizontal circulating loop of current and the electric surface current is vertically directed. By making suitable transformations [13], one can approximate the field due to the magnetic current as a constant times the field produced by the electric current acting alone [10]. The effect of the equivalent magnetic current is usually negligible anyway and thus the effect of the load can be accounted for by impressing an equivalent electric current on the surface of the small cylinder enclosing the load in an *empty* cavity. The total equivalent current is just the total load current I_L.

Characteristic equation for the resonant frequency— There are *two* expressions for the load voltage that one can write which when equated, yield the characteristic equation for the resonant frequency of the loaded cavity. One expression is that the load voltage V_L is the driving-point impedance of the *empty* cavity jX_{11} times the load current I_L, where X_{11} is the driving-point reactance. The second expression is the defining relationship for the load itself,

$$V_L = -jX_L I_L,$$

where X_L is the load reactance. Combining these two equations yields the characteristic equation,

$$X_L + X_{11} = 0.$$

A very useful graphical interpretation of this characteristic equation can be obtained if the microstrip cavity is modeled as seen from the load terminal pair as illustrated in Fig. 1. The resonant circuit shown in the figure represents the contribution to the driving-point impedance from the resonant mode of the empty cavity whose resonant frequency is nearest that of the corresponding loaded cavity mode of interest. The reactive contribution due to all other modes of the empty cavity in the Foster expansion of the driving-point impedance is what we call the "feed reactance," X_f. We have de-

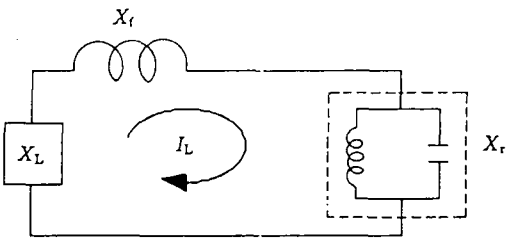

Figure 1. Circuit model for the input impedance of a microstrip cavity.

picted this as a simple inductive reactance although it does not really correspond to a single inductor. In most cases, particularly cases in which degenerate- or nearly degenerate-mode pairs of the empty cavity do not exist, the feed reactance is indeed positive and slowly varying over the band of both the loaded-cavity and empty-cavity modes of interest. Regardless of how it is depicted, it is computed using the full modal analysis of the cavity and as such, it is precise. Using this model, the characteristic equation becomes

$$-(X_L + X_f) = X_r. \tag{1}$$

An even simpler way to obtain this characteristic equation is to apply Kirchoff's voltage law to the circuit illustrated in Fig. 1 with the load reactance attached. Since a resonant mode of the loaded element is a source-free mode, the sum of the voltage drops around the loop must vanish implying that

$$(X_L + X_f + X_r)I_L = 0.$$

This yields the characteristic equation (1) since I_L must not be zero.

In order to develop important design concepts, it is useful to solve equation (1) graphically. Such a graphical solution is illustrated in Fig. 2(a). The simple case a short-circuit load $X_L = 0$ is considered first. The intersection of the dashed line in Fig. 2, representing $-X_f$ alone, with the solid line representing X_r marks the resonant frequency of the loaded cavity.

Several design principles emerge from this figure, particularly in reference to the rectangular element illustrated in Fig. 3.

1. It is immediately clear that the introduction of a short circuit will increase the resonant frequency of the cavity.

2. The resonant reactance corresponding say to the $m = 0$, $n = 1$ mode of the rectangular element (the mode most commonly used) is

$$X_r = -j\mu t \frac{2c^2}{ab}\omega \frac{\cos^2(\pi y/b)}{\omega^2 - c^2k_{01}^2}, \tag{2}$$

where the patch dimensions are $a \times b \times t$, c is the speed of light in the cavity dielectric, $k_{01} = \pi/b$ is the resonant wavenumber of the $(0,1)$-mode, and y is the y coordinate of the load position. When y approaches either edge, $y = 0$ or $y = b$, the resonant reactance given in equation (2) becomes stationary. As $y \rightarrow b/2$, the resonant reactance approaches zero. In graphical terms, the reactance curve begins as a very slender departure from zero for load points near $y = b/2$ and then fattens out as y moves away from the centerline. For load points near the edge, the X_r curve changes little. This trend is illustrated in Fig. 2(b) by the sequence of three X_r curves labeled 1–3 corresponding to feed points 1–3.

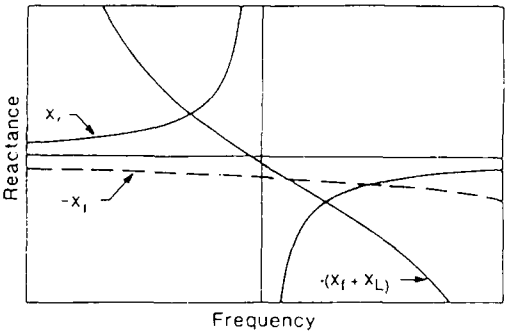

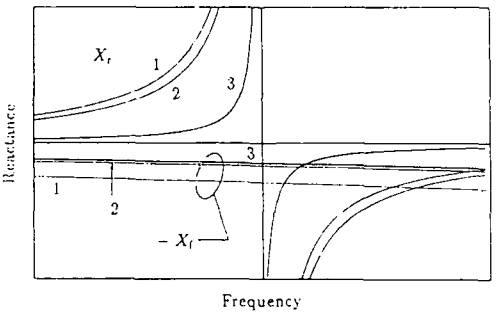

Figure 2. (a) Plot of X_r, $-(X_f + X_L)$ versus frequency; (b) Plot of X_r, $-X_f$ for three different feed locations.

This observation illustrates how load placement affects the resonant frequency. A short placed near the centerline changes the resonant frequency little. As the load is moved away from the centerline in either direction toward an edge the resonant frequency increases rapidly at first and then more slowly as the load point nears the edge.

This graphical interpretation, which will be found very useful in later applications, is consistent with the observation that the load will have more effect on the resonant frequency when placed where the empty-cavity field is strongest and no effect where the cavity field is zero.

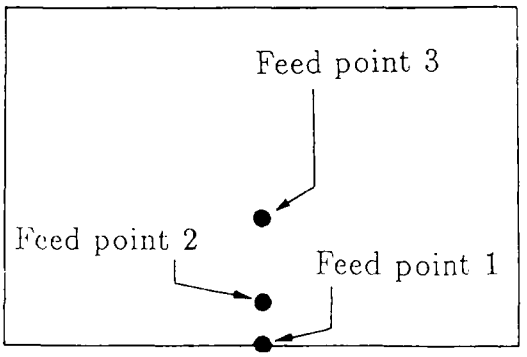

Figure 3. Rectangular element with three different load locations.

3. The preceding observation about the dependency of resonant frequency on load position made the tacit assumption that the feed reactance is independent of of feed position. Nothing could be further from the truth. In fact, the feed reactance can vary by a factor of three or more as the feed point is moved from place to place on the patch [13]. The feed reactance typically increases as the feed point is moved near an edge. The increase is rapid when the feed point is very near the edge. This feed reactance is predicted fairly well by the cavity model, particularly for thinner elements, except for feed points right on the edge. There, the cavity model substantially overestimates the feed reactance because the equivalent electric currents on the magnetic wall that would make the cavity model precise have been neglected. These equivalent currents tend to oppose the impressed source current (in this application, the load current) and ignoring them results in an increased inductive reactance.

   The effect of this variation is that as the load point moves toward the edge, the $-X_f$ curve moves downward. This is illustrated by the sequence of three curves in Fig. 2(b). Thus, it is expected that the resonant frequency should begin at the resonant frequency of the empty cavity when y is on the centerline, it should increase rapidly at first due to a widening X_r curve, and finally decrease somewhat due to a rapidly increasing feed reactance for load points near the edge. This is, in fact, exactly what is observed by measurements.

Determination of feed reactance— In order to graph the $-X_f$ curve, the input reactance of a microstrip cavity must be computed. This can be obtained by using the Green's function,

$$G(r|r') = j\omega\mu \sum_A \frac{\psi_{mn}(r)\psi_{mn}(r')}{k^2 - k_{mn}^2},$$

where A is the set of all pairs of non-negative integers, (m,n), and $\psi_{mn}(r)$ is the mn^{th} mode of the cavity satisfying

$$\nabla^2\psi_{mn}(r) = -k_{mn}^2\psi_{mn}(r), \quad r \in S,$$

$$\nabla\psi_{mn}(r)\cdot\hat{n} = 0, \quad r \in \partial S.$$

The source and observation position vectors are $r = x\hat{x} + y\hat{y}$ and $r' = x'\hat{x} + y'\hat{y}$, S is the set of points making up the patch, ∂S is the set of points on the patch edge, and $\hat{n}$ is the outward-pointing unit normal to the patch edge. In the case of rectangular elements,

$$\psi_{mn}(r) = \frac{2}{\sqrt{(1+\delta_{m0})(1+\delta_{n0})ab}} \cos\left(\frac{m\pi x}{a}\right)\cos\left(\frac{n\pi y}{b}\right).$$

The series for $G(r|r')$ diverges as $r \to r'$. This is because the inductive reactance associated with a filament is infinite. In order to obtain the input reactance associated with the *actual* load current, one must integrate this Green's function over the load current distribution. It is assumed that the load current is distributed uniformly on a circular cylinder of diameter d. The "location" of the load is the center of the cylinder's cross section. The required integration needs to be computed efficiently since the nonlinear characteristic equation for the resonant frequency must be solved numerically, or enough points plotted to solve it graphically. A very efficient SEM expansion of the cavity field with a quasistatic correction has been developed [10], the details of which are too lengthy for presentation here. Once the integration has been carried out, the result, when multiplied by $-jt$ yields the total reactance X_{tl} at the load point from which the resonant reactance can be subtracted leaving X_f.

Determination of the modal distribution— Once the resonant frequency is determined, the task turns to computing the modal distribution of the loaded cavity. For the case of a single load, the unnormalized mode function $\Psi(r)$ of the *loaded cavity* in terms of the modes of the *empty cavity* is

$$\Psi(r) = j\omega\mu \sum_A \frac{\psi_{mn}(r)\psi_{mn}(r_1)}{k^2 - k_{mn}^2}, \tag{3}$$

where k is the resonant wavenumber of the resonant mode of the loaded cavity and r_1 is the position vector for locating the center of the load. No integration is used in this expression since it is not used to compute the field in the region of the source (i.e., load) current. The evaluation of this series is also facilitated by the use of an SEM expansion with a quasistatic correction.

It is apparent from equation (3) that the closer that the resonant wavenumber k is to a given k_{mn} associated with a particular mode of the empty cavity, the closer the loaded-cavity mode will resemble the $\psi_{mn}(r)$ empty-cavity mode. More will be said about this for specific applications discussed in the next section.

Quality factor, pattern, and impedance— Once the modal distribution has been obtained, the pattern can be approximated as the field due to a filamentary magnetic loop of current coinciding with the edge of the patch. The current at a given point r on the loop is $\Psi(r)$ and is impressed over a grounded dielectric slab with the patch removed. Once the pattern is obtained, the power radiated in the space and surface waves can be computed. The average energy stored in the electric field is computed using

$$\omega W_e = \frac{1}{2}t\epsilon_r\mu_r^2 k_0^3\eta_0 \sum_A \frac{\psi_{mn}^2(r_1)}{(k^2 - k_{mn}^2)^2} + \omega W_L,$$

Where W_L is the average electric energy stored by the load. From the radiated power P_r and the stored electric energy W_e, the radiative quality factor

$$Q_r = \frac{4\pi f_0 W_e}{P_r}$$

is computed where f_0 is the resonant frequency of the loaded antenna. In addition to the radiative quality factor, the quality factors associated with the power consumed in heating the dielectric and metal cladding are $Q_d = 1/\delta$ and $Q_m = t/\Delta$, where δ is the *actual* loss tangent of antenna dielectric, and Δ is the skin depth in the metal cladding. From these quality factors, the quality factor of the antenna is determined using

$$Q = \left(\frac{1}{Q_r} + \frac{1}{Q_d} + \frac{1}{Q_m}\right)^{-1}.$$

To compute the input impedance (at least for the case of loaded elements in which only one resonant mode contributes significantly in the band of interest), one can use the circuit model illustrated in Fig. 4. The admittance of the resonant circuit is

$$Y_r = G\left[1 + jQ\left(\left(\frac{f}{f_0}\right)^2 - 1\right)\right].$$

The conductance G can be determined by using the relation

$$|V_t|^2 G = P,$$

where voltage V_t across the resonant circuit is

$$V_t = -t\Psi(r_f),$$

r_f being the location of the feed of the loaded element. The power P is the total power absorbed by the antenna element corresponding

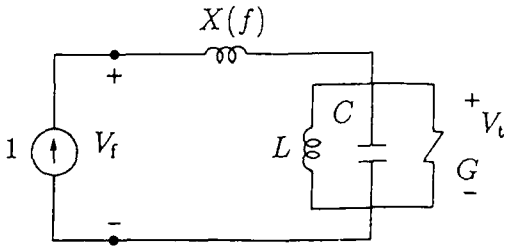

Figure 4. Circuit model of the loaded microstrip antenna.

the resonant mode $\Psi(r)$ computed earlier to determine the antenna quality factor. Note that V_t is *not* the feed voltage since $\Psi(r_f)$ does not include the effect of the feed reactance. (The feed reactance of the *empty* cavity at the load point, of course, *does* affect the V_t. The feed reactance referred to here is the feed reactance at the actual feed point of the *loaded* cavity).

The feed reactance can be modeled as

$$X_f = X_{f0} + (f - f_0)X_{f1}.$$

Let

$$f_+ = \left(1 + \frac{1}{2Q}\right) f_0, \quad f_- = \left(1 - \frac{1}{2Q}\right) f_0.$$

The coefficients X_{f0} and X_{f1} can be approximated as

$$X_{f0} \approx \frac{1}{2}(X(f_+) + X(f_-)) + \frac{R}{4Q},$$

and

$$X_{f1} \approx \frac{Q}{f_0}[X(f_+) - X(f_-) + 2R],$$

where $R = 1/G$. What remains is to determine the input reactance of the ideal cavity at the upper and lower frequencies f_+ and f_-.

To do this, one simply views the input reactance at the feed port as the input reactance of a loaded two-port network. The z parameters of the two-port network are the z parameters of the *empty* cavity with port 2 located at the feed and port 1 located at the load. The mutual reactance between the ports with respective position vectors r_1 and r_2 is just

$$X_{12} = j\omega G(r_1|r_2).$$

The input reactance is then

$$X = X_{22} - \frac{X_{12}^2}{X_{11} + X_L},$$

where X_{22} is the input reactance of the empty cavity at r_2 and is computed in the same way as X_{11}.

Extension to multiple loads— All of the preceding was geared to a *single* load. This was done, initially, because very useful design principles could be developed. Although the nice graphical interpretation of the characteristic equation will be lost, the results can be easily modified to accommodate the case of multiple loads [10]. This extension is most valuable in a number of applications since symmetric pairs of loads can then be used to suppress large cross-polarized fields that would otherwise be generated by a single load.

3 Applications

A number of applications of loaded microstrip antennas are discussed in this section. Many were discovered by purely experimental investigations, but all benefit from the simple design principles and the theory developed in the preceding section.

Frequency-agile antennas— One of the first applications recognized [3] was that one could change the resonant frequency of microstrip antennas by shorting the patch at one or more locations. What is just as important is that one could vary the resonant frequency over a wide range *without significantly changing the radiation pattern or input impedance*. This means that these elements could be loaded with PIN diodes at a number of points and the center frequency could be varied over a wide range by simply biasing different diodes on or off.

The computed voltage distribution of the loaded mode around the edge of the patch for a mode shorted at a single point is illustrated in Fig. 5. The voltage distribution at first appears to be severely perturbed from that of the (0, 1) mode of the corresponding unloaded antenna. A closer look, however, will show that voltage distribution of the loaded antenna can be thought of as that of the unloaded element plus an oscillating magnetic current which has little effect on the radiation pattern. Thus, much the character of what might be termed the "parent" mode—the unloaded antenna mode from which the loaded mode was adapted—is carried over to the loaded antenna mode. The predicted results are consistent with experimental data as shown in a typical case illustrated in Fig. 6.

Polarization-diverse antennas— Microstrip antennas can also be designed to produce a field along the broadside direction whose polarization can be adjusted by turning on or off one or more PIN diodes [3], or by adjusting the bias on one or more varactor diodes [12]. Two nearly degenerate modes can be excited by a single feed with one mode producing a far-field component which is orthogonal to that of the other mode. By altering the difference in the resonant frequencies of the two modes, one can adjust the relative phasing of the modes. Thus, one can control the polarization of the total far field produced by the two modes. Elements have been built whose polarization could be altered continuously between left- and right-hand circular polarization. A drawback of this type of element is that the band over which the axial ratio is under 3dB is quite narrow ($35/Q$ percent) [12].

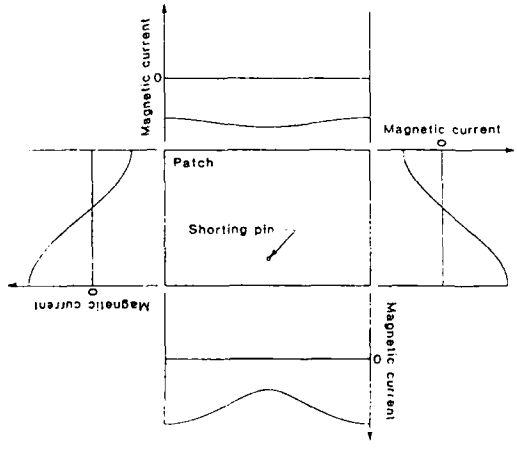

Figure 5. Magnetic current distribution of the resonant mode of a frequency-agile element with a single short located at $x = 5.72$ cm and $y = 1.52$ cm. The patch dimensions are $11.43 \times 7.62 \times 0.152$ cm and the dielectric constant is 2.43

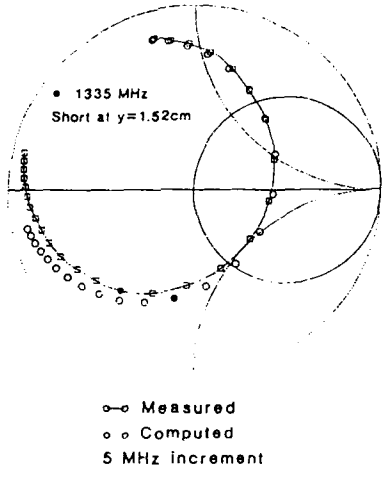

Figure 6. Input impedance of a frequency-agile element described in Fig. 5 with the feed point is at (2.54, 1.27).

Dual-band elements— In some applications, two or more rather narrow, discrete frequency bands of operation are often required with band separations of only a few percent. One technique that has been used is to stack elements of different sizes [14], [15]. One experimental result using a reactive load was reported in [2]. The present theory shows the type of load that is needed and how to control the band separation.

Figure 2(a) illustrates the uses of a load reactance which has a pole lower than the resonant frequency of the empty cavity resonant parent mode. If adjusted properly, two intersections between the X_r curve and the $-(X_f + X_L)$ curve occur corresponding to two daughter resonant modes of the loaded cavity. The band separation can be controlled in two ways.

1. If the magnitude of the slope of the $-(X_f + X_L)$ curve is increased, the band separation is reduced.
2. If the load is placed closer to a zero of the parent mode function, then the X_r curve becomes thinner again reducing the band separation.

Of these two methods, the latter is the easiest to implement. The resonant load can be simply an open- or a short-circuited transmission line, which can be etched on the same plane as the patch itself. In this case, the patch may need to be slotted and the line recessed as illustrated in Fig. 7 in order to control the band separation and still maintain at least bilateral symmetry in the element to reduce cross polarization.

It is clear from Fig. 2(a) that there is a continuous set of possible pairs of dual resonant frequencies obtainable by varying the resonant frequency of the load. However, it turns out that there is really only one pair of resonant frequencies which yields resonant modes whose input impedances are approximately the same. For all other pairs, the maximum input resistance of one is larger than the other. In extreme cases, one mode is so poorly matched that it is useless. Figure 8 contains the measured input impedance of both modes of a typical dual-band element.

DC mode applications— In all of the applications discussed above, the parent mode used almost exclusively was the (0,1) mode of a rectangular element. This mode produces a pattern with a beam maximum in a direction perpendicular to the patch. If mounted on a large grounded dielectric slab, the pattern falls off to zero in any direction parallel to the patch. If the dielectric is truncated at the patch edge, the gain also falls, but not to zero. *For the purposes of the present discussion, we will assume that the dielectric is so truncated.* Another mode of a nonloaded microstrip antenna is the DC mode—a mode resonant at zero frequency which has a constant voltage distribution from point to point on the patch. If this mode could be excited at an RF frequency, the pattern it would produce is basically the same as that of an electric monopole element mounted perpendicular to the ground plane. This yields a pattern which has a broadside null and a maximum along the ground plane. The first question to be addressed is how to resonate this mode at a useful frequency instead of at DC.

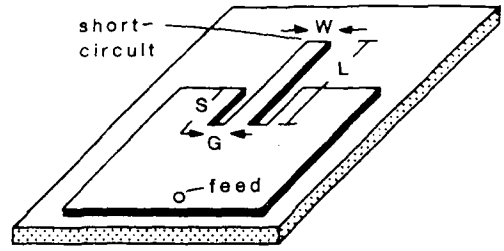

Figure 7. A monolithic dual-band element using a short-circuited transmission line recessed into the patch.

To answer this question, we consider the DC mode to be a parent mode and plot its corresponding X_r and $-X_f$ curves as illustrated in Fig. 9. It turns out that if $X_L = 0$, the resonant frequency (occurring where the dashed curve and the X_r curve intersect in Fig. 9) is still a little too low to be useful. To raise the frequency even higher, an appropriate amount of capacitance can be added. If the load capacitor is placed in the center of the square patch, then the resonant frequencies of the (0,1) and (1,0) modes of the antenna are unaffected and all *three* modes can be made to resonate at the same frequency. An alternative to using a capacitive load is to use four short circuits as illustrated in Fig. 10. The voltage distribution along

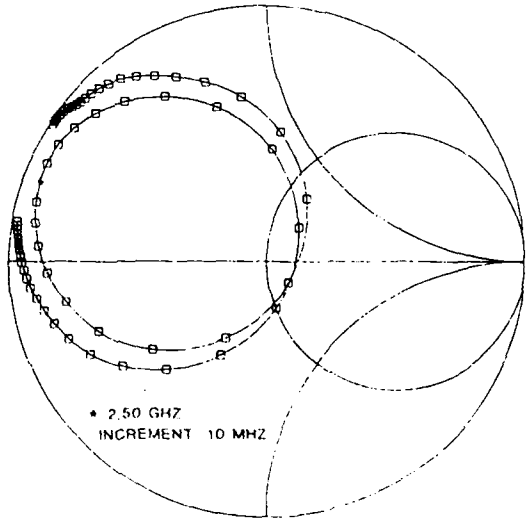

Figure 8. Measured input impedances of both modes of a typical dual-band element using a shorted transmission line as its resonant load.

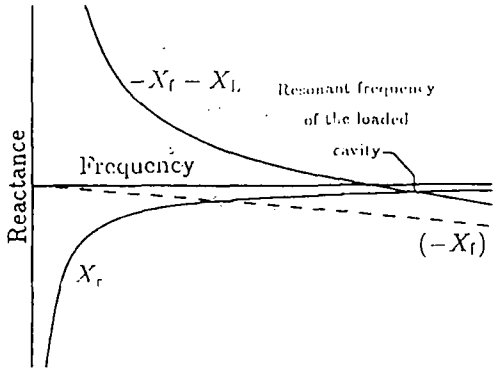

Figure 9. Plot the of x_r, $-X_f$, and $-(X_f + X_L)$ curves for a square patch element's DC mode. The X_L corresponds to a capacitive load.

one edge of the patch is also illustrated—the distributions along the remaining edges are identical. This again illustrates the principle that the daughter, loaded mode has the features of its parent mode, although it is not identical. The magnetic current distribution is basically constant around the edge with an oscillating perturbation having little significance in the far field. At least three applications of this DC mode can be imagined.

End-fire element. By combining with the proper magnitude and phase, the magnetic current associated with the DC mode, which circulates in one direction around the patch, and the magnetic current of a (0,1) mode, which is directed oppositely on opposite radiating edges, one can achieve an end-fire pattern. By "end-fire" we mean a pattern with a beam maximum in one direction parallel to the patch. This is not possible using a *single* mode of a microstrip antenna. Moreover, it is probably not possible using a pair of naturally occurring degenerate modes (such as the (0,1) and (1,0) modes of a square patch) since such modes typically yield *differently* polarized fields—such pairs of degenerate modes are useful for creating circular polarization, however. In order to excite both the loaded-DC mode and the (0,1) mode *independently*, one must feed each mode either at a point where the other mode is zero, or with a symmetry opposite to that of the other mode. The element illustrated in Fig. 11 uses a combination of these two methods. The dashed circular curve in the figure illustrates a line along which the electric field of the loaded-DC mode is zero. In principle, one should be able to feed the (0,1) mode at that point without coupling to the DC mode. A symmetrical feed is introduced at a pair of points at which the field of the (0,1) mode is zero thus preventing coupling to this mode. In addition, the (1,0) has odd symmetry and thus is also not excited by the symmetrical feed. The only mode that this symmetrical feed can couple to is the loaded DC mode. This element was built and its performance was consistent with the design principles outlined here.

Adaptive element. The element described in the preceding paragraph is essentially a two-element array within a single patch and, as such, has a pattern that can be adapted by changing the excitation of the two modes. Another type of adaptive element requiring a single feed is again that shown in Fig. 10, but with the short circuits implemented as PIN diodes. When biased on, the element would produce a monopole pattern. When they are biased off, the element produces the usual (0,1) mode pattern.

Monopulse element. By having a combination of four feeds located at the center of each edge of the patch, one can produce a sum and difference pattern by appropriate even or odd excitation of oppo-

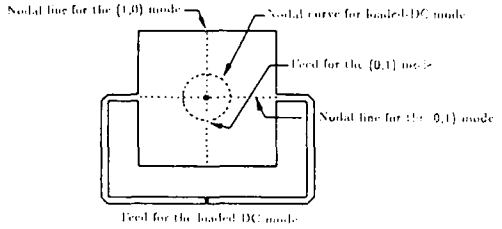

Figure 11. An element supporting three degenerate modes: the loaded-DC mode, the (0,1) mode, and the (1,0) mode.

site pairs of feeds. This application calls for the capacitively center-loaded square patch supporting degenerate loaded-DC, (0,1), and (1,0) modes. If a pair of feeds on opposite edges are excited in phase, then only the DC mode is excited. Exciting the pair out of phase would excite only either the (0,1) mode or the (1,0) mode depending on which pair of feeds were used.

Adaptive impedance matching— Another application is to change the input impedance of an element dynamically in response to a changing environment in which the element is placed, for example in a phased array. In this application, one seeks to hold the resonant frequency and the pattern constant. If one introduces a symmetrically located pair of short circuits that lie along the curve illustrated in Fig. 12, the maximum input resistance varies as shown in Fig. 13.

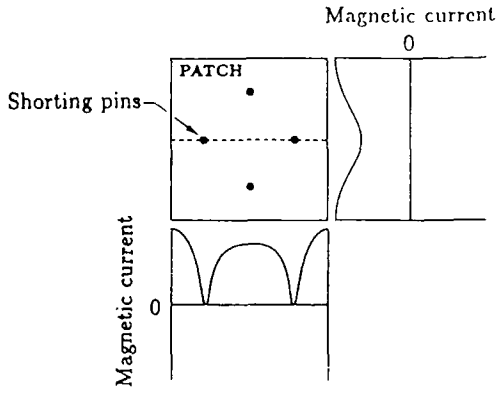

Figure 10. Square patch element with four short circuits producing a loaded-DC mode. The voltage distributions along one edge and along a cut through a centerline of the element are also shown.

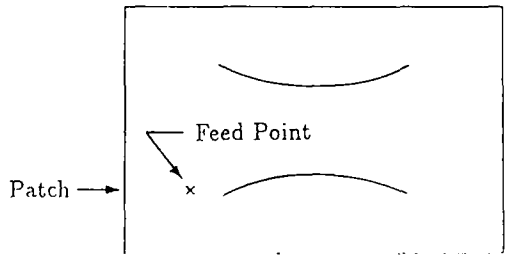

Figure 12. The locus of points along which a symmetrically placed pair of shorts will result in a constant resonant frequency and an essentially constant pattern.

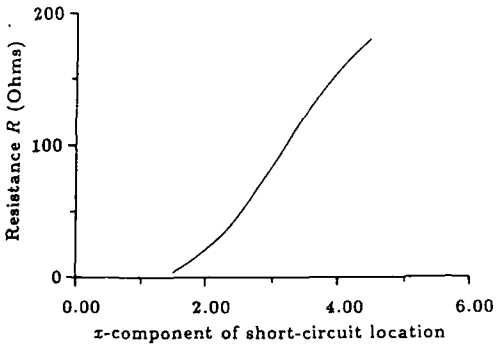

Figure 13. Variation of the maximum input resistance as the load pair is moved along the curves illustrated in Fig. 12.

Pattern shaping— There is not a lot of shaping of the pattern that one can do with a microstrip element since it is not electrically large and the magnetic current distribution must be essentially real-valued. However, one can, in principle, obtain a more nearly isotropic pattern in the E-plane by appropriately loading one edge of the element. (Again, the dielectric must be truncated at the edge of the patch). The concept in this application is to place loads at one edge so that the net magnetic current at that edge is zero as illustrated in Fig. 14. The magnetic current at the opposite edge is not zero resulting in a single magnetic dipole for this pair of edges. There is a net magnetic dipole on the remaining pair of edges, but they do not contribute any field in the E-plane and their maximum field strength in the H-plane has been computed to be down by about 9dB from the main beam. This yields the desired isotropic pattern. Some shaping of this pattern is possible by adjusting the net magnetic current at the loaded edge.

4 Conclusions

The basic theory of loaded microstrip antennas and numerous practical applications have been discussed. Proper selection and location of reactive loads can be used to control the resonant frequency, polarization, impedance, and radiation pattern. These characteristics can then be made electronically adaptable to various systems needs if the loads are PIN or varactor diodes.

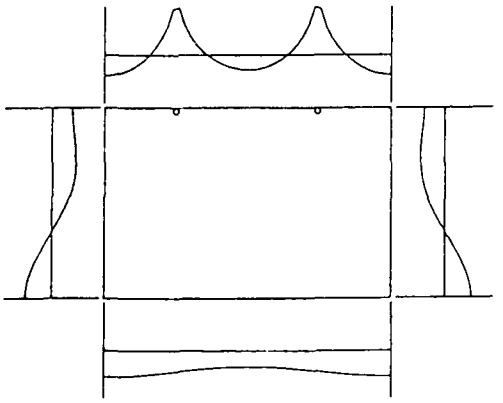

Figure 14. Voltage distribution along the edge of a rectangular patch loaded with a pair of capacitors. The net magnetic current on one edge is zero, but is not zero on the other.

References

[1] John Huang, "Circularly polarized conical patterns from circular microstrip antennas," *IEEE Trans. Antennas Propagat.*, vol. AP-32, pp. 991-994, Sept. 1984.

[2] J.I. Kerr, "Microstrip antenna development," *Proceedings of the Workshop on Printed-Circuit Antenna Technology*, Las Cruces, NM, pp. 3.1-3.20, Oct. 1979.

[3] D.H. Schaubert, F.G. Farrar, A.R. Sindoris, and S.T. Hayes, "Microstrip antennas with frequency agility and polarization diversity," *IEEE Trans. Antennas Propagat.*, vol. AP-29, pp. 118-123, Jan. 1981.

[4] B.F. Wang and Y.T. Lo, "Microstrip antennas for dual-frequency operation," *IEEE Trans. Antennas Propagat.*, vol. AP-32, pp. 938-943, Sept. 1984.

[5] W.F. Richards, S.E. Davidson, and S.A. Long, "Dual band, reactively loaded microstrip antenna," *IEEE Trans. Antennas Propagat.*, vol. AP-33, pp. 556-561, May 1985.

[6] S.E. Davidson, S.A. Long, and W.F. Richards, "Dual-band microstrip antennas with monolithic reactive loading," *Electronics Letters*, vol. 21, no. 20, pp. 936-937, Sept. 26, 1985.

[7] W.F. Richards and S.A. Long, "Pattern adaptation using loaded, dual-mode microstrip antennas," *IEEE Antennas Propagat. Symposium Digest*, Vancouver, BC, pp. 93-96, June 1985.

[8] W.F. Richards and S.A. Long, "Matching microstrip antennas using reactive loads," *IEEE Antennas Propagat. Symposium Digest*, Philadelphia, PA, pp. 431-434, June 1986.

[9] D.L. Sengupta, "Analysis of tunable rectangular patch antennas," *IEEE Antennas Propagat. Symposium Digest*, Boston, MA, pp. 267-270, June 1984.

[10] W.F. Richards and Y.T. Lo, "Theoretical and experimental investigation of a microstrip radiator with multiple lumped linear loads," *Electromagnetics*, vol. 4, no. 3-4, pp. 371-385, Sept. 1983.

[11] Y.T. Lo, D. Solomon, and W.F. Richards, "Theory and experiment on microstrip antennas", *IEEE Trans. Antennas Propagat.*, vol. AP-27, pp. 137-145, Mar. 1979.

[12] W.F. Richards, Y.T. Lo, and D.D. Harrison, "An improved theory for microstrip antennas and applications," *IEEE Trans. Antennas Propagat.*, vol. AP-29, pp. 38-46, Jan. 1981.

[13] W.F. Richards, J.R. Zinecker, R.D. Clark, and S.A. Long, "Experimental and theoretical investigation of the inductance associated with a microstrip antenna feed," *Electromagnetics*, vol. 4, no. 3-4, pp. 327-346, Sept. 1983.

[14] J.S. Dahele, K.F. Lee, and P.Y. Lee, "Experimental study of the characteristics of coupled top-loaded microstrip monopoles," *IEEE Trans. Antennas Propagat.*, vol. AP-31, pp. 530-531, May 1983.

[15] S. A. Long and M. D. Walton, "A dual-frequency stacked circular-disk antenna," *IEEE Trans. Antennas Propagat.*, vol. AP-27, pp. 270-273, 1979.

International Journal of Infrared and Millimeter Waves, Vol. 7, No. 4, 1986

THE INPUT IMPEDANCE OF THE DIELECTRIC RESONATOR ANTENNA

Stuart A. Long and Mark W. McAllister
Department of Electrical Engineering
University of Houston, University Park
Houston, Texas 77004

Received January 13, 1986

Abstract

Dielectric cylinders of very high permittivity have been used in the past as resonant cavities, but since the structure is not enclosed by metallic walls, electromagnetic fields do exist beyond the geometrical boundaries of the structure and part of the power is radiated. Through the proper choice of geometry and permittivity this radiation can become the dominant feature of the structure and become an efficient antenna for use at millimeter wave frequencies. Both experimental and theoretical investigations of a variety of these dielectric resonator antennas have been undertaken. In particular, the input impedance of a probe-fed cylindrical structure was examined in detail and a comparison of theoretical and experimental results was made.

0195-9271/86/0400-0555$01.00/0

Introduction

There is, today, strong interest on the part of both military and commercial users, in antenna systems which can operate efficiently in the millimeter wave region (100-300 GHz) and above. Reducing the size of currently-used microwave frequency antennas to obtain higher resonant frequencies will usually be unsuccessful, either because the small size prohibits economical fabrication or because the inherently larger conduction losses at the higher frequencies result in inefficient operation.

The above limitations could possibly be overcome if the antennas had simple shapes and few conducting surfaces. This explains the success of the dielectric rod antenna, in which radiation is "leaked" from the surface of the dielectric as a travelling wave passes through the rod. The use of a standing wave, rather than a travelling wave, to produce radiation from a dielectric structure, is the subject of the present investigation. This structure has been denoted as a "dielectric resonator antenna."

Antennas of three basic shapes have been studied: cylindrical, rectangular, and hemispherical. In each case a piece of high-permittivity dielectric of the appropriate shape is situated atop a conducting ground plane and excited by a probe fed from beneath the ground plane into the dielectric. Geometries for the three types of antennas are shown in figures 1-3. It has been analytically implied, and experimentally shown, that such structures can provide reasonably efficient radiation in the direction normal to the ground plane if the shapes, permittivities, probe lengths, probe positions, and excitation frequencies are correctly chosen.

The analysis began with a model for the internal fields (and resonant frequencies) of the antennas: the fields were shown to be approximately those of a magnetic-walled dielectric-filled cavity above a ground plane. For each shape the lowest-frequency modes were identified and feed probe locations for exciting these modes were found. The antenna far-field patterns were computed using magnetic surface currents as equivalent radiation sources.

Experimentally, antennas were fabricated with dimensions on the order of one inch and relative

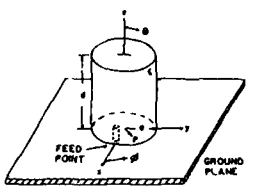

Fig. 1 Cylindrical geometry.

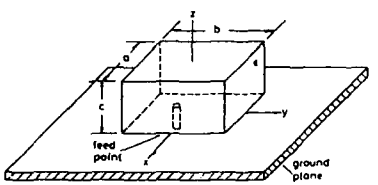

Fig. 2 Rectangular geometry.

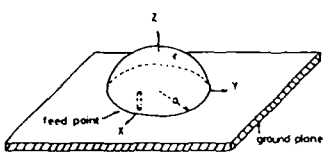

Fig. 3 Hemispherical geometry.

permittivities between 8 and 17, resulting in resonant frequencies between 1 GHz and 6 GHz. (Although these frequencies are not in the millimeter wave region mentioned above, the emphasis of this study was on the fundamental properties of the antenna, not on a particular higher-frequency application). Measurements of input impedance versus frequency for various shapes, permittivities, probe lengths, and probe positions have been taken. Pattern measurements, taken in an anechoic chamber, have been compared with calculated far-field patterns.

Resonant Frequency

Cylindrical Geometry

For the calculation of a first-order approximation of the resonant frequency the feed probe of the cylindrical sample shown in figure 1 is temporarily ignored and image theory applied to replace the ground plane by an imaged portion of the cylinder. An approximate solution for the interior fields was then calculated by assuming that the surfaces are all perfect magnetic conductors. An expression for the resonant frequency can then be derived [1].

$$f_{npm} = \frac{1}{2\pi a\sqrt{\mu\varepsilon}} \sqrt{\left\{ \begin{matrix} X_{np}^2 \\ X_{np}'^2 \end{matrix} \right\} + \left[\frac{\pi a}{2d}(2m+1)\right]^2} \qquad (1)$$

where $J_n(X_{np})=0$ and $J_n'(X_{np}')=0$ and J_n is the Bessel Function of the first kind. The lowest order mode is the TM_{110} with n=1, p=1, m=0. Using $X_{11}'=1.841$

$$f_{110} = \frac{1}{2\pi a\sqrt{\mu\varepsilon}} \sqrt{(1.841)^2 + \left(\frac{\pi a}{2d}\right)^2} \qquad (2)$$

Equivalent magnetic surface currents were then found and used as sources for the far-field radiation patterns [2]. Linearly polarized fields with broad

beamwidths normal to the ground plane were found in both the E- and H-planes as long as the a/d ratio was not allowed to become too small ($a/d \geq 0.5$). For smaller values of a/d a null began to develop along the direction normal to the plane of the radiator. Experimental measurements of both resonant frequency and radiation pattern were made for a variety of different dielectric materials ($4.5 < \varepsilon_r < 15.2$) with varying aspect ratios ($0.15 < a/d < 1.67$). Reasonable correlation between theory and experiment was found.

Rectangular Geometry

A similar theoretical derivation was carried out for the rectangular geometry shown previously in figure 2. In this case, the general formula reduces to [2]

$$f_{|01|} = \frac{1}{2\sqrt{\mu\varepsilon}} \sqrt{\frac{1}{a^2} + \frac{1}{4c^2}} \tag{3}$$

for the dominant $TM_{|01|}$ mode where it is assumed there are no field variations in the y-direction.

Broad lobes normal to the ground plane are once again found when the radiation patterns are calculated. In a similar analogy to the previously discussed cylindrical radiator the rectangular block may not be allowed to be too tall or dips in the pattern begin to occur. As long as the height is kept smaller than the base dimensions ($c < a,b$) the maximum radiation will be in the proper direction [3]. Once again, experimental verification was obtained for varying sizes of blocks and different dielectric constants.

Hemispherical Geometry

The third antenna shape that was considered was the hemisphere on a ground plane as shown in figure 3. Its analysis is different in that no approximations are needed to find the internal and external fields. The geometry is separable and an exact solution can be obtained. This analysis results in a transcendental equation for the complex resonant wavenumbers which has been solved numerically [4]. The principal plane

radiation patterns are quite similar to the previous two shapes. Experimental measurements once again show good correlation for both the resonant frequency and field patterns.

Theoretical Impedance

The experimental impedance curves for a probe-fed cylindrical resonator antenna resemble those which would be obtained by measuring the impedance of a parallel RLC circuit. Such a circuit can be used as an approximate model for the impedance as seen by the probe. Values of R, L, and C as functions of the antenna parameters can be derived for the case of the cylindrical resonant antenna.

The circuit model is based on the variational formula for the input impedance of a probe in a cavity, which is [5]

$$Z_{in} = -\frac{1}{I^2} \iiint \vec{E} \cdot \vec{J}^a \, dV \tag{4}$$

where $\vec{J}^a$ is the assumed current distribution on the probe and I is the magnitude of the input current at the bottom of the probe. $\vec{E}$ is the normalized total electric field in the cavity. It has been shown [5] that the field in such a cavity with electric sources present can be expanded in terms of modal eigenvectors

$$\vec{E} = \sum_i \frac{j\omega \vec{E}_i}{\omega^2 - \omega_i^2} \iiint \vec{J} \cdot \vec{E}_i^* \, dV \tag{5}$$

where the $\vec{E}_i$ are normalized such that

$$\iiint \varepsilon \vec{E}_i \cdot \vec{E}_j^* \, dV = \delta_{ij} \tag{6}$$

and ω_i is the resonant frequency of the i^{th} mode.

For the first-order approximation, only the i=0

term is taken; i.e., only the single mode of interest is assumed to be present in the cavity. Substituting Equation (5) into Equation (4) gives

$$Z_{in} = \frac{-j\omega}{I^2} \frac{a_o^2}{\omega^2 - \omega_o^2} \tag{7}$$

where

$$a_o = \iiint \vec{E}_o \cdot \vec{J}^a \, dV \tag{8}$$

Since losses are present, ω_o is complex, i.e.,

$$\omega_o^2 = \omega_{or}^2 (1 + j/Q) \tag{9}$$

where Q is the total quality factor and ω_{or} is the real part of the resonant frequency. Near resonance, then, Equation (7) can be approximated by

$$Z_{in} = - \frac{j\omega (a_o/I)^2}{\omega^2 - \omega_{or}^2 (1 + j/Q)} \tag{10}$$

This can be compared to the formula for the impedance of a parallel RLC circuit:

$$Z_{RLC} = - \frac{j\omega/C}{\omega^2 - \omega_{or}^2 (1 + j/Q)} \tag{11}$$

where $\omega_{or}^2 = 1/LC$, $Q = R/\omega L = R/\omega_{or} L$. The elements of the circuit are thus

$$R = \frac{Q}{\omega_{or}} \left(\frac{a_o}{I}\right)^2 \quad L = \frac{1}{\omega_{or}^2} \left(\frac{a_o}{I}\right)^2 \quad C = \left(\frac{a_o}{I}\right)^{-2} \tag{12}$$

Since Equation (11) will always produce a reactance curve which is symmetrical about the real axis on either side of resonance, it provides a model valid only for a limited range of probe lengths. Experimental results [2] indicate that this range will be approximately between one-fourth and three-eights of a wavelength in the dielectric.

In order to evaluate the term a_o/I, a probe current distribution must be assumed. A reasonable approximate choice is

$$J^a = I \frac{\sin k(\ell - z)}{\sin k\ell} \delta(\phi) \delta(\rho - \rho_o) (1/\rho_o) \hat{z} \tag{13}$$

where ℓ is the probe length, k is the wavenumber in the dielectric, and ρ_o is the probe radial location. This gives a filamentary current which is zero at the end of the probe and has magnitude I at the bottom of the probe. Clearly this is a rough approximation since the experimental probes are quite thick (probe diameter/probe length ≈ 1/10); however, as a starting assumption it is reasonable.

The quantity (a_o/I) can then be evaluated for the cylindrical resonant antenna. From previous work [2] an expression for E_z which is normalized according to Equation (6) is

$$E_z = \frac{1}{\sqrt{W}} \frac{1}{\omega\epsilon} \left(\frac{1.841}{a}\right)^2 J_1(k_\rho \rho) \cos\phi \cos(z\pi/2d) \tag{14}$$

where

$$W = \frac{\pi d}{2\omega^2 \epsilon} \left[\frac{.995}{d^2} + \frac{2.731}{a^2}\right] \tag{15}$$

After expanding the sin $k(\ell - z)$ term in Equation (13) and applying Equation (8), the following integral is derived:

$$a_o/I = \frac{1}{\sqrt{W}} \frac{1}{\omega\epsilon} \left(\frac{1.841}{a}\right)^2 J_1(k_\rho \rho_o) \, .$$

$$\int_0^{\ell} \cos kz \cos(\pi z/2d)dz - \cot k\ell \int_0^{\ell} \sin kz \cos(\pi z/2d)dz \tag{16}$$

The integrals are evaluated:

$$\int_0^{\ell} \cos kz \cos(\pi z/2d)dz = \frac{\sin((k-\pi/2d)\ell)}{2(k-\pi/2d)} + \frac{\sin((k+\pi/2d)\ell)}{2(k+\pi/2d)} \tag{17}$$

$$\int_0^{\ell} \sin kz \cos(\pi z/2d)dz = -\frac{1}{2}(k-\pi/2d)^{-1}[\cos((k-\pi/2d)\ell)-1]$$

$$-\frac{1}{2}(k+\pi/2d)^{-1}[\cos((k+\pi/2d)\ell)-1] \tag{18}$$

A computer program was written to evaluate Equation (16), solve for R, L, and C, and to plot the resulting impedance curve over a range of frequencies near resonance. Figures (4 and 5) show purely theoretical resistance and reactance curves (solid curves) for two different cylinders along with experimental data taken previously [1]. The theoretical Q's were found to be higher than experimental ones for all except high a/d cylinders, and thus, the narrower peaks on most of the theoretical resistance curves are to be expected. Resistance at resonance is fairly well predicted -- the errors in applying Equation (7) are apparently nicely balanced by the aforementioned errors in the theoretical Q's.

To further check the validity of Equation (12) in predicting R, a set of measurements was taken on a cylindrical antenna with $a/d = 0.5$ and $\epsilon_r = 13.2$. Six different probe lengths were utilized: 1.47 cm, 1.40 cm, 1.32 cm, 1.22 cm, 1 09 cm and 0.97 cm. The top curves in Figures 6-8 are the experimental impedance curves for three of the probe lengths. The program mentioned above was run for all six cases, with measured Q's from the experimental curves as inputs. The bottom graphs in Figures 6-8 are the resulting "semi-theoretical" plots. Since the scaling is occasionally different between identical-parameter curves, the resistance at resonance as a function of probe length has been plotted in Figure 9. The agreement is seen to be quite good considering all the

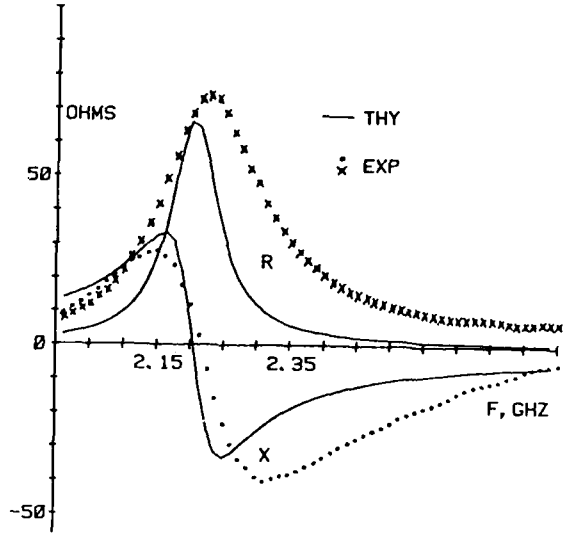

Fig. 4 Theoretical and experimental impedance, a = 1.27 cm, a/d = 0.67, ϵ_r = 13.2, tanδ = 0.0064, probe length= 0.81 cm.

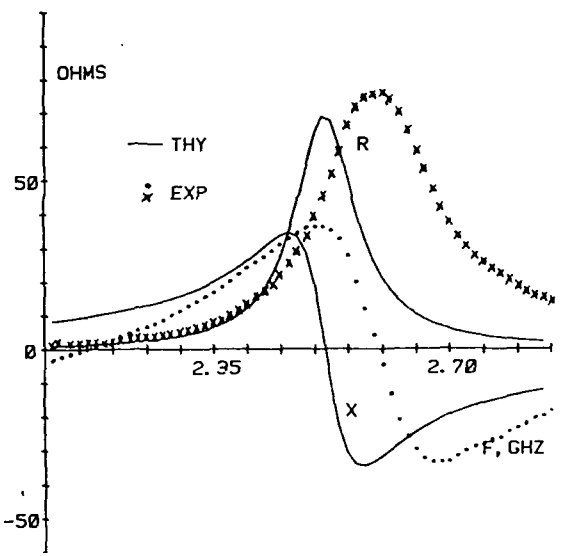

Fig. 5 Theoretical and experimental impedance, a = 1.27 cm, a/d = 1.0, ε_r = 13.2, tanδ = 0.0064, probe length = 0.81 cm.

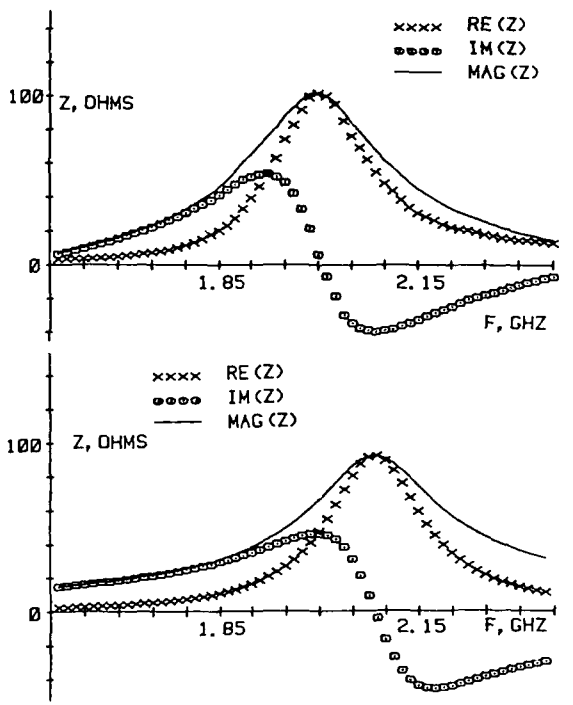

Fig. 6 Experimental (top) and theoretical using measured Q (bottom) impedance, a = 1.27 cm, a/d = 0.5, ε_r = 13.2, tanδ = 0.0064, probe length = 1.22 cm.

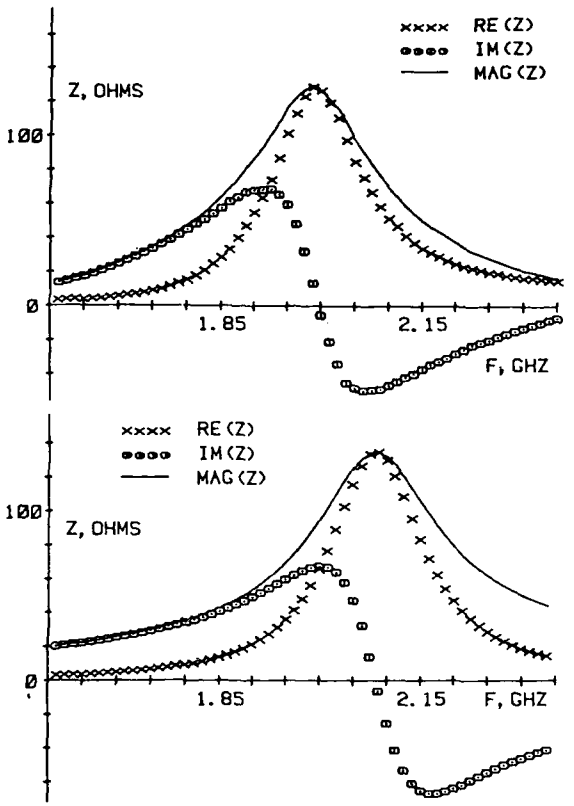

Fig. 7 Experimental (top) and theoretical using measured Q (bottom) impedance, a = 1.27 cm, a/d = 0.5, ε_r = 13.2, tanδ = 0.0064, probe length = 1.32 cm.

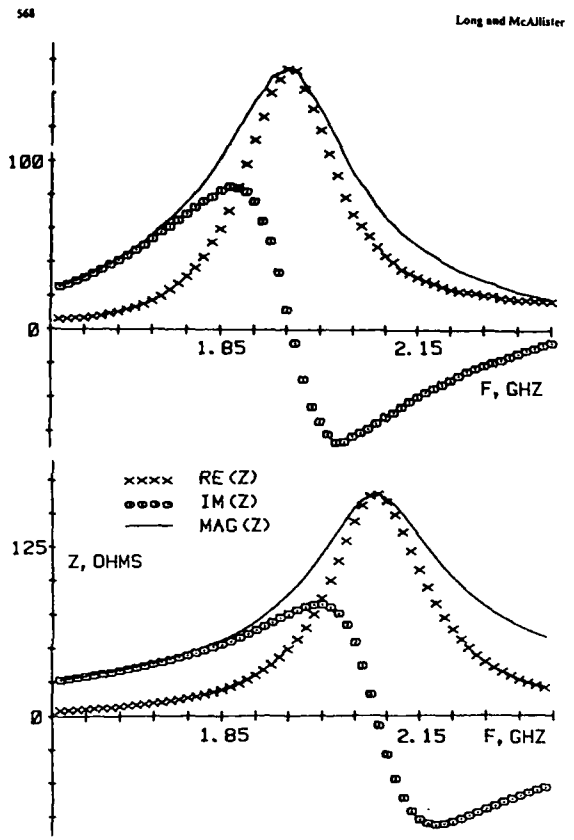

Fig. 8 Experimental (top) and theoretical using measured Q (bottom) impedance, a = 1.27 cm, a/d = 0.5, ε_r = 13.2, tanδ = 0.0064, probe length = 1.40 cm.

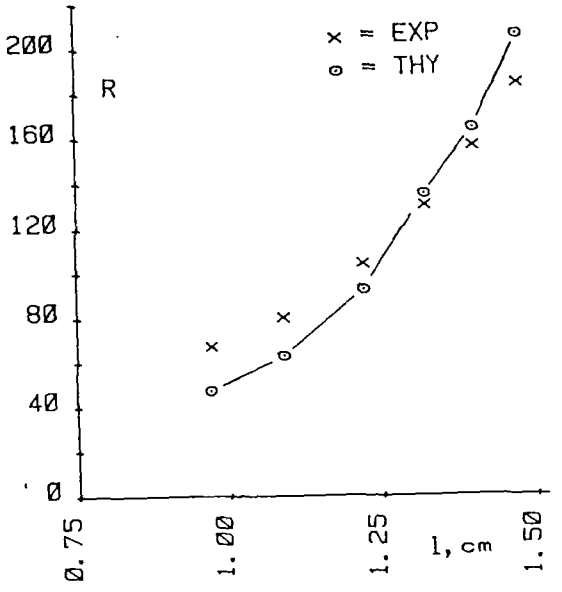

Fig. 9 Resistance at resonance versus probe length, [illegible]

approximations that were made.

Conclusions

It has been shown, that at least qualitatively, the impedance behavior of the dielectric resonator antenna can be predicted from a simple resonant circuit model. Experimental data of the impedance as a function of frequency were taken for a variety of radiators and the results compared to theoretical computations.

Acknowledgements

This work was supported in part by the U.S. Army Research Office under contract DAAG-29-84-K-0166.

References

[1] S.A. Long, M.W. McAllister, and L.C. Shen, "The resonant cylindrical dielectric cavity antenna," IEEE Trans. Antennas and Propagation, AP-31, p. 406, May 1983.

[2] M.W. McAllister, "The resonant dielectric antenna: Experiment and theory," Dissertation, Department of Electrical Engineering, University of Houston-University Park, Dec. 1983.

[3] M.W. McAllister, S.A. Long, and G.L. Conway, "Rectangular dielectric resonantor antenna," Electron. Lett., vol. 19, p. 218, March 17, 1983.

[4] M.W. McAllister and S.A. Long, "Resonant hemispherical dielectric antenna," Electron. Lett., vol. 20, p. 657, Aug. 2, 1984.

[5] R.F. Harrington, Time-Harmonic Electromagnetic Fields, New York, McGraw-Hill, 1961, pp. 434-435.

An Asymptotic Extraction Technique for Evaluating Sommerfeld-Type Integrals

DAVID R. JACKSON, MEMBER, IEEE, AND
NICÓLAOS G. ALEXÓPOULOS, SENIOR MEMBER, IEEE

Abstract—An asymptotic extraction process is developed which leads to an efficient method for the evaluation of the electric field from a

Manuscript received February 11, 1986; revised May 27, 1986. This work was supported under U.S. Army Research Contracts DAAG 29-83-K-0067 and DAAG-29-84-K-0163.

D. R. Jackson is with the Electrical Engineering Department, University of Houston, Houston, TX 77004.

N. G. Alexopoulos is with the Electrical Engineering Department, University of California, Los Angeles, CA 90024.

IEEE Log Number 8610053.

0018-926X/86/1200-1467$01.00

Hertzian dipole in a layered geometry. This technique allows for a rapidly converging expression for the electric field which remains well behaved as the source and observation heights z', z coincide. A useful application of this method is in the calculation of mutual impedance between printed dipoles.

I. Introduction

For the rigorous analysis of microstrip antenna problems, a key step is usually the evaluation of Sommerfeld-type integrals to compute the reaction between current functions. This is often the most time-consuming part of the total calculation, due to slow convergence. Furthermore, because the Sommerfeld integral for the electric field from a Hertzian dipole becomes nonconvergent as the source and observation heights z' and z coincide, certain techniques must be used for calculations in the real-space domain [1]. An alternative approach is the plane-wave spectrum method [2], [3]. This method eliminates the nonconvergent behavior when $z = z'$. Self-term problems are also eliminated, making the method very attractive for the numerical analysis of antenna problems. One disadvantage of this method, however, is that the convergence of the resulting integral expression depends on the Fourier transforms of the current functions when $z = z'$. The integrand thus oscillates more rapidly as the separation between currents increases, and the convergence becomes worse as the size of the current functions decreases. Hence it is difficult to compute the reaction between small basis functions of current which are widely separated. One technique for overcoming this difficulty has been introduced by Pozar [4]. In this technique a homogeneous-space term is extracted from the integrand in the spectral domain, resulting in a more rapid convergence. This technique is well-suited for an efficient analysis of patch and dipole antennas. The convergence of the resulting integrand is still slow for small current functions when $z = z'$, however.

In this communication an asymptotic extraction technique for directly evaluating the electric field of a Hertzian dipole is introduced, in which convergence is obtained for all values of z and z'. Because the extraction technique is performed in the real-space domain, the method efficiently computes the reaction between basis functions of arbitrarily small size. The resulting expression is also rapidly convergent, allowing for an efficient computation even for large basis function separations.

II. Asymptotic Extraction Technique

The geometry of a Hertzian dipole embedded in a layered structure over a ground plane is shown in Fig. 1. Although the general method to be discussed is applicable to an arbitrary number of layers, an explicit solution will only be given for the case of a dipole within a single layer of thickness B, as shown in the figure. Likewise, the method is applicable to layers of arbitrary loss, although results will only be shown for the lossless case. The Hertzian dipole is assumed oriented in the x direction, at a distance z' from the ground plane. The relative permittivity and permeability of the layer are denoted as ϵ_r, μ_r, with $n = \sqrt{\epsilon_r \mu_r}$ the index of refraction.

The starting point of the analysis is the Sommerfeld solution for the Hertzian potential components Π_x, Π_z at x, y, z due to the dipole at x', y', z'. This solution may be written in the form (suppressing $e^{+j\omega t}$) [5]

$$\Pi_x = \int_0^\infty f(\lambda) J_0(\lambda r)\, d\lambda \tag{1}$$

$$\Pi_z = \int_0^\infty g(\lambda) J_1(\lambda r) \cos\phi\, d\lambda \tag{2}$$

in which

$$r = [(x-x')^2 + (y-y')^2]^{1/2}, \qquad \cos\phi = \frac{x-x'}{r}$$

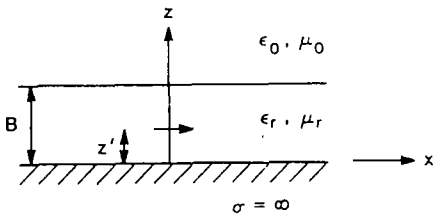

Fig. 1. Hertzian dipole embedded in a single layer.

and $f(\lambda)$, $g(\lambda)$ are complicated functions of the integration variable λ which also depend on z and z', although this dependence is not explicitly shown here. For the case of a single layer with $z, z' \le B$, the functions f and g are given by

$z \le z' \le B$

$$f(\lambda) = \frac{2}{D_e(\lambda)} \frac{\lambda}{u_1} \left[\frac{1}{\mu_r} u_1 \cosh u_1(B-z') + u \sinh u_1(B-z') \right] \sinh u_1 z \tag{3}$$

$z' \le z \le B$

$$f(\lambda) = \frac{2}{D_e(\lambda)} \frac{\lambda}{u_1} \left[\frac{1}{\mu_r} u_1 \cosh u_1(B-z) + u \sinh u_1(B-z) \right] \sinh u_1 z' \tag{4}$$

and in either region,

$$g(\lambda) = \frac{2}{D_e(\lambda) D_m(\lambda)} \frac{(1-n^2)}{\mu_r} \lambda^2 \sinh u_1 z' \cosh u_1 z \tag{5}$$

where

$$D_e(\lambda) = u \sinh u_1 B + \frac{1}{\mu_r} u_1 \cosh u_1 B \tag{6}$$

$$D_m(\lambda) = \frac{1}{\mu_r} u n^2 \cosh u_1 B + u_1 \sinh u_1 B \tag{7}$$

with

$$u = (\lambda^2 - k_0^2)^{1/2}, \quad u_1 = (\lambda^2 - k_1^2)^{1/2}, \text{ and } k_1 = k_0 n.$$

In (3)-(5) a normalization factor $-j\omega\mu_0\mu_r/4\pi k_1^2$ has been suppressed. An important feature of the coefficient functions $f(\lambda)$ and $g(\lambda)$ is that they are both $0(1)$ as $\lambda \to \infty$ when $z = z'$, and they both decay exponentially as $\lambda \to \infty$ otherwise. This general property holds true for any arbitrary number of layers. These functions also exhibit surface-wave poles at the roots of the functions $D_e(\lambda)$ and $D_m(\lambda)$ in the region $k_0 \le \lambda \le k_0 n$, as well as branch points at $\lambda = \pm k_0$. The integration in (1) and (2) is along a Sommerfeld contour which goes above these poles, and which maintains the proper branch interpretation of u [1].

To illustrate the extraction technique the E_x component of the electric field is considered, given by

$$E_x = k^2 \Pi_x + \frac{\partial^2 \Pi_x}{\partial x^2} + \frac{\partial^2 \Pi_z}{\partial x \partial z}. \tag{8}$$

where k is the wavenumber at x, y, z.

To calculate E_x, (2) is first differentiated as

$$\frac{\partial \Pi_z}{\partial z} = \int_0^\infty h(\lambda) J_1(\lambda r) \cos\phi \ \lambda \ d\lambda \tag{9}$$

where

$$h(\lambda) = \frac{1}{\lambda} \frac{\partial g}{\partial z}. \tag{10}$$

The function $h(\lambda)$ is also O(1) as $\lambda \to \infty$ when $z = z'$, and exponentially decaying otherwise. Hence (9) is nonconvergent when $z = z'$. To overcome this problem, an asymptotic extraction term may be formulated, which asymptotically approximates the behavior of the integrands in (1) and (9). Such a form may be obtained by approximating the hyperbolic sinh and cosh functions appearing in the f and h functions with exponential functions of λ. In particular, the following relations are used:

$$\sinh(u_i a) \sim \frac{1}{2} \delta_a e^{+\lambda a}$$

$$\cosh(u_i a) \sim \frac{1}{2} (2 - \delta_a) e^{+\lambda a}$$

as $\lambda \to \infty$, with

$$\delta_a = \begin{cases} 1, & a > 0 \\ 0, & a = 0. \end{cases}$$

Using these, the coefficient functions are seen to become asymptotic to the following forms as $\lambda \to \infty$:

$$f(\lambda) \sim \sum_{n=1}^{N} \frac{a_n}{k_0} e^{-\lambda \xi_n} \equiv f_a(\lambda) \tag{11}$$

$$h(\lambda) \sim \sum_{n=1}^{N} \frac{b_n}{k_0} e^{-\lambda \zeta_n} \equiv h_a(\lambda). \tag{12}$$

The number N depends on the number of layers in the problem, with $N = 1$ for the single layer case. The constants a_n, b_n depend only on the layer thicknesses and material parameters, while the constants ξ_n, ζ_n depend on z and z' as well as the layer thicknesses. For example, for the single layer case, the following results are obtained from (3)–(7) for the case $z \le z'$:

$$a_1 = \frac{1}{\mu_r + 1} [2 - \delta_{B-z'} + \mu_r \delta_{B-z'}] \tag{13}$$

$$\xi_1 = z' - z \tag{14}$$

and

$$b_1 = \frac{2(1 - n^2)}{(\mu_r + 1)(\epsilon_r + 1)} \tag{15}$$

$$\zeta_1 = 2B - z - z'. \tag{16}$$

In (13), (15) a factor $-30j\mu_r/n^2$ has been suppressed.

The asymptotic terms $f_a(\lambda)$ and $h_a(\lambda)$ are now subtracted and added from the integrands in (1) and (9), respectively. The resulting expressions from the added terms may be evaluated in closed form, using the relations

$$\int_0^\infty J_0(\lambda r) e^{-\lambda \beta} \, d\lambda = \frac{1}{(r^2 + \beta^2)^{1/2}} \tag{17}$$

and

$$\frac{\partial}{\partial x} J_0(\lambda r) = -J_1(\lambda r)(\lambda \cos\phi). \tag{18}$$

Substituting the results into (8) and differentiating then results in

$$E_x = \int_0^\infty F(\lambda) \, d\lambda + k^2 \sum_{n=1}^{N} \frac{a_n}{k_0} T_{1n} - \sum_{n=1}^{N} \frac{a_n}{k_0} T_{2n} + \sum_{n=1}^{N} \frac{b_n}{k_0} T_{3n} \tag{19}$$

where

$$F(\lambda) = [f(\lambda) - f_a(\lambda)] E_1(\lambda) + [h(\lambda) - h_a(\lambda)] E_2(\lambda) \tag{20}$$

with

$$E_1(\lambda) = (k^2 - \lambda^2 \cos^2\phi) J_0(\lambda r) - \lambda^2 (1 - 2\cos^2\phi) \frac{J_1(\lambda r)}{\lambda r} \tag{21}$$

$$E_2(\lambda) = \lambda^2 \cos^2\phi J_0(\lambda r) + \lambda^2 (1 - 2\cos^2\phi) \frac{J_1(\lambda r)}{\lambda r} \tag{22}$$

and

$$T_{1n} = \frac{1}{(r^2 + \xi_n^2)^{1/2}} \tag{23}$$

$$T_{2n} = \frac{r^2 + \xi_n^2 - 3(x - x')^2}{(r^2 + \xi_n^2)^{5/2}} \tag{24}$$

$$T_{3n} = \frac{r^2 + \zeta_n^2 - 3(x - x')^2}{(r^2 + \zeta_n^2)^{5/2}}. \tag{25}$$

The functions $f(\lambda)$ and $h(\lambda)$ approach their corresponding asymptotic forms fairly quickly in general, as shown in Fig. 2 for the case of a single teflon layer with $z = z' = B$ (the asymptotic functions are constants in this case, since ξ_1 and ζ_1 are both zero). The terms $f(\lambda) - f_a(\lambda)$ and $h(\lambda) - h_a(\lambda)$ are $O(1/\lambda^2)$ as $\lambda \to \infty$, so the integration in (19) converges for all z and z'.

Because of the surface-wave poles the integration in (19) may be broken into two regions: $(0, A)$ and (A, ∞), where A is larger than all surface-wave poles. A pole extraction technique may then be used to evaluate the integration over the first region [1]. The integration over the second region may be improved by noting that

$$\lim_{\lambda \to \infty} \lambda^2 [f(\lambda) - f_a(\lambda)] = c_1 \tag{26}$$

and

$$\lim_{\lambda \to \infty} \lambda^2 [h(\lambda) - h_a(\lambda)] = c_2 \tag{27}$$

where c_1, c_2 are constants which are nonzero when $z = z'$.

Assuming that the limiting results of (26), (27) are valid when $\lambda > M$ for some sufficiently large value M, the integration from M to ∞ may be evaluated analytically as

$$\int_M^\infty F(\lambda) \, d\lambda = \frac{c_2 - c_1}{r} [(1 - \cos^2\phi) I(Mr) + (1 - 2\cos^2\phi) J_1(Mr)] - c_1 n^2 r [I(Mr) + J_1(Mr) - J_0(Mr)/Mr] \tag{28}$$

where

$$I(x) \equiv \int_x^\infty J_0(t) \, dt = -J_1(x)(1 - x^{-2}) + \frac{J_0(x)}{x} (1 - 3x^{-2}) + O(x^{-9/2}) \tag{29}$$

as $x \to \infty$.

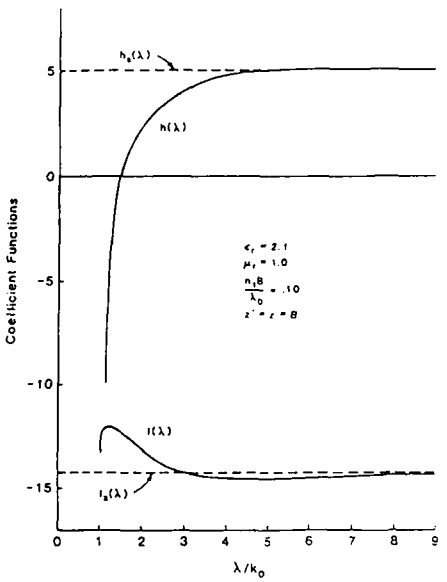

Fig. 2. A plot of the coefficient functions $f(\lambda)$, $h(\lambda)$, and the corresponding asymptotic functions $f_a(\lambda)$, $h_a(\lambda)$ (in all functions a factor j/k_0 has been suppressed).

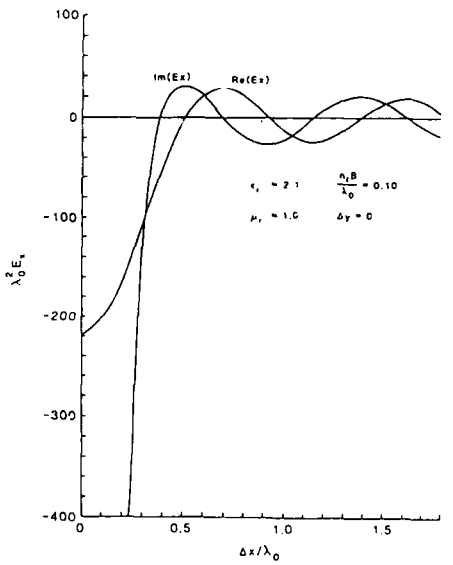

Fig. 3. E_x versus $\Delta x/\lambda_0$ for a dipole on a teflon layer with $z' = z = B$.

Choosing $M/k_0 = 25$ will usually insure that the limiting approximations of (26), (27) as well as that of (29) are valid. Hence the integration in λ need not usually extend past this value of M in order to obtain accurate results for all values of z and z'.

As an illustration of results obtained with this method, the real and imaginary parts of the E_x-field are plotted versus x-axis separation in Fig. 3 ($\Delta x = x - x'$) for the case $\phi = 0$ with a teflon layer. The E_x-field decays slowly with r in this case due to the endfire nature of the dominant TM_1 surface-wave mode.

One practical use of the E-field computation by this method is in the calculation of mutual impedance between dipoles [8]. When using the method of moments with subdomain basis functions, the reaction between widely separated basis functions on different dipoles may be computed efficiently by approximating the currents as point sources, which reduces the computation to a single E-field evaluation. The plane-wave spectrum method may be used for reactions along the same dipole, thus using both methods in a complimentary way.

III. Conclusion

An asymptotic extraction technique for the efficient real-space evaluation of the electric field from a Hertzian dipole in a layered media has been presented. The method involves the extraction of z-dependent terms from the integrands in the Sommerfeld expressions for the Hertzian potential components, resulting in an expression which converges rapidly for all values of z and z'. This method is well suited for finding the reaction between basis functions of current which are small and widely separated, for which a point dipole approximation may be used.

References

[1] I. E. Rana and N. G. Alexopoulos, "Current distribution and input impedance of printed dipoles," *IEEE Trans. Antennas Propagat.*, vol. AP-29, pp. 99–105, Jan 1981. (Note that (13) and (14) have a factor of 2, which is a misprint.)

[2] N. K. Uzunoglu, N. G. Alexopoulos, and J. G. Fikioris, "Radiation properties of microstrip dipoles," *IEEE Trans. Antennas Propagat.*, vol. AP-27, pp. 853–858, Nov. 1979. (See also correction, *IEEE Trans. Antennas Propagat.*, vol. AP-30, p. 526, May 1982.)

[3] D. M. Pozar, "Input impedance and mutual coupling of rectangular microstrip antennas," *IEEE Trans. Antennas Propagat.*, vol. AP-30, pp. 1191–1196, Nov. 1982.

[4] D. M. Pozar, "Improved computational efficiency for the moment method solution of printed dipoles and patches," *Electromagn.*, vol. 3, no. 3-4, pp. 299–309, July-Dec. 1983.

[5] A. Sommerfeld, *Partial Differential Equations*. New York: Academic, 1962.

[6] N. G. Alexopoulos and I. E. Rana, "Mutual impedance computation between printed dipoles," *IEEE Trans. Antennas Propagat.*, vol. AP-29, pp. 106–111, Jan. 1981.

[7] D. R. Jackson, "Fundamental superstrate effects on printed circuit antennas," Ph.D. dissertation, Univ. California, Los Angeles, Dec. 1985.

[8] D. R. Jackson and N. G. Alexopoulos, "Analysis of planar-strip geometries in a substrate-superstrate configuration," *IEEE Trans. Antennas Propagat.*, vol. AP-34, pp. 1430–1439, this issue.

Analysis of Planar Strip Geometries in a Substrate-Superstrate Configuration

DAVID R. JACKSON, MEMBER, IEEE, AND NICÓLAOS G. ALEXÓPOULOS, SENIOR MEMBER, IEEE

Abstract—A moment method procedure is used to analyze the behavior of several different configurations consisting of planar strips in a substrate-superstrate geometry. These include the microstrip transmission line, center-fed dipole, the mutual impedance between two dipoles, and the transmission-line coupled dipole. In each case some of the basic superstrate effects are discussed.

I. INTRODUCTION

RECENTLY, some of the basic effects of a superstrate (cover) layer on printed circuit antenna performance were investigated, based on the analysis of a Hertzian (infinitesimal) dipole. By properly choosing the layer thicknesses and material constants, it was observed that several different phenomena could occur, each of which could be used in a different way to improve the radiation characteristics of the dipole [1]–[4]. These results extend directly to apply to the radiation characteristics of full-size printed antennas. However, for the full-size antenna, input impedance and mutual coupling problems are also of concern, and these require calculation of the near-field together with a suitable numerical technique. The purpose of this investigation is the numerical analysis of four representative classes of full-size geometries in a substrate-superstrate configuration, each composed of planar strips. These four geometries, shown in Fig. 1, include the microstrip transmission line, the center-fed dipole, the mutual impedance between two dipoles, and the transmission-line coupled dipole. In each case the conductive strips of width w are embedded within a two-layered structure consisting of a grounded substrate of thickness B with relative permittivity and permeability ϵ_1, μ_1 with a superstrate of thickness t on top, having parameters ϵ_2, μ_2. The strip axes are taken to be in the x direction in all cases. An illustration of the layer geometry is shown in Fig. 2 for the case of the microstrip line. A convenient analysis for each of these cases can be provided by using a plane-wave spectrum formulation for the reaction between two arbitrary x-directed current sources, together with a Galerkin moment method formulation.

After the formulation of each problem is given, results are shown and the effects of a superstrate layer are discussed. For the microstrip transmission line, the effect of the superstrate on the line dispersion is demonstrated. For the center-fed dipole, the superstrate effect on the resonant length and input resistance is seen, and simple formulas are given to approximately calculate these quantities. The effect of a superstrate layer on the mutual impedance between two dipoles is then discussed, and it is demonstrated that a superstrate may be

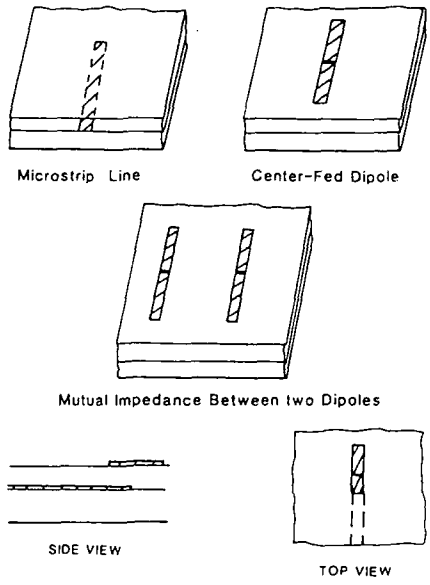

Fig. 1. Planar-strip geometries in a substrate-superstrate configuration.

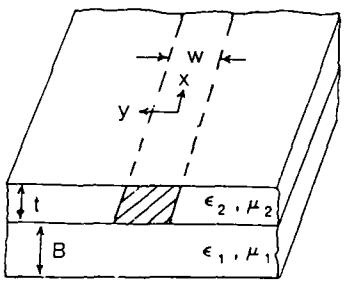

Fig. 2. Substrate-superstrate geometry.

Manuscript received February 7, 1986; revised May 29, 1986. This work was supported under U.S. Army Research Contract DAAG 29-83-K-0067 and Northrop Contract 82-110-1006.

D. R. Jackson is with the Electrical Engineering Department, University of Houston, Houston, TX 77004.

N. G. Alexópoulos is with the Electrical Engineering Department, University of California, Los Angeles, CA 90024.

IEEE Log Number 8610051.

0018-926X/86/1200-1430$01.00

used to significantly reduce the mutual impedance for dipoles in an endfire configuration. Finally, the effect of a superstrate layer on the coupling between a dipole and transmission line is examined, and the capacitive nature of the coupling is demonstrated.

II. Formulation for Current Reaction

A foundation for the numerical analysis of full-size planar strip structures is the calculation of the reaction between two x-directed currents. Denoting $J_1(x, y)$ and $J_2(x, y)$ as two such currents located at $z = z_1$ and $z = z_2$, respectively, the reaction is defined as

$$r_{12} = \langle J_1, J_2 \rangle = \int_{-\infty}^{+\infty} \int_{-\infty}^{+\infty} E_{x1}(x, y) J_2(x, y)\, dx\, dy \quad (1)$$

where E_{x1} is the E_x-field from current $J_1(x, y)$ and the integration is performed in the plane z_2. A starting point for this calculation is the Sommerfeld solution for the magnetic Hertzian vector potential at (x, y, z) due to an electric Hertzian dipole source at (x', y', z') where $z' = z_1$. This can be written in cylindrical coordinates as

$$\Pi_x = \int_0^{\infty} f(\lambda) J_0(\lambda r)\, d\lambda \quad (2)$$

$$\Pi_z = \cos\phi \int_0^{\infty} g(\lambda) J_1(\lambda r)\, d\lambda \quad (3)$$

where

$$r = [(x - x')^2 + (y - y')^2]^{1/2}$$

and $f(\lambda)$, $g(\lambda)$ are complicated functions of λ which also depend on z, z', although this dependence is not explicitly shown here (the time dependence $e^{+j\omega t}$ is also being suppressed throughout the analysis). These functions are given explicitly in [2]. The E_x-field in the plane z_2 is then found from

$$E_{x1}(x, y, z_2) = \int_{-\infty}^{+\infty} \int_{-\infty}^{+\infty} J_1(x', y') \cdot \left(k^2 \Pi_x + \frac{\partial^2 \Pi_x}{\partial x^2} + \frac{\partial^2 \Pi_z}{\partial x \partial z} \right)_{z = z_2} dx'\, dy' \quad (4)$$

where the integration is performed in the plane z_1, and k is the wavenumber at $z = z_2$, given as $k = k_0 n_i$ when z is in the ith layer, with n_i being the index of refraction of the ith layer. Because of the differentiation appearing in (4), it is convenient to write

$$\frac{\partial \Pi_z}{\partial z} = \cos\phi \int_0^{\infty} h(\lambda) J_1(\lambda r) \lambda\, d\lambda \quad (5)$$

where

$$h(\lambda) = \frac{1}{\lambda} \frac{\partial g}{\partial z}. \quad (6)$$

Equation (5) may be put into a similar form as (2) by using

$$\frac{\partial}{\partial x} J_0(\lambda r) = -\lambda \cos\phi\, J_1(\lambda r). \quad (7)$$

Both (2) and (5) are then in the form of cylindrical (Fourier-Bessel) transforms, and a conversion to rectangular (Fourier) form may be accomplished. Substituting (4) into (1) then results in the plane-wave spectrum form

$$r_{12} = \frac{1}{2\pi} \int_{-\infty}^{+\infty} \int_{-\infty}^{+\infty} \frac{1}{\lambda} [(k^2 - \lambda_x^2) f(\lambda) + \lambda_x^2 h(\lambda)] \cdot \tilde{J}_1(\lambda_x, \lambda_y) \tilde{J}_2(-\lambda_x, -\lambda_y)\, d\lambda_x\, d\lambda_y \quad (8)$$

where

$$\tilde{J}(\lambda_x, \lambda_y) = \int_{-\infty}^{+\infty} \int_{-\infty}^{+\infty} J(x', y') e^{-j(\lambda_x x' + \lambda_y y')}\, dx'\, dy'$$

and

$$\lambda = \sqrt{\lambda_x^2 + \lambda_y^2}.$$

Defining new origins (x_1, y_1) and (x_2, y_2) for currents J_1, J_2, and assuming the currents are even functions in x and y about the new origins, (8) can be written as

$$r_{12} = \frac{2}{\pi} \int_0^{\pi/2} \int_C [(k^2 - \lambda_x^2) f(\lambda) + \lambda_x^2 h(\lambda)] \tilde{J}_1(\lambda_x, \lambda_y) \cdot \tilde{J}_2(\lambda_x, \lambda_y) \cdot \cos(\lambda_x \Delta x) \cos(\lambda_y \Delta y)\, d\lambda\, d\tilde{\phi} \quad (9)$$

where $\Delta x = x_1 - x_2$, $\Delta y = y_1 - y_2$, and $\tilde{\phi} = \tan^{-1}(\lambda_y/\lambda_x)$.

The contour C in the Sommerfeld integration is from 0 to ∞, above the surface-wave poles. A root extraction technique is used to remove the singular behavior of the integrand [5], [6], and other numerical techniques are used to improve computational efficiency. A matrix storage of the complicated part of the integrand in brackets is one such technique, and the use of a Filon-type integration to account for the oscillatory nature of the cosine terms is another. In the application of Galerkin's method to the antenna geometries, a convenient choice of basis functions is

$$b(x, y) = \xi(x) \eta(y) \quad (10)$$

where

$$\xi(x) = \frac{\sin k_\epsilon (d - |x|)}{\sin k_\epsilon d}, \qquad |x| \le d \quad (11)$$

$$\eta(y) = \frac{4}{5w} \left(1 + \left| \frac{2}{w} y \right|^3 \right), \qquad |y| \le \frac{w}{2} \quad (12)$$

[7], [8]. An advantage of using (12) over the Maxwell current is faster convergence of the transform [8]. The planar strips of width w are then divided into N subsections of length d in the x direction, and the representation

$$J(x, y) = \eta(y) \sum_{n=1}^{N-1} I_n \xi(x - nd + L/2) \quad (13)$$

is used for each strip, with L the strip length and x measured from the strip center.

One of the difficulties in using (9) is that the cosine terms oscillate faster for increasing separation Δx, Δy between basis

functions. Furthermore, convergence is provided by the Fourier transforms $\tilde{J}_1$, $\tilde{J}_2$ when $z_1 = z_2$ since $f(\lambda)$ and $h(\lambda)$ are $0(1)$ as $\lambda \to \infty$, so the integration in λ must extend to further values as the size of the basis functions decrease. This makes the necessary computation for mutual impedance very time consuming when computing the reaction between basis functions which are small and widely separated. In this case it is convenient to formulate the reaction in the real-space domain. If the basis functions are approximated as point dipoles of current this is equivalent to simply evaluating the E_x-field of a Hertzian dipole, and this may be formulated in an efficient manner [9].

III. Microstrip Transmission Line

Using (8), an analysis of the propagation on a microstrip line is straightforward. A current expansion function of the form

$$J_1(x, y) = \eta(y) e^{-j\beta x} \tag{14}$$

is assumed on the line, and a testing function

$$J_2(x, y) = \delta(x)\delta(y) \tag{15}$$

is used, which forces the E_x-field at the strip center to be zero. This is equivalent in principle to the original formulation of Denlinger [8], although the approach is based here on the three-dimensional Green's function. Using the integral representation of the δ-function, the result

$$\int_0^\infty \frac{1}{\lambda} \tilde{\eta}(\lambda_y)[(k^2 - \beta^2) f(\lambda) + \beta^2 h(\lambda)] \, d\lambda_y = 0 \tag{16}$$

is obtained, where

$$\lambda = \sqrt{\beta^2 + \lambda_y^2}$$

and $\tilde{\eta}(\lambda_y)$ is the one-dimensional transform of $\eta(y)$. As pointed out in [11] the value of β must be greater than all surface-wave poles, since a residue contribution would result in a complex value for the integration, and a real-valued solution for β would not be possible.

Equation (16) allows for a convenient solution for the propagation on an infinitely thin strip. As $w \to 0$, $\tilde{\eta}(\lambda_y) \to 1$ and does not provide any convergence, so the term in brackets must vanish as $\lambda \to \infty$, resulting in

$$\beta^2 \sim k^2 \frac{f(\infty)}{f(\infty) - h(\infty)} \tag{17}$$

as $w \to 0$. From this formula the classical results for an infinitely thin wire may be obtained [12], [13], where the effective permittivity and permeability are

$$\epsilon_e = \frac{1}{2}(\epsilon_i + \epsilon_j), \quad \mu_e = \left[\frac{1}{2}(\mu_i^{-1} + \mu_j^{-1})\right]^{-1} \tag{18}$$

when the strip is at the interface between the ith and jth layers, and $\epsilon_e = \epsilon_i$, $\mu_e = \mu_i$ if the line is embedded within the ith layer. Equation (18) may be used as a basis for choosing k_e in (11), with $k_e = k_0\sqrt{\mu_e \epsilon_e}$ [6].

Results for a line at the interface ($z = B$) are shown in Fig. 3(a) for the case of a GaAs superstrate ($\epsilon_2 = 12.5$) over a teflon substrate ($\epsilon_1 = 2.1$). As the frequency increases, $\epsilon_e \to \epsilon_2$ since $\epsilon_2 > \epsilon_1$. The dispersion is less for the smaller line width at lower frequencies, but regardless of line width the solution is above the dominant TM_1 surface-wave mode here. As the superstrate thickness increases the amount of dispersion does as well, seen from Fig. 3(b). This is due to the fact that ϵ_2 is significantly larger than ϵ_1. If a superstrate with $\epsilon_2 = \epsilon_1$ is used instead, the dispersion would be less than without a superstrate.

IV. Center-Fed Dipole

For the three antenna geometries shown in Fig. 1, a moment solution using Galerkin's method is used. For the center-fed dipole the current distribution (13) is assumed, and a δ-gap excitation is taken at $x = 0$. The Z_{mn} coefficients of the Galerkin matrix then represent the reaction between basis functions centered at $x = md - L/2$ and $x = nd - L/2$ where L is the length of the dipole. The Galerkin set of matrix equations

$$[Z_{mn}][I_n] = [E_n] \tag{19}$$

is then formulated, where the excitation column vector E has components $E_n = \delta_{np}$ for N even, where $p = N/2$. A variational expression for the input impedance is [14]

$$Z_{in} = \frac{1}{I(0)^2} \sum_{m,n} Z_{mn} I_m I_n \tag{20}$$

where $I(0)$ is the current at $x = 0$. Using (19), this formula immediately reduces to the usual result $Z_{in} = 1/I(0)$. Once input impedance is found in this way, the resonant length may easily be determined. If the resonant length L_r is small compared to a wavelength, an approximate formula for the input resistance is [15]

$$R_r \simeq 120 \left(\frac{L_r}{\lambda_0}\right)^2 \frac{P_T}{15\pi^2/\lambda_0^2} \, (\Omega) \tag{21}$$

where p_T is the total (radiated + surface wave) power (in watts) delivered by a Hertzian dipole of strength 1 A-m at the same z location.

In Fig. 4(a) the exact resonant length of a dipole at the interface is shown, and compared with the approximate value

$$L_r/\lambda_0 \simeq 1/\sqrt{2(\epsilon_1 + \epsilon_2)} \tag{22}$$

as predicted by (18) when fringing fields are neglected in the infinitely narrow nonmagnetic case. When the thickness t becomes comparable to w the resonant length changes rapidly, becoming asymptotic to a limiting half-space value close to the value predicted by (22). In Fig. 4(b) the resonant input resistance is shown for the same case of Fig. 4(a), and compared with (21). From (21) it is seen that a superstrate affects resonant input resistance in two ways; by shortening the resonant length, and by changing P_T. The latter effect is discussed in [1].

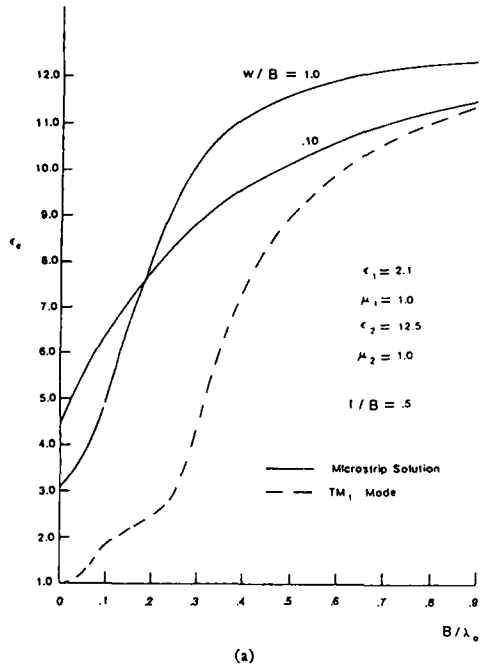

Fig. 3. (a) Effective dielectric constant versus substrate thickness for two different strip widths. (b) Effective dielectric constant versus substrate thickness for different superstrate thicknesses.

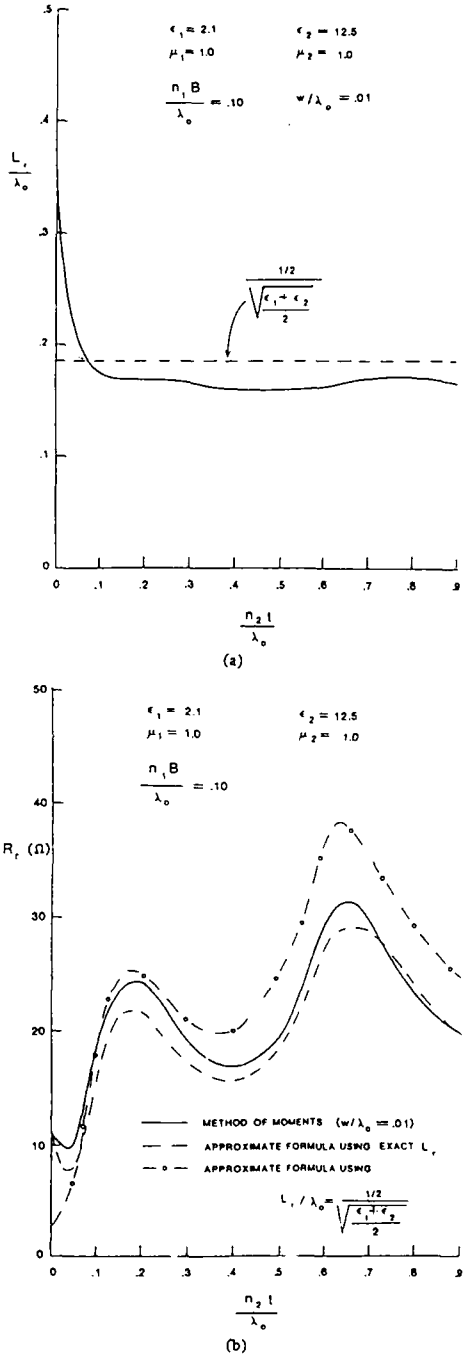

Fig. 4. (a) Resonant length versus superstrate thickness showing a comparison of exact and approximate values. (b) Resonant input resistance versus superstrate thickness showing a comparison of exact and approximate values.

V. Mutual Impedance Between Two Dipoles

The mutual impedance between two center-fed dipoles has been analyzed in two ways: by using the method of moments, and by using the electromotive force (emf) method. In the moment method approach basis functions are assumed on each dipole, with dipole 1 excited by a delta-gap source and dipole 2 short circuited. A partitioned Galerkin matrix set of equations is then solved to find the dipole currents. Using $[Z] = [Y]^{-1}$ where $[Y]$ is the admittance matrix results in the formula

$$Z_{12} = \frac{-1}{I_1(0)} \left[\frac{I_2(0)/I_1(0)}{1 - \left(\frac{I_2(0)}{I_1(0)} \right)^2} \right]. \tag{23}$$

Other formulas for Z_{12} may be derived, but an advantage of this form is the avoidance of numerical difficulties when $|I_2(0)| \ll |I_1(0)|$, which occurs for larger dipole separations.

In the emf method the mutual impedance is given by

$$Z_{12} = \frac{-1}{I_1(0) I_2(0)} \iint_{S_2} E_{x1}(x, y) J_2(x, y)\, dx\, dy \tag{24}$$

where E_{x1} is the field from the current J_1 on dipole 1 when excited in the absence of dipole 2, and J_2 is the current on dipole 2 (region denoted S_2) with dipole 1 open-circuited. Currents J_1 and J_2 are usually assumed, making the method approximate. In the case of infinitely narrow dipoles the currents become sinusoidal with an effective k_e as discussed in Section III however, allowing for an exact calculation. Since no self-term problems are encountered for separated dipoles, an efficient calculation of Z_{12} may be achieved using integration in real space. For narrow dipoles this approach is computationally more efficient, and has the advantage of being numerically stable as $w \to 0$ since there are no self-term problems.

For simplicity, results will be confined to the special case of both dipoles at $z = z_0$. First, a comparison of the moment solution with the emf method is shown in Fig. 5, for dipoles in an endfire configuration on a single teflon layer ($z_0 = B$). The real and imaginary parts of the mutual impedance, R_{12} and X_{12}, are plotted for several different strip widths. The moment method solution is used for the nonzero strip widths, and the emf method is used for the zero strip width. As can be seen from the figure, the moment solution converges toward the emf solution for narrower strip widths, supporting the validity of the assumed current using (18). Because all of the basic superstrate effects on mutual impedance can be seen from the infinitely narrow dipole case, the remainder of the results shown in this section will be for this case.

The basic properties of mutual impedance for dipoles in broadside or endfire configuration can be seen from Fig. 6, for dipoles on a single layer. The mutual impedance decays fairly rapidly with separation in the broadside case (Fig. 6(a)), but much slower in the endfire case (Fig. 6(b)). This is due to the fact that the far-field surface wave pattern of a transverse magnetic (TM)-mode wave is strongest in the endfire direction, having a null in the broadside direction [16]. The

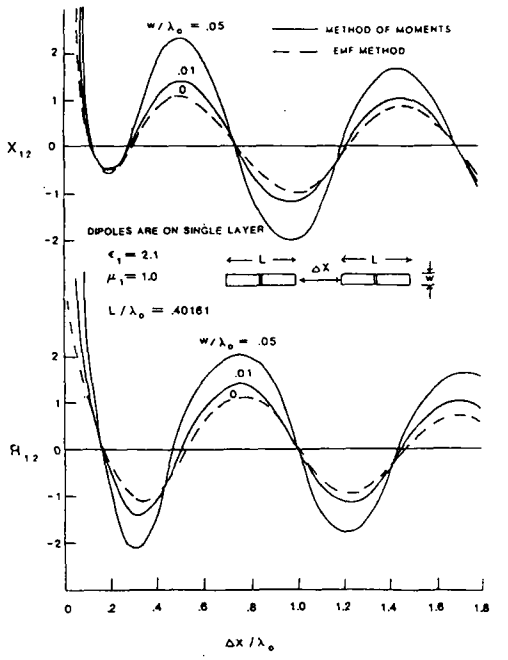

Fig. 5. Mutual impedance versus separation showing a comparison of the moment method solution for two different strip widths and the emf solution for zero strip width.

opposite is true for a transverse electric (TE)-mode wave, but for the layer thickness used here only the dominant TM mode exists. This strong endfire coupling is even more pronounced for dipoles on a magnetic layer, since the TM_1 mode is much more strongly excited. Such a case is shown in Fig. 7, where $\mu_1 = 10.0$. This strong endfire coupling can be reduced by using a superstrate layer to reduce or eliminate the surface waves. An example of this is shown in Fig. 8, in which a magnetic layer with $\mu_2 = 10.0$ is used as a superstrate over a teflon substrate, with $z_0 = B$. The superstrate thickness is chosen from

$$\frac{n_2 t_c}{\lambda_0} = \frac{n_2}{2\pi\sqrt{n_2^2 - n_1^2}} \tan^{-1} \left[\frac{\epsilon_2 \sqrt{n_1^2 - 1}}{\sqrt{n_2^2 - n_1^2}} \right] \tag{25}$$

which results in an elimination of all surface waves in this case. As discussed in [1], the elimination of surface waves is often difficult to achieve when using a nonmagnetic superstrate, because of the thin substrate limitation. However another way to reduce surface waves is by embedding the dipoles within the substrate layer and using a superstrate with a higher index of refraction. This reduces surface wave excitation due to the exponentially decaying nature of the surface-wave fields inside the substrate. An example showing mutual impedance for this configuration is presented in Fig. 9, where $z_0 = B/2$. Once the separation becomes sufficiently large in this case, the mutual impedance is very small. Also of interest

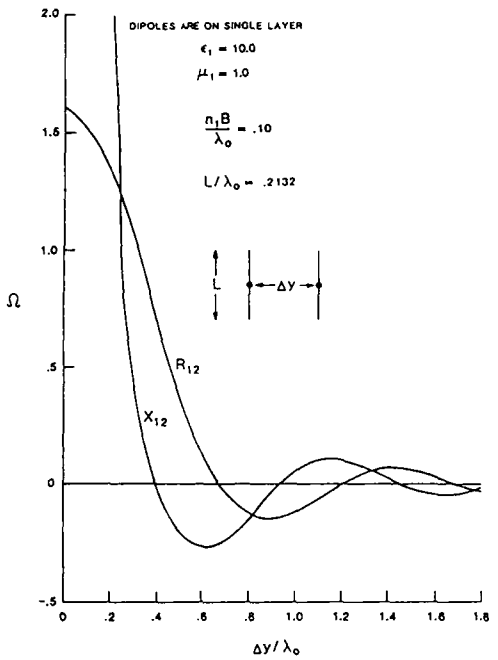

(a)

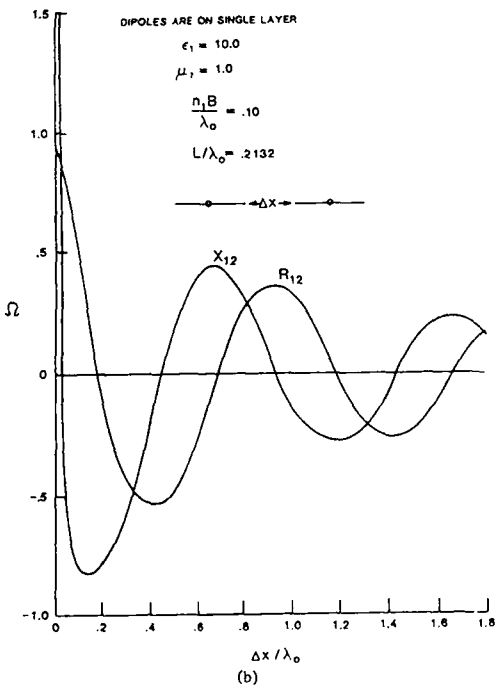

(b)

Fig. 6. (a) Mutual impedance versus separation for dipoles in broadside configuration on a single layer. (b) Mutual impedance versus separation for dipoles in endfire configuration on a single layer.

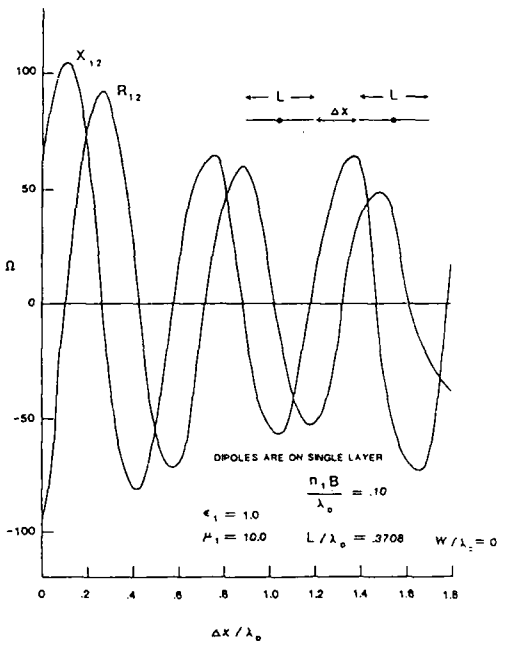

Fig. 7. Mutual impedance versus separation for dipoles in endfire configuration on a single magnetic layer.

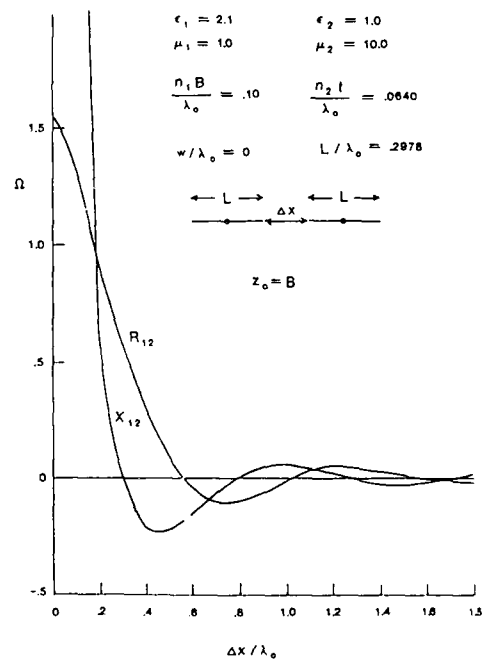

Fig. 8. Mutual impedance versus separation for dipoles in endfire configuration with a superstrate used to eliminate surface waves.

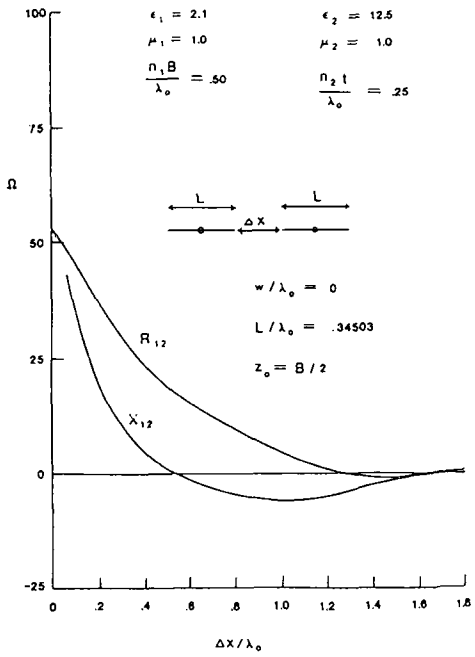

Fig. 9. Mutual impedance versus separation for dipoles in endfire configuration embedded in the middle of the substrate.

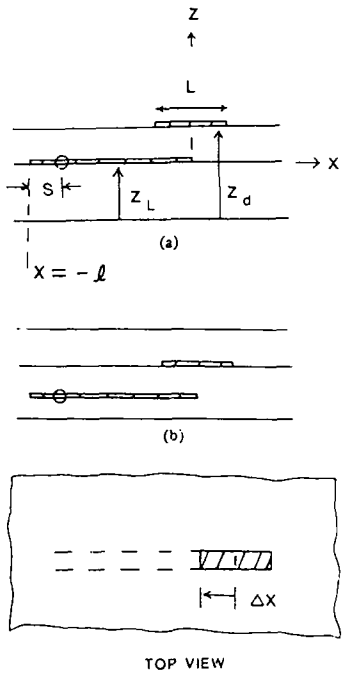

Fig. 10. Geometry of coupling between dipole and transmission line. (a) Dipole on top of superstrate. (b) Dipole at the interface.

is the almost monotonic nature of the curves in this case, which can be explained by assuming the superstrate acts as a conductor for the space-wave fields, and using image theory. The images will add in phase for z_0 and $B - z_0$ an odd number of electrical quarter-wavelengths in the substrate.

VI. Dipole Excitation by Transmission-Line Coupling

Another configuration which has been analyzed using the moment approach is the strip dipole excited by electromagnetic coupling to a microstrip transmission line, shown in Fig. 10. This problem has been successfully analyzed with the moment method in the past for the line and dipole within a single layer [17]. A δ-gap source is placed near the end of the line as shown, and the same procedure as for the mutual impedance is used to find the line and dipole currents. From this information the normalized admittance Y/Y_0 may be found, referred to the dipole-end of the line. For fixed line and dipole heights z_L and z_d, an input match may be achieved by varying the dipole length L and offset in either the x or y directions, provided z_L and z_d are sufficiently close. An offset variation in the x direction was chosen here in order to take advantage of an efficient matrix storage procedure for the reaction values. The offset is then taken in integral number of subsections, $\Delta x = N \cdot d$.

One of the main objectives in feeding a dipole in this manner is to minimize the radiation from the line while maintaining a significant radiation from the dipole. This implies keeping z_L small, while simultaneously keeping a prescribed level of coupling between the two. Also, to have a significant bandwidth, z_d should not be too small. However, decreasing z_L lowers the coupling for a fixed z_d, so it is important to investigate ways of increasing the coupling. One approach is to stack multiple dipoles above the line [18]. Another approach is to choose a different material between the line and dipole. Qualitatively, the coupling between the line and dipole may be regarded as largely capacitive, which suggests an improved coupling using $\epsilon_2 > \epsilon_1$ in the geometry of Fig. 10(a). To verify this, the end admittance is plotted versus offset for different dipole lengths in Figure 11(a) for the case of $\epsilon_1 = \epsilon_2 = 2.1$. As can be seen, the coupling is not sufficient to allow for an input match with the layer thicknesses used. In Fig. 11(b) the same layer electrical thicknesses are used, but with $\epsilon_2 = 10.0$. In this case the coupling is sufficiently strong to allow for an input match, for $L/\lambda_0 \simeq 0.186$ and $\Delta x/\lambda_0 \simeq 0.123$. In Fig. 11(c) a magnetic superstrate is used, with $\mu_2 = 10.0$. The coupling in this case is not significantly different than the case of Fig. 11(a), supporting the conclusion of a capacitive-like coupling mechanism. A similar improvement in coupling is possible when using stacked dipoles. The stacked dipole approach allows for an even greater improvement in bandwidth, but the total physical layer thickness will be larger when using $\epsilon_2 \simeq \epsilon_1$.

The dipole can also be placed at the interface and excited by a line in the substrate, as shown in Fig. 10(b). In this case the superstrate is not improving coupling, but may be used to increase the efficiency of the dipole or achieve other desired effects [1].

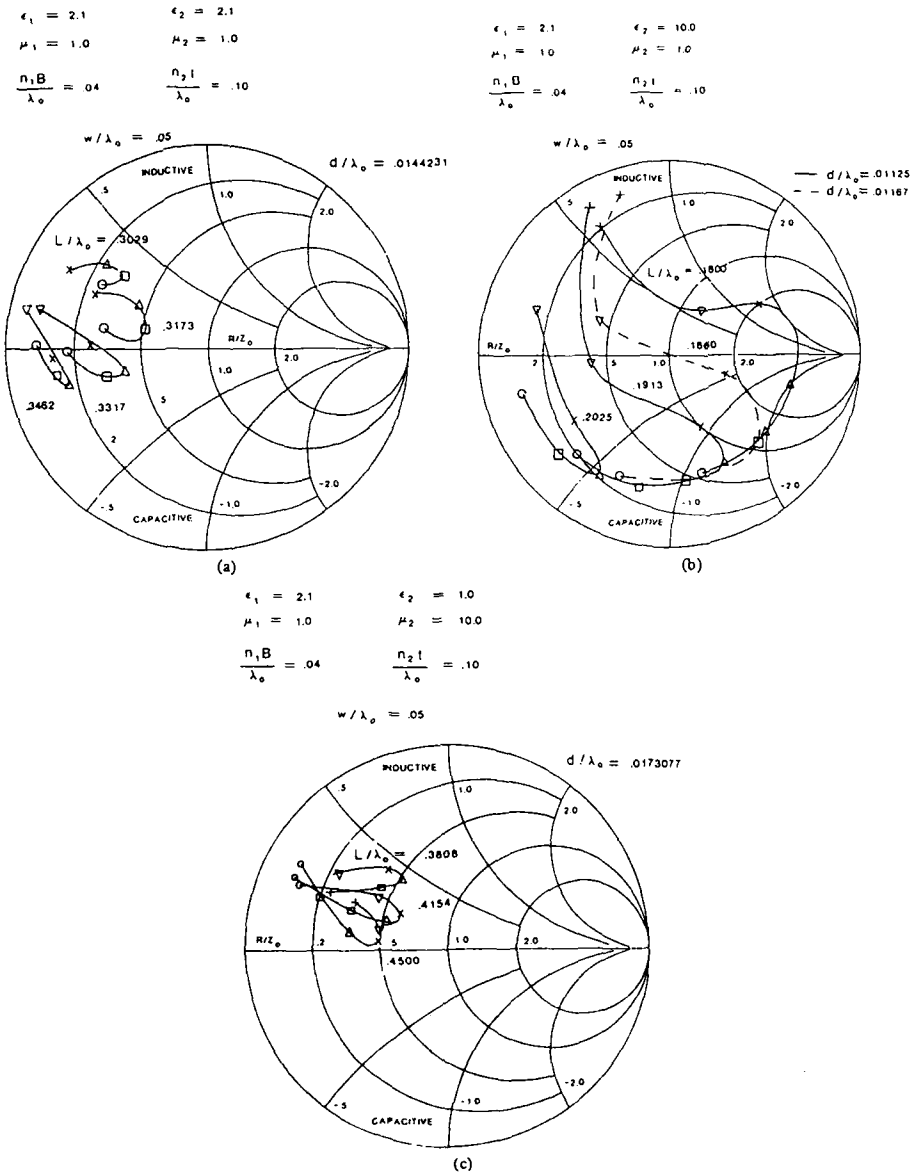

Fig. 11. (a) Normalized end admittance versus offset for different dipole lengths with $\epsilon_2 = \epsilon_1 = 2.1$. The offset along each curve is specified by $\Delta x = N \cdot d$ with $N = 4, 8, 12, 16, 20$ corresponding to points O, □, Δ, X, ▽, respectively. (b) Normalized end admittance versus offset for different dipole lengths with $\epsilon_2 = 10.0$, $\epsilon_1 = 2.1$. The dashed curve shows a dipole length which allows for an input match. The offset along each curve is specified by $\Delta x = N \cdot d$ with $N = 3, 5, 7, 10, 11, 12$ corresponding to points O, □, Δ, X, ▽, +, respectively. (c) Normalized end admittance versus offset for different dipole lengths with $\mu_2 = 10.0$, $\epsilon_1 = 2.1$. The offset along each curve is specified by $\Delta x = N \cdot d$ with $N = 8, 12, 14, 16, 18, 20$ corresponding to points O, □, Δ, X, ▽, +, respectively.

VII. Conclusion

Four geometries consisting of planar strips in a substrate-superstrate configuration have been analyzed, including the microstrip transmission line, the center-fed dipole, the mutual impedance between two dipoles, and the transmission-line coupled dipole. The starting point in the analysis of each of these was the plane-wave spectrum formulation for the reaction between two current sources. A real-space evaluation technique for finding the electric field was also used, which improved the efficiency of the moment-method calculation for mutual impedance, and also allowed for an easy determination of the mutual impedance between infinitely narrow dipoles.

For the microstrip transmission line, the amount of dispersion was seen to significantly increase as a superstrate is added when ϵ_2 is much larger than ϵ_1. The dispersion decreases as the line width decreases, although β must always be above the largest surface-wave pole. In the case of the center-fed dipole, the resonant length and input resistance were found from the moment method and compared with simple approximate formulas. These approximate formulas allow for an easy extension of Hertzian dipole results to the resonant strip dipole. The mutual impedance between dipoles was then investigated using both the moment method and the emf method. The emf method allows for an efficient computation for the case of very narrow dipoles, and gives accurate results when the proper value of k_e is used in the assumed current. It was demonstrated that a superstrate may be used to significantly decrease the mutual impedance between dipoles, especially for dipoles in an endfire configuration, by reducing or eliminating surface waves. Finally, results were shown for the case of a dipole excited by coupling to a transmission line, and it was verified that the coupling mechanism is predominantly capacitive. Hence the coupling is improved by using a material with a higher dielectric constant between the line and dipole.

References

[1] N. G. Alexopoulos and D. R. Jackson, "Fundamental superstrate (cover) effects on printed circuit antennas," *IEEE Trans. Antennas Propagat.*, vol. AP-32, pp. 807-816, 1984.

[2] ——, "Fundamental superstrate (cover) effects on printed circuit antennas," UCLA Rep. ENG-83-50, Oct. 1983.

[3] N. G. Alexopoulos, D. R. Jackson, and P. B. Katehi, "Criteria for nearly omnidirectional radiation patterns for printed antennas," *IEEE Trans. Antennas Propagat.*, vol. AP-33, pp. 195-205, Feb. 1985.

[4] D. R. Jackson and N. G. Alexopoulos, "Gain enhancement methods for printed circuit antennas," *IEEE Trans. Antennas Propagat.*, vol. AP-33, pp. 976-987, Sept. 1985.

[5] N. K. Uzunoglu, N. G. Alexopoulos, and J. G. Fikioris, "Radiation properties of microstrip dipoles," *IEEE Trans. Antennas Propagat.*, vol. AP-27, pp. 853-858, Nov. 1979. (See also correction, *IEEE Trans. Antennas Propagat.*, vol. AP-30, p. 526, May 1982.)

[6] D. M. Pozar, "Input impedance and mutual coupling of rectangular microstrip antennas," *IEEE Trans. Antennas Propagat.*, vol. AP-30, pp. 1191-1196, Nov. 1982.

[7] I. E. Rana and N. G. Alexopoulos, "Current distribution and input impedance of printed dipoles," *IEEE Trans. Antennas Propagat.*, vol. AP-29, pp. 99-106, Jan. 1981.

[8] E. J. Denlinger, "A frequency dependent solution for microstrip transmission lines," *IEEE Trans. Microwave Theory Tech.*, vol. MTT-19, pp. 30-39, Jan. 1971.

[9] D. R. Jackson and N. G. Alexopoulos, "An asymptotic extraction technique for evaluating Sommerfeld-type integrals," *IEEE Trans. Antennas Propagat.*, pp. 1467-1470, this issue.

[10] D. M. Pozar, "Improved computational efficiency for the moment method solution of printed dipoles and patches," *Electromagn.*, vol. 3, no. 3-4, pp. 299-309, July-Dec. 1983.

[11] R. W. Jackson and D. M. Pozar, "Full-wave analysis of microstrip open-end and gap discontinuities," *IEEE Trans. Microwave Theory Tech.*, vol. MTT-33, pp. 1036-1042, Oct. 1985.

[12] J. R. Wait, "Theory of wave propagation along a thin wire parallel to an interface," *Radio Sci.*, vol. 7, pp. 675-679, June 1972.

[13] R. A. Pucel and D. J. Masse, "Microstrip propagation on magnetic substrates—Part I: design theory," *IEEE Trans. Microwave Theory Tech.*, vol. MTT-20, pp. 304-308, May 1972.

[14] V. H. Rumsey, "Reaction concept in electromagnetic theory," *Phy. Rev.*, vol. 94, pp. 1483-1491, June 1954.

[15] D. R. Jackson and N. G. Alexopoulos, "Microstrip dipoles on electrically thick substrates," *Int. J. Infrared and Millimeter Waves*, Jan. 1986.

[16] N. G. Alexopoulos and I. E. Rana, "Mutual impedance computation between printed dipoles," *IEEE Trans. Antennas Propagat.*, vol. AP-29, pp. 106-111, Jan. 1981.

[17] P. B. Katehi and N. G. Alexópoulos, "On the modeling of electromagnetically coupled microstrip antennas—The printed strip dipole," *IEEE Trans. Antennas Propagat.*, vol. AP-32, pp. 1179-1186, Nov. 1984.

[18] ——, "A bandwidth enhancement method for microstrip antennas," in *1985 IEEE Antennas Propagat. Soc. Symp. Dig.*, vol. 1, pp. 405-408.

[19] A. J. M. Soares, S. B. A. Fonseca, and A. J. Giarola, "The effect of a dielectric cover layer on the current distribution and input impedance of printed dipoles," *IEEE Trans. Antennas Propagat.*, vol. AP-32, pp. 1149-1153, Nov. 1984.

David R. Jackson (S'83-M'84), for a photograph and biography please see page 816 of the August 1984 issue of this TRANSACTIONS.

Nicólaos G. Alexópoulos (S'68-M'69-SM'82), for a photograph and biography please see page 39 of the January 1983 issue of this TRANSACTIONS.

RESONANT FREQUENCY OF ELECTRICALLY THICK RECTANGULAR MICROSTRIP ANTENNAS

Indexing terms: Antennas, Microstrip

An algebraic formulation for the resonant frequency of a rectangular microstrip antenna has been derived which is valid for electrically thick substrates. Predicted values of resonance are compared with previous theories, as well as actual experimental measurements, for radiators approaching one-quarter wavelength in thickness.

Introduction: Rectangular microstrip patch antennas are among the most widely used printed-circuit antennas. A comprehensive analysis of the configuration has been carried out by a number of authors, resulting in simple design equations for the resonant frequency, input impedance, beamwidth and bandwidth.[1,2] The bandwidth of the rectangular patch is typically very small for low-profile, electrically thin configurations. One of the techniques to increase the bandwidth is to increase the thickness proportionately. However, most of the design equations for the resonant frequency are only accurate for thin patches, normally of the order of $h/\lambda \leq 0{\cdot}02$, where h is the thickness of the dielectric substrate and λ is the wavelength in the substrate. In this letter we present a simple semi-empirical design equation for the resonant frequency of an electrically thick rectangular patch.

Analysis: The design equation is based on the simple observation that the open-end extension of a rectangular patch is related to the edge extension of a similar transmission line. In the case of striplines or triplate lines these extensions are given by b ln $(2/\pi)$, independent of the dielectric constant of the substrate and frequency for wide strips ($W/b \gg 0{\cdot}10$). However, in the case of microstrip such a simple behaviour is not expected to exist because of the inhomogeneity of the medium above the ground plane.

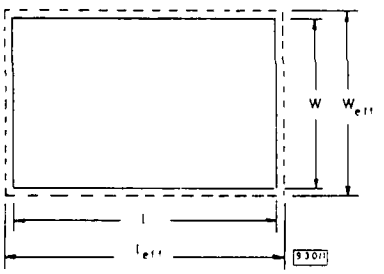

Fig. 1 *Geometry of rectangular microstrip antenna*

The resonant frequency f_{mn} of a rectangular patch of width W and length l, both comparable to $\lambda/2$, is given by

$$f_{mn} = \frac{c}{2\sqrt{(\varepsilon_d)}} \sqrt{\left[\left(\frac{m}{W_{eff}}\right)^2 + \left(\frac{n}{l_{eff}}\right)^2\right]} \tag{1}$$

where ε_d is the dynamic dielectric constant for the patch defined by Wolff and Knoppik,[3] and W_{eff} and l_{eff} are the effective dimensions taking into account the energy stored in the fringing fields. The physical and effective dimensions of the patch are shown in Fig. 1. To determine W_{eff} we consider $W_{eff} = W + \Delta W$, where ΔW is the open-end effect, which according to the observation above is related to the edge effect of a microstrip line of width l. This is given by

$$\Delta W = f(\varepsilon_r)(l_{eq} - l) \tag{2}$$

where l_{eq} is the equivalent dimension obtained from the planar waveguide model:[4]

$$l_{eq} = \frac{120\pi h}{Z_0(l)\sqrt{\varepsilon_{re}(l)}} \tag{3}$$

The function $f(\varepsilon_r)$ describes the influence of the dielectric inhomogeneity on ΔW. It is taken to be the same as previously found for the open end of the microstrip line:

$$f(\varepsilon_r) = \frac{1}{2}\,\frac{\varepsilon_{re}(l) + 0{\cdot}3}{\varepsilon_{re}(l) - 0{\cdot}258} \tag{4}$$

In eqn. 4, $\varepsilon_{re}(l)$ means that ε_{re} is the effective dielectric constant of a microstrip line of width l. Using eqns. 2 and 3 in the expression for W_{eff}, we obtain

$$W_{eff} = W + \left(\frac{l_{eq} - l}{2}\right)\frac{\varepsilon_{re}(l) + 0{\cdot}3}{\varepsilon_{re}(l) - 0{\cdot}258} \tag{5}$$

Similarly, l_{eff} is given by

$$l_{eff} = l + \left(\frac{W_{eq} - W}{2}\right)\frac{\varepsilon_{re}(W) + 0{\cdot}3}{\varepsilon_{re}(W) - 0{\cdot}258} \tag{6}$$

Results: For evaluating ε_{re} the simple expression due to Schneider[5] was used:

$$\varepsilon_{re} = \frac{\varepsilon_r + 1}{2} + \frac{\varepsilon_r - 1}{2}\left[1 + \frac{10}{W/h}\right]^{-1/2} \tag{7}$$

For calculating Z_0 for a given value of W/h, the equations provided by Wheeler were used.[4] The effect of dispersion was ignored. The resonant frequency f_{10} obtained using the design equation given here is compared with that due to James *et al.*[2]

Table 1 CALCULATED AND MEASURED NORMALISED RESONANT FREQUENCIES

l	W	h/λ	f_0	f_{mn}	f_{en}	f_{jn}	f_{hn}
5·70	3·80	0·037	2·586	0·893	0·918	0·889	0·920
4·55	3·05	0·047	3·222	0·897	0·899	0·866	0·900
2·95	1·95	0·068	5·039	0·841	0·848	0·816	0·861
1·95	1·30	0·094	7·559	0·773	0·786	0·754	0·810
1·70	1·10	0·110	8·934	0·761	0·754	0·724	0·785
1·40	0·90	0·125	10·919	0·705	0·715	0·683	0·750
1·20	0·80	0·141	12·284	0·673	0·693	0·662	0·733
1·05	0·70	0·148	14·039	0·651	0·664	0·633	0·710
0·90	0·60	0·166	16·378	0·626	0·629	0·600	0·683
1·70	1·10	0·229	8·934	0·529	0·513	0·484	0·590

$\varepsilon_r = 2{\cdot}33$, $h = 0{\cdot}3175$ cm (except last entry, where $h = 0{\cdot}9525$ cm)

and Hammerstad[6] in Table 1. The set of parameters for the rectangular patch are those given by Chang *et al.*[6] In each case a normalised resonant frequency is found by dividing the actual value of resonant frequency by f_0, the zero-order prediction assuming the substrate is infinitesimally thin and that W is one-half wavelength in the dielectric. For units of c in

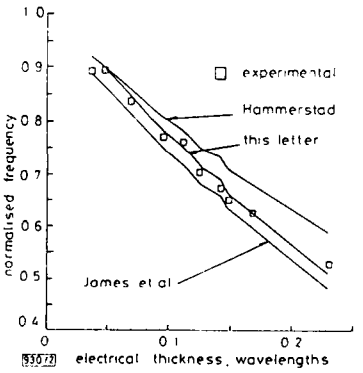

Fig. 2 *Calculated and measured normalised resonant frequencies*

$\varepsilon_r = 2{\cdot}33$, $h = 0{\cdot}3175$ cm (except last entry, where $h = 0{\cdot}9525$ cm)

Reprinted from ELECTRONICS LETTERS 8th October 1987 Vol. 23 No. 21 pp. 1149-1151

metres/second and those of W in centimetres, $f_0 = 15/(W\sqrt{\varepsilon_r})$ GHz. The entries for f_{mn}, f_{en}, f_{jn} and f_{hn} thus represent, respectively, the values measured, calculated by this method, calculated by James *et al.*, and calculated by Hammerstad divided by the appropriate f_0. The graphical representation of these data in Fig. 2 shows that the resonant frequencies predicted here lie in between those calculated by the other two methods, and are closer to measured values for most of the cases. An overall accuracy of approximately 3% was found for values of electrical thickness $h/\lambda \leq 0{\cdot}229$.

Acknowledgments: This work was supported by the US Army Research Office through contract DAAG29-84-K-0166 and by a grant from the Texas Advanced Technology Research Programme.

R. GARG
S. A. LONG

Department of Electrical Engineering
University of Houston
Houston, TX 77004, USA

18th August 1987

References

1 BAHL, I. J., and BHARTIA, P.: 'Microstrip antennas' (Artech House, 1980)

2 JAMES, J. R., HALL, P. S., and WOOD, C.: 'Microstrip antennas—theory and design' (Peter Peregrinus, 1981)

3 WOLFF, I., and KNOPPIK, N.: 'Rectangular and circular microstrip disk capacitors and resonators', *IEEE Trans.*, 1974, MTT-22, pp. 857–864

4 GUPTA, K. C., GARG, R., and BAHL, I. J.: 'Microstrip lines and slotlines' (Artech House, 1979)

5 SCHNEIDER, M. V.: 'Microstrip lines for microwave integrated circuits', *Bell Syst. Tech. J.*, 1969, **48**, pp. 1422–1444

6 CHANG, E., LONG, S. A., and RICHARDS, W. F.: 'An experimental investigation of electrically thick rectangular microstrip antennas', *IEEE Trans.*, 1986, AP-34, pp. 767–772

Communications

An Improved Formula for the Resonant Frequencies of the Triangular Microstrip Patch Antenna

RAMESH GARG AND STUART A. LONG, SENIOR MEMBER, IEEE

***Abstract*—An improved formula is derived to predict the resonant frequency of the triangular microstrip patch antenna. The technique previously used for the case of a circular disk is modified to produce greater accuracy than previous investigations.**

INTRODUCTION

Recently, Dahele and Lee [1] have reported on the resonant frequencies of an equilateral triangular microstrip patch. The calculated values of these frequencies, based on an effective length a_{eff} and an effective relative permittivity ϵ_{eff}, have been compared with measured values. A comparison with measured values, however, shows some reasonable difference between the two. Here, we show that if a different effective length and just the actual substrate permittivity are used, the computed values are much closer to the measured values.

CALCULATIONS

To compute the resonant frequency of an equilateral triangular patch, the effect of the fringing field can be assumed the same as that of an equivalent circular disk which has the same metalized area as the given triangular patch. Previously, the effective radius a_e of the circular disk was given [2]:

$$a_e = a\sqrt{1+\frac{2h}{\pi\epsilon_r a}\left(\ln\frac{\pi a}{2h}+1.7726\right)} \tag{1}$$

where a is the radius of the disk and h is the substrate thickness. This formula can then be modified to provide a reasonably accurate prediction of the resonant frequency of the triangular patch by substituting an equivalent sidelength, a_{eq}, into (1) in the place of a to then produce a new effective sidelength. This can be done by defining a_{eq} such that $S = \pi a_{eq}$ where S is the area of the original triangular patch. Then this value of a_e can be used in the formula for the resonant frequency [1]:

$$f_{m,n,l} = \frac{2c}{3a_e(\epsilon_r)^{1/2}}(m^2+mn+n^2)^{1/2} \tag{2}$$

where c is the velocity of light and the integers m, n, l satisfy the condition $m + n + l = 0$.

This approach was first suggested by Suzuki and Chiba [3] for the case of a pentagonal patch. The results are shown in Table I, along with the previous theories [1] and experimental data. As can be seen the new method consistently predicts resonant frequencies more accurately through the first five resonances.

Manuscript received August 20, 1987. This work was supported in part by the U.S. Army Research Office under Contract DAAG29-84-K-0166 and by a grant from the Texas Advanced Technology Research Program.

The authors are with the Department of Electrical Engineering, University of Houston, Houston, TX 77004.

IEEE Log Number 8719160.

RESONANT FREQUENCIES OF AN EQUILATERAL TRIANGULAR PATCH ANTENNA (a = 10 cm, ϵ_r = 2.32, AND h = 0.159 cm)

Mode	Measured GHz	Calculated (GHz) a_{eff} and ϵ_{eff} [1]	Calculated (GHz) a_{eff} and ϵ_r [1]	Calculated (GHz) a_e and ϵ_r
$TM_{1,0,-1}$	1.280	1.413	1.299	1.273
$TM_{1,1,-2}$	2.242	2.447	2.252	2.239
$TM_{2,0,-2}$	2.550	2.826	2.599	2.546
$TM_{2,1,-3}$	3.400	3.738	3.439	3.419
$TM_{3,0,-3}$	3.824	4.238	3.899	3.819

REFERENCES

[1] J. S. Dahele and K. F. Lee, "On the resonant frequencies of the triangular patch antenna," *IEEE Trans. Antennas Propagat.*, vol. AP-35, pp. 100-101, Jan. 1987.

[2] L. C. Shen and S. A. Long, "The resonant frequency of a circular disc, printed-circuit antenna," *IEEE Trans. Antennas Propagat.*, vol. AP-25, pp. 595-596, July 1977.

[3] Y. Suzuki and T. Chiba, "Computer analysis method for arbitrarily shaped microstrip antenna with multiterminals," *IEEE Trans. Antennas Propagat.*, vol. AP-32, pp. 585-590, June 1984.

0018-926X/88/0400-0570$01.00

IEEE TRANSACTIONS ON ANTENNAS AND PROPAGATION, VOL. 36, NO. 7, JULY 1988

A Leaky-Wave Analysis of the High-Gain Printed Antenna Configuration

DAVID R. JACKSON, MEMBER, IEEE, AND ARTHUR A. OLINER, LIFE FELLOW, IEEE

Abstract—A leaky-wave analysis is used to explain the narrow-beam "resonance gain" phenomenon, in which narrow beams may be produced from a printed antenna element in a substrate-superstrate geometry. The leaky-wave approach furnishes insight into the physical processes involved, provides new practical information, and permits the derivation of simple asymptotic formulas for the leaky-wave properties and for the radiation behavior. Results are presented as a function of frequency, the scan angle, and the ϵ of the superstrate.

I. Introduction

RECENTLY, a method for increasing the gain of a printed-circuit antenna involving the use of a superstrate layer was discussed [1]. In this method the antenna element is embedded within a two-layered geometry consisting of a bottom (substrate) layer of thickness b having relative permittivity and permeability ϵ_1, μ_1, and a top (superstrate) layer having parameters ϵ_2, μ_2, as shown in Fig. 1. As explained in [1], a narrow beam about any desired angle θ_p may be obtained for $\epsilon_2 \gg 1$ or $\mu_2 \gg 1$ when the layer thicknesses are chosen properly. In particular, the following dual types of "resonance conditions" are discussed in [1].

Case 1:

$$\frac{n_1 b}{\lambda_0}\sqrt{1-\sin^2\theta_p/n_1^2}=\frac{m}{2} \tag{1}$$

$$\frac{n_2 t}{\lambda_0}\sqrt{1-\sin^2\theta_p/n_2^2}=\frac{(2p-1)}{4} \tag{2}$$

for $\epsilon_2 \gg 1$.

Case 2:

$$\frac{n_1 b}{\lambda_0}\sqrt{1-\sin^2\theta_p/n_1^2}=\frac{(2m-1)}{4} \tag{3}$$

$$\frac{n_2 t}{\lambda_0}\sqrt{1-\sin^2\theta_p/n_2^2}=\frac{(2p-1)}{4} \tag{4}$$

for $\mu_2 \gg 1$, where $n_1 = \sqrt{\epsilon_1\mu_1}$, $n_2 = \sqrt{\epsilon_2\mu_2}$ and m, n are positive integers.

When (1), (2) or (3), (4) are satisfied, the gain at θ_p becomes increasingly large as $\epsilon_2 \to \infty$ or $\mu_2 \to \infty$, respectively, with a resultant decrease in beamwidth. Asymptotic formulas for gain and beamwidth are presented in [1]. Although providing for convenient formulas, this derivation does not by itself provide any *insight* into the fundamental cause of the narrow-beam phenomenon.

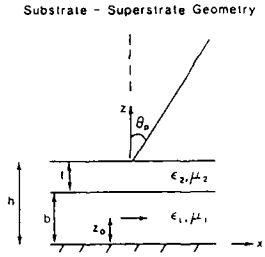

Fig. 1. Two-layered geometry with embedded dipole antenna element from which narrow beam can be radiated. ϵ_2 (or μ_2) of superstrate (upper layer) must be greater than ϵ_1 (or μ_1) of substrate. Horizontal antenna element is located at height z_0 and peak of radiated beam occurs at angle θ_p.

In this article it is shown that the resonance gain effect may be elegantly described in terms of *leaky waves.* It is demonstrated that the phenomenon is attributable to the presence of both transverse electric (TE)- and transverse magnetic (TM)-mode leaky waves which are excited on the structure. Asymptotic formulas for the leaky-wave properties are derived, which demonstrate that the attenuation rate of the leaky waves decreases as the gain of the pattern increases. The migration with frequency of the leaky-wave poles in the steepest-descent plane is also discussed, and it is shown that several important physical effects are confirmed by that investigation. Radiation patterns based on the relevant leaky wave are then compared with the exact patterns to demonstrate the dominant role of the leaky waves in determining the pattern. One practical result of this investigation is a simple rule for determining the size of the structure necessary to produce the narrow-beam patterns, a result which would be difficult to obtain otherwise.

Due to the similarity of results, only case 1 ($\epsilon_2 \gg 1$) will be discussed. This is the more practical of the two cases, since low-loss high-permeability materials are difficult to obtain.

II. Leaky-Wave Poles and the Steepest-Descent Representation

The theory of leaky waves and their role in determining the radiation behavior of certain antennas is well established [2]–[7]. To emphasize the main points, the analysis for the case of a horizontal Hertzian electric dipole in the stratified medium

Manuscript received March 20, 1987; revised September 24, 1987. This work was supported in part by the Army Research Office under Contract DAAG29-84-K-0166.

D. R. Jackson is with the Cullen College of Engineering, University of Houston, 4800 Calhoun Road, Houston, TX 77004.

A. A. Oliner is with the Polytechnic University, 333 Jay Street, Brooklyn, NY 11201.

IEEE Log Number 8820226.

0018-926X/88/0700-0905$01.00

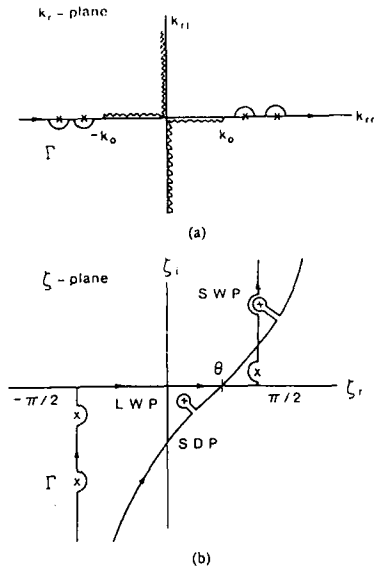

Fig. 2. (a) k_z-plane, where k_z is wavenumber transverse to z direction. Surface-wave poles lie along real axis (denoted by x's) and branch cuts (wiggly lines) emanate from branch points $\pm k_0$. Integration path Γ is deformed around surface-wave poles in accordance with conventional assumption of infinitesimal loss (and $e^{j\omega t}$ time dependence). Branch cuts are chosen so that upper Riemann sheet is proper, whereas lower Riemann sheet is improper. Leaky-wave poles occur on improper (lower) sheet. (b) Steepest-descent plane corresponding to time dependence $e^{j\omega t}$. Saddle-point is present at $\zeta = 0$ on real axis, and example is given of leaky-wave pole and surface-wave pole captured by deformation from original path Γ to steepest-descent path.

of Fig. 1 will be considered. Starting with the classical Sommerfeld solution [8], the expressions for the fields are written in terms of the Hertzian magnetic vector potential $\bar{\Pi}$ as

$$\bar{H} = j\omega\epsilon \nabla \times \bar{\Pi} \tag{5}$$

$$\bar{E} = k^2 \bar{\Pi} + \nabla(\nabla \cdot \bar{\Pi}). \tag{6}$$

After solving the boundary-value problem for $\bar{\Pi}$, the two components of the potential Π_x and Π_z may be written in the region $z > h$ as (suppressing $e^{+j\omega t}$)

$$\Pi_x(r, z) = \int_{-\infty}^{+\infty} \frac{f(k_r r)}{D_e(k_r)} e^{-jk_z(z-h)} H_0^{(2)}(k_r r)\, dk_r \tag{7}$$

$$\Pi_z(r, z) = \cos\phi \int_{-\infty}^{+\infty} \frac{g(k_r r)}{D_e(k_r) D_m(k_r)} e^{-jk_z(z-h)} H_1^{(2)}(k_r r)\, dk_r \tag{8}$$

where

$$r = \sqrt{x^2 + y^2}$$

$$k_z = (k_0^2 - k_r^2)^{1/2}.$$

In these expressions f, g, D_e, and D_m are complicated functions [9] of the integration variable k_r. D_e and D_m have zeros on the real axis of the k_r plane in the range $k_0 \le k_r \le \max(k_i)$, where k_i is the wavenumber in the ith layer. These zeros correspond to TE- and TM-mode surface waves, respectively. The integration path goes around these poles, as shown in Fig. 2(a). Branch cuts from the branch points at $\pm k_0$ are also necessary to define the proper branch interpretation of k_z, which is $\mathrm{Im}(k_z) < 0$, corresponding to fields that decay as z increases.

The steepest-descent transformation

$$k_r = k_0 \sin\zeta \tag{9}$$

$$k_z = k_0 \cos\zeta \tag{10}$$

then results in an integration along the contour Γ in the steepest-descent ζ-plane, shown in Fig. 2(b). This contour may be deformed into the steepest-descent path (SDP) which passes through the saddle point at $\zeta = \theta$, where R, θ, ϕ describe the observation point in spherical coordinates with $r = R\sin\theta$, $z - h = R\cos\theta$. The far-field evaluations of (7), (8) may be obtained via the saddle point method in the usual way [7]. It is important to recognize that the single-sheeted steepest-descent plane as a whole is neither proper nor improper, but in fact portions of it are proper and other portions improper. The semi-infinite strip for which $0 < \zeta_r < \pi/2$ and $\zeta_i < 0$ is an improper region ($\mathrm{Im}(k_z) > 0$). Complex zeros of $D_e(k_r)$, $D_m(k_r)$ may exist in this region at $\zeta_{rp} + j\zeta_{ip}$, which result in TE- and TM-mode "leaky-wave" poles (LWP). Complex poles can only occur in the improper region for the lossless case when $\epsilon_i > 1$, $\mu_i > 1$ [2]. Hence the only other poles in the ζ-plane are the surface wave poles (SWP), which lie along the lines $\zeta_r = \pm\pi/2$, as shown.

If θ is sufficiently large, some leaky-wave poles will in general be captured during the path deformation, as shown in Fig. 2(b). The leaky-wave fields increase exponentially with z, but decrease exponentially with R within the region in which they are defined, since $\theta > \zeta_{rp}$ when they are captured [2]. The leaky-wave phase and attenuation constants are given by

$$\beta = \mathrm{Re}(k_{rp}) = \mathrm{Re}(k_0 \sin\zeta_p) = k_0 \sin\zeta_{rp} \cosh\zeta_{ip} \tag{11}$$

$$\alpha = -\mathrm{Im}(k_{rp}) = -\mathrm{Im}(k_0 \sin\zeta_p) = -k_0 \cos\zeta_{rp} \sinh\zeta_{ip}, \tag{12}$$

respectively, where $\beta - j\alpha$ is the pole location in the k_r-plane (on the improper sheet). If a leaky-wave pole is close to the real axis so that α is sufficiently small, the leaky-wave field will dominate the total field at the air-dielectric interface, provided the residue is not too small [3]. In this case the radiation pattern exhibits a sharply peaked behavior at $\theta = \theta_p$ where

$$\beta = k_0 \sin\theta_p. \tag{13}$$

A more detailed discussion of leaky-wave properties is given in [2], [3].

III. Asymptotic Evaluation of the Leaky-Wave Properties

In view of the previous discussion, it may be expected that leaky waves could be responsible for the high-gain effect. This

presumption may be verified by a straightforward, but lengthy, asymptotic solution for the leaky-wave pole locations of the characteristic equations, which are as follows.

TE-Mode:

$$D_e = 0 = \cos(k_{z2}t)[\mu_1(jk_{z0}b) + (k_{z1}b)\cot(k_{z1}b)] - \frac{\sin(k_{z2}t)}{k_{z2}t}\left[\frac{\mu_1}{\mu_2}(k_{z2}t)(k_{z2}b) - j\mu_2(k_{z1}b)(k_{z0}t)\cot(k_{z1}b)\right]. \quad (14)$$

TM-Mode:

$$D_m = 0 = \cos(k_{z2}t)[j(k_{z0}b)\epsilon_1 - (k_{z1}b)\tan(k_{z1}b)] - \frac{\sin(k_{z2}t)}{k_{z2}t}\left[\frac{\epsilon_1}{\epsilon_2}(k_{z2}t)(k_{z2}b) + j\epsilon_2(k_{z1}b)(k_{z0}t)\tan(k_{z1}b)\right] \quad (15)$$

where

$$k_{z0} = (k_0^2 - k_r^2)^{1/2}$$
$$k_{z1} = (k_1^2 - k_r^2)^{1/2}$$
$$k_{z2} = (k_2^2 - k_r^2)^{1/2}.$$

The sign taken for the square root of k_{z1}, k_{z2} is arbitrary since these signs occur in even function fashion in (14) and (15), but $\mathrm{Im}(k_{z0}) > 0$ is used to ensure the improper pole interpretation.

To solve for complex pole locations asymptotically, k_r is written as a perturbation about the expected high-gain value as

$$k_r = k_0 \sin\theta_p + k_0(\delta_r + j\delta_i). \quad (16)$$

The arguments of the tan and cot functions may then be approximated for the cases $\theta_p > 0$ and $\theta_p = 0$ and then substituted into (14), (15), with only the dominant terms kept as $\epsilon_2 \to \infty$. After straightforward but lengthy simplification, the results summarized below are obtained.

TE-Mode:

$\theta_p > 0$:

$$\beta/k_0 \sim \sin\theta_p \quad (17a)$$

$$\alpha/k_0 \sim a_1/\epsilon_2. \quad (17b)$$

$\theta_p = 0$:

$$\beta/k_0 \sim \alpha/k_0 \sim c_1/\sqrt{\epsilon_2}. \quad (17c)$$

TM-Mode:

$\theta_p > 0$:

$$\beta/k_0 \sim \sin\theta_p \quad (18a)$$

$$\alpha/k_0 \sim b_1/\epsilon_2. \quad (18b)$$

$\theta_p = 0$:

$$\beta/k_0 \sim \alpha/k_0 \sim c_1/\sqrt{\epsilon_2} \quad (18c)$$

where

$$a_1 = \frac{1}{m\pi}\frac{\mu_2}{\mu_1}(n_1^2 - \sin^2\theta_p)^{3/2}\cot\theta_p \quad (19a)$$

$$b_1 = \frac{1}{m\pi}\epsilon_1\mu_2(n_1^2 - \sin^2\theta_p)^{1/2}(\sin\theta_p\cos\theta_p)^{-1} \quad (19b)$$

$$c_1 = \frac{1}{\sqrt{m\pi}}\sqrt{\mu_2/\mu_1}\, n_1^{3/2}. \quad (19c)$$

Several important conclusions follow from these results. First, there exists a TE-mode and a TM-mode leaky-wave pole which both become dominant ($\alpha \to 0$) for $\epsilon_2 \gg 1$. For these dominant poles $\beta/k_0 \sim \sin\theta_p$ when $\theta_p > 0$, in agreement with the conclusion of a peaked beam at θ_p due to the leaky waves. For $\theta_p > 0$ the attenuation constant α behaves as $O(1/\epsilon_2)$. For the case $\theta_p = 0$, β/k_0 tends to zero, but relatively slowly, behaving as $O(1/\sqrt{\epsilon_2})$. In this case, α/k_0 has the same asymptotic form as β/k_0, and hence the leaky-wave pole asymptotically approaches the origin along the diagonal line, in either the k_r-plane or the ζ-plane. Furthermore, in this case the form is the same for both the TE- and TM-mode poles.

To verify the validity of the asymptotic formulas, results showing a comparison of the exact and asymptotic leaky-wave propagation wavenumbers for the TE-mode case are presented in Fig. 3 for a broadside beam, and in Fig. 4 for a scanned beam ($\theta_p = 45°$), for the lowest mode ($m = 1$, $p = 1$). The exact values are found by a secant-method search in the complex plane. The agreement is good in all cases, and improves as ϵ_r increases.

One of the *practical uses* of these formulas for the leaky-wave properties is in determining the required structure size in the x, y directions to realize the narrow beam patterns. The size required is such that the leaky waves emanating from the dipole are sufficiently attenuated at the perimeter. If the structure radius is r_s, then $\alpha r_s \gg 1$ is required.

IV. Leaky-Wave Radiation Patterns

The TE-mode leaky wave primarily determines the E_ϕ component of the far field, while the TM-mode wave primarily determines E_θ. The TM-mode leaky wave thus determines beamwidth in the E-plane, while the TE-mode wave determines beamwidth in the H-plane. Because the asymptotic form for α/k_0 is the same for the TE- and TM-modes when $\theta_p = 0$, a broadside pencil beam is produced which is circular in shape. For a scanned beam the forms are different, so a conical beam having different beamwidths in the two planes is created.

For the H-plane, it is possible to predict easily the leaky-wave radiation pattern using scalar diffraction theory. This is because the H-plane pattern of the dipole is the same as that for an infinite line source in the x direction. Because of the two-dimensional nature of the line-source problem, a scalar Kirchhoff-Huygens formulation may be used to determine the radiation field from the amplitude distribution of the leaky-wave on the layer surface. Derived in [3], the formula for the

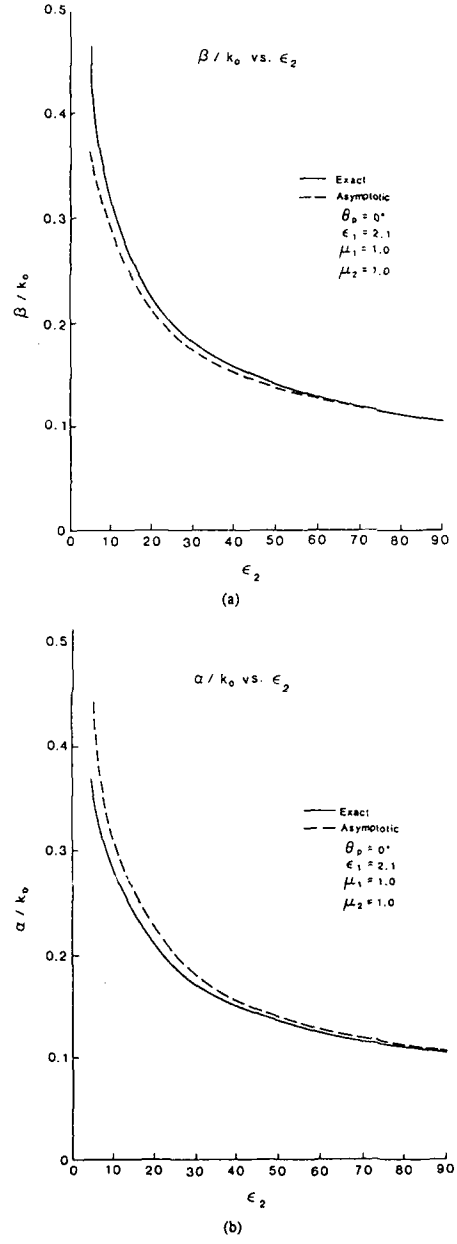

Fig. 3. Comparisons between exact and asymptotic TE-mode leaky-wave propagation wavenumbers as function of dielectric constant ϵ_2 of superstrate, for lowest mode with $\theta_p = 0°$ (broadside beam). (a) Phase constant β/k_0 versus ϵ_2. (b) Attenuation constant α/k_0 versus ϵ_2.

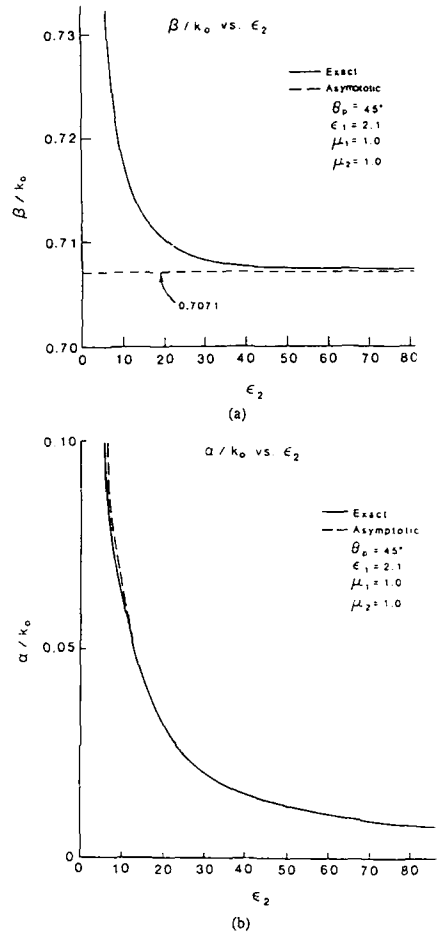

Fig. 4. Same as Fig. 3, but for $\theta_p = 45°$ (scanned beam). Note tha 4(a), for β/k_0, ordinate scale is greatly enlarged.

radiated power pattern is

$$R(\theta) = \left| \frac{\cos\theta}{\sin^2\zeta_p - \sin^2\theta} \right|^2.$$

To provide a convincing demonstration of the don nature of the leaky waves in determining the pattern, the H-plane radiation pattern (from a reciprocity method [compared with (20) for the lowest mode ($m = p = 1$) ir 5(a) and (b) for $\theta_p = 0°$ and $\theta_p = 45°$, respectively patterns are normalized to 1.0 at the maximum). agreement is excellent in both cases.

Since the asymptotic formulas for α/k_0 do not depend o dipole position z_0 but only on the layer parameters. beamwidth and gain of the pattern are likewise independe z_0 in the asymptotic limit. The amount of radiated powe however, dependent on the dipole position. The optir

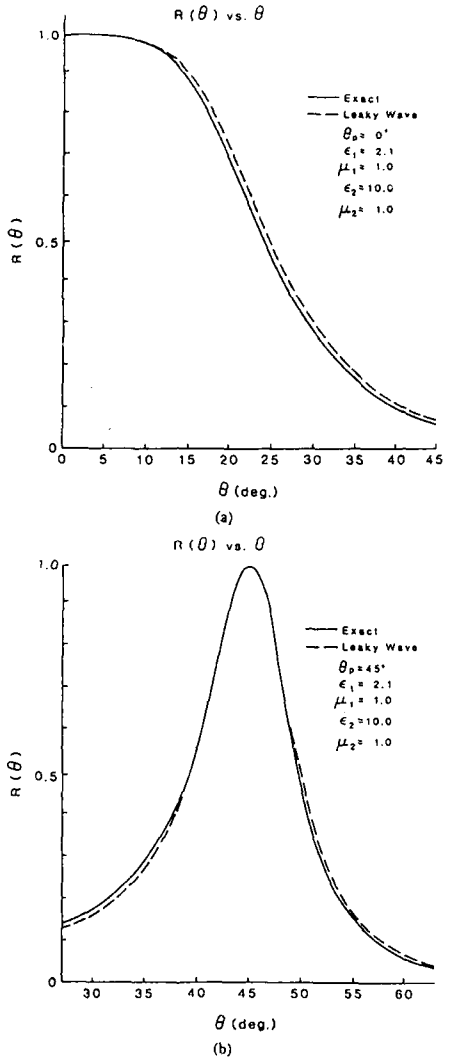

Fig. 5. Comparisons of exact and leaky-wave H-plane radiation patterns for lowest mode with $\epsilon_2 = 10$. (a) $\theta_p = 0°$. (b) $\theta_p = 45°$. Agreements are seen to be excellent.

dipole height to maximize radiated power is

$$\frac{n_1 z_0}{\lambda_0}\sqrt{1-\sin^2\theta_p/n_1^2}=\frac{1}{4}(2n-1), \qquad n=1, 2, \cdots \quad (21)$$

where $z_0 < b$. This places z_0 at a voltage maximum position in a transmission-line model of the layered structure [1].

V. Pole Migration With Frequency

Some interesting features can be observed as the leaky-wave pole positions are traced as a function of frequency in the steepest-descent plane. In Fig. 6, such a plot is obtained by

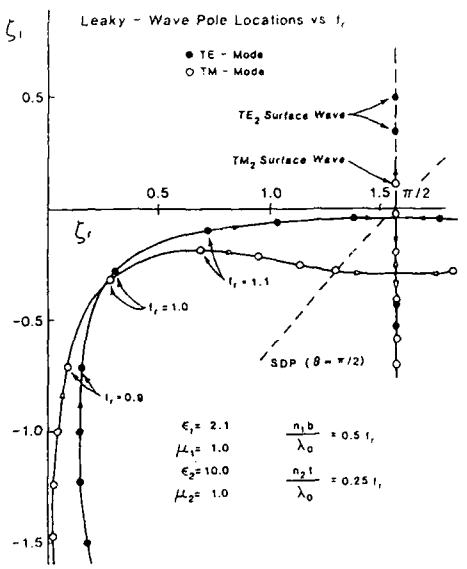

Fig. 6. Migration of leaky-wave poles in steepest-descent plane with normalized frequency f_r, for lowest mode with $\epsilon_2 = 10$. Interval between data points is 0.10.

introducing a frequency ratio f_r, and then using layer thicknesses according to

$$\frac{n_1 b}{\lambda_0}=0.5 f_r \quad (22a)$$

$$\frac{n_2 t}{\lambda_0}=0.25 f_r \quad (22b)$$

with $\epsilon_1 = 2.1$, $\epsilon_2 = 10$, and $\mu_1 = \mu_2 = 1$.

At low frequency the radiated beam has a maximum at broadside with a relatively low gain. For low frequency both the TE- and TM-mode poles lie significantly below the real axis, as seen in Fig. 6. As f_r increases toward 1.0 the broadside beam narrows, with a maximum broadside gain obtained for $f_r \simeq 1.0$. At this point conditions (22a) and (22b) then correspond to the resonance condition for $\theta_p = 0$ for the lowest mode ($m = 1$, $p = 1$) as given by (1) and (2). In the steepest-descent plane both poles are seen to come near to the origin at $f_r = 1$. At this point $-\zeta_i \simeq \zeta_r$, in accordance with the prediction, made in association with (17c) and (18c), that for large ϵ_2 the poles would lie near to the origin along the diagonal line.

As f_r increases past 1.0 the beam scans, since (1) is then satisfied for larger values of θ_p; (2) will then not be satisfied exactly, but this feature is not too significant in determining the resonance condition. It is primarily the substrate thickness that determines the beam scan angle. The scanned beam is conical in shape, having a narrower beamwidth in the H-plane than in the E-plane. These results are in agreement with the pole behavior for $f_r > 1.0$ in Fig. 6. As f_r increases, ζ_r increases for both poles. However, $|\zeta_i|$ decreases steadily

for the TE-mode pole but begins increasing for the TM-mode pole. The attenuation constant α is thus smaller for the TE-mode pole, in accordance with (17b), (18b) which predict that the TE-mode pole is less attenuated when $\epsilon_2 \gg 1$.

Also shown in Fig. 6 is a portion of the steepest descent path (dashed line) for the case of a saddle point at $\zeta = \theta = \pi/2$, with the path described by $\sin \zeta_r \cosh \zeta_i = 1$. All leaky-wave poles to the left of this line will be captured for some angle θ, while those to the right are never captured. This path also serves as a dividing line between fast waves ($\beta < k_0$) to the left and slow waves ($\beta > k_0$) to the right, seen from (11). Hence all leaky-waves poles which are captured, and thus directly contribute to the fields, are fast waves. From Fig. 6 it is seen that both the TE-mode and TM-mode poles cross the $\pi/2$ steepest-descent curve, but at different frequencies. The poles continue to proceed into the slow wave region, intersecting the line $\zeta_r = \pi/2$. In the lossless case, poles in the ζ-plane are symmetrically located about the line $\zeta_r = \pi/2$ [2]. Hence, at the intersection frequencies the poles merge with their symmetrical counterparts, which are also improper poles. As f_r increases further, the pole pairs split. For each pair, one pole proceeds downward along the line $\zeta_r = \pi/2$, and represents an improper surface wave pole, which is never captured for any angle θ. The other pole moves upward from the intersection point along the line $\zeta_r = \pi/2$, starting as an improper surface-wave pole. This pole crosses the $\zeta = \pi/2$ point (real axis) at the frequency corresponding to a TE or TM surface-wave cutoff frequency, for the respective pole type. The pole continues to move upward as f_r increases, becoming a proper surface-wave pole. The two upward-moving poles may then be identified as the usual TE_2 and TM_2 surface-wave poles, respectively (for the indexing used here, the TM_0 and TE_1 modes have the lowest cutoff frequencies of their respective mode types, with the TM_0 mode having zero cutoff frequency).

Although only the TE_2 and TM_2 poles are shown in Fig. 6, there are an infinite number of both TE- and TM-mode leaky-wave poles [6], although only a finite number are captured by the steepest-descent path (and hence contribute directly to the field) at any given frequency. Only the TE_2 and TM_2 poles are dominant, however, with the others being further away from the real axis. All of the leaky waves exhibit a similar behavior regarding the intersection with a symmetrical image pole on the $\pi/2$ line, however, with the upward-moving pole crossing the $\pi/2$ point at some frequency, corresponding to a surface-wave cutoff frequency. In this way all leaky-wave poles may be indexed according to their corresponding surface wave type and number.

VI. Conclusion

The narrow-beam resonance gain phenomenon discussed in [1] is shown to be attributable to the excitation of weakly attenuated leaky waves on the structure. Both a TE- and a TM-mode leaky wave become dominant for $\epsilon_2 \gg 1$, where subscript 2 refers to the superstrate. The attenuation constant α of the leaky waves tends to zero as ϵ_2 increases, beha $O(1/\epsilon_2)$ for a scanned beam ($\theta_p > 0$), and as $O(1/\sqrt{\epsilon}$ broadside beam ($\theta_p = 0$). The phase constant β of th waves tends to $k_0 \sin \theta_p$ for $\theta_p > 0$ and tends t asymptotically in the same form as α when θ_p Asymptotic formulas for the explicit behavior have presented. One practical application of these formula simple rule for determining how large the structure ra needs to be to realize the narrow beam: $\alpha r_s \gg 1$.

The TE-mode leaky wave determines the H-plane p while the TM-mode leaky wave determines the E pattern. In the H-plane, the pattern due to the leaky wa itself may be computed from Huygen's principle, ar results show excellent agreement with the total rad pattern, furnishing additional proof that the fields at the interface are indeed dominated by the leaky waves. The l wave approach discussed in this paper provides both si cant insight into the physical processes involved in the na beam resonance gain phenomenon, and methods to deri relevant expressions in much simpler ways.

References

[1] D. R. Jackson and N. G. Alexopoulos, "Gain enhancement m for printed circuit antennas," *IEEE Trans. Antennas Propagat* AP-33, pp. 976-987, Sept. 1985.

[2] T. Tamir and A. A. Oliner, "Guided complex waves: Part 1, Fi an interface," *Proc. Inst. Elec. Eng.*, vol. 110, pp. 310-324 1963.

[3] ——, "Guided complex waves: Part 2, Relation to radiation patt *Proc. Inst. Elec. Eng.*, vol. 110, pp. 325-334, Feb. 1963.

[4] ——, "The influence of complex waves on the radiation field of excited plasma layer," *IRE Trans. Antennas Propagat.*, vol. A pp. 55-65, Jan. 1962.

[5] S. Barone, "Leaky wave contributions to the field of a line s above a dielectric slab," Microwave Res. Inst., Polytechnic Brooklyn, Rep. R-532-56, PIB-462, Nov. 1956.

[6] S. Barone and A. Hessel, "Part II—Leaky wave contributions t field of a line source above a dielectric slab," Microwave Res. Polytechnic Inst. Brooklyn, R-698-58, PIB-626, Dec. 1958.

[7] L. B. Felsen and N. Marcuvitz, *Radiation and Scatterin Waves*. Englewood Cliffs, NJ: Prentice-Hall, 1973.

[8] A. Sommerfeld, *Partial Differential Equations*. New York: demic, 1962.

[9] N. G. Alexopoulos and D. R. Jackson, "Fundamental super effects on printed circuit antennas," *IEEE Trans. Antennas Pr gat.*, vol. AP-32, pp. 807-816, Aug. 1984.

David R. Jackson (S'83-M'84) was born i Louis, MO, on March 28, 1957. He obtainec B.S.E.E. and M.S.E.E. degrees from the Uni sity of Missouri, Columbia, in 1979 and 1 respectively, and the Ph.D. degree in elect engineering from the University of California, Angeles, in 1985.

He is currently an Assistant Professor in Electrical Engineering Department at the Univer of Houston, Houston, TX. His research interest present include microstrip antennas and pri antennas for millimeter wave applications.

Arthur A. Oliner (M'47-SM'52-F'61-LF'87) for a photograph and bio phy please see page 1294 of the December 1985 issue of this TRANSACTI

APPENDIX J

Electronic Letters, Vol. 24. no. 18, pp 1156-1157, Sept 1, 1988

MICROSTRIP TRANSMISSION LINE EXCITATION OF DIELECTRIC RESONATOR ANTENNAS

Indexing terms: Dielectric resonators, Microstrip, Antennas, Dielectrics and dielectric devices

A systematic investigation of the excitation of a cylindrical dielectric resonator antenna was undertaken to illustrate the possibility of such a feed structure and to characterise the coupling behaviour and radiation patterns of the system.

Introduction: Previous work by McAllister[1-3] has shown the dielectric resonator antenna to be an efficient and practical radiator, but this work concentrated on the coaxial probe feed which is not normally acceptable for higher frequency applications. This investigation concentrates on the use of a microstrip feed structure which may be applicable to frequencies well within the millimetre wave bands.

Geometry and structure: The dielectric resonator antenna simply consists of a block of relatively high permittivity material (ε_r = 6 to 30) situated on top of a conducting ground plane. For the case considered in this work, the radiator was chosen to be cylindrical in shape and placed on top of a common microstrip substrate for its excitation as shown in Fig. 1. The microstrip line was 3·2 mm wide and on a 1·19 mm thick Teflon-fibreglass substrate with a relative dielectric constant, ε_{rs} = 2·5, to give a characteristic impedance of 50 Ω. The cylinders used were of radius 12·7 mm, with heights from 2·54 mm to 12·7 mm and relative dielectric constants from 8·1 to 1 mm to 25·4 mm.

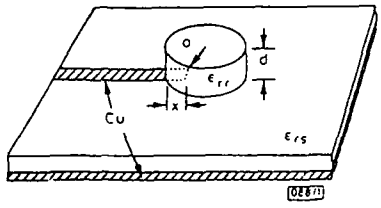

Fig. 1 *Geometry of dielectric resonator antenna fed by microstrip transmission line*

Results: Typical impedance and insertion loss plots are shown in Fig. 2 and Fig. 3 for the case ε_r = 20·8, d = 8·5 mm, a = 12·7 mm and x = 5 mm. The resonant frequency is seen to be 2·72 GHz while the predicted theoretical resonance should occur at 2·46 GHz (a resulting error of 10·6%). Radiation patterns for both the E-plane (the plane going through the centre of the microstrip line and perpendicular to the substrate surface) and H-plane are shown in Fig. 4 and are typical of the performance of the antenna as long as the ratio d/a does not exceed 1·5.

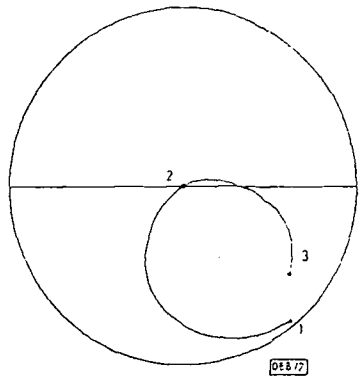

Fig. 2 *Impedance*

ε_r = 20·8, d = 8·5 mm, a = 12·7 mm and x = 5 mm (point 1 = 2·00 GHz; point 2 = 2·72 GHz; point 3 = 3·00 GHz)

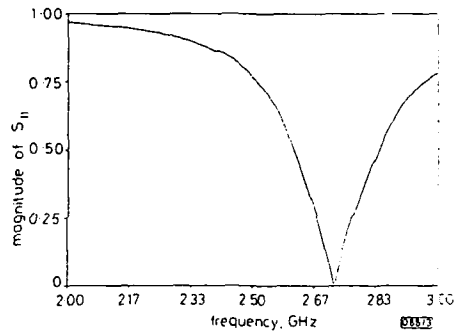

Fig. 3 *Insertion loss*

ε_r = 20·8, d = 8·5 mm, a = 12·7 mm and x = 5 mm

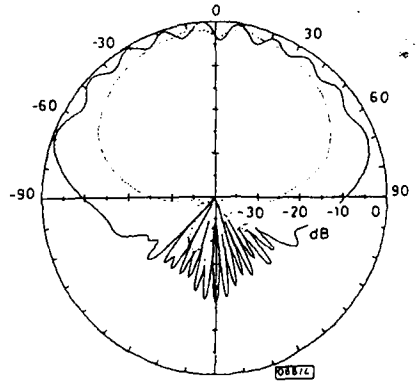

Fig. 4 *E-plane (solid line) and H-plane (dotted line) radiation patterns*

ε_r = 20·8, d = 8·5 mm, a = 12·7 mm and x = 5 mm (f = 2·72 GHz)

The critical parameter that determines the amount of coupling and the particular mode excited by the microstrip transmission line is the overlap distance x. Its effect on the coupling is illustrated in Fig. 5 which shows the insertion loss against overlap distance for the cylinder mentioned in the previous paragraph. It can be seen that the strongest coupling occurs

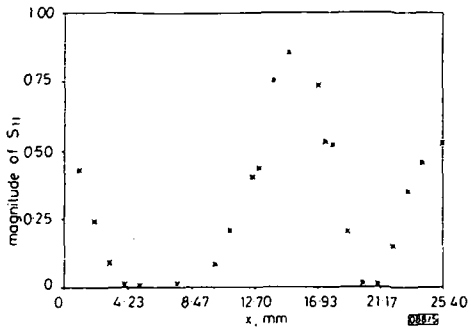

Fig. 5 *Insertion loss against overlap distance x*
$\varepsilon_r = 20{\cdot}8$, $d = 8{\cdot}5$ mm, and $a = 12{\cdot}7$ mm

around $x = 5$ mm and $x = 21$ mm, which are the points where the termination of the line is slightly less than one quarter of a dielectric wavelength from the edge of the cylinder. It is also noted that the radiation patterns deteriorated around $x = 15$ mm, where the end of the line was near the centre of the cylinder and thus not able to excite the proper lowest-order mode. More detailed results are available in Reference 4.

The investigation has shown that a microstrip line can be strongly coupled to the dielectric resonator antenna. This coupling results in an efficient and practical antenna system for frequencies well within the millimetre waveband.

Acknowledgments: This work was supported by the U.S. Army Research Office through contract DAAG29-84-K-0166 and by a grant from the Texas Advanced Technology Research Programme.

R. A. KRANENBURG
S. A. LONG
Department of Electrical Engineering
University of Houston
Houston, TX 77204-4793, USA

19th July 1988

References

1 LONG, S. A., MCALLISTER, M. W., and SHEN, L. C.: 'The resonant cylindrical dielectric cavity antenna', *IEEE Trans.*, 1983, AP-31, pp. 406–412
2 MCALLISTER, M. W., LONG, S. A., and CONWAY, G. L.: 'Rectangular dielectric resonator antenna', *Electron. Lett.*, 1983, 19, pp. 218–219
3 MCALLISTER, M. W., and LONG, S. A.: 'Resonant hemispherical dielectric antenna', *Electron. Lett.*, 1984, 20, pp. 657–659
4 KRANENBURG, R. A.: 'Planar transmission line excitation of dielectric resonator antennas'. Masters thesis, Department of Electrical Engineering, University of Houston, 1988